Investigation of MEMS Inertial Sensors and Aircraft Dynamic Models in Global Positioning System Integrity Monitoring for Approaches with Vertical Guidance

By

Troy S. Bruggemann
B. Eng (Hons)
M. Eng

School of Engineering Systems
Faculty of Built Environment of Engineering
Queensland University of Technology

A thesis submitted for the partial fulfilment of the requirements for the degree of Doctor of Philosophy

2009

Key Words

Approach with Vertical Guidance, Global Positioning System, Inertial Measurement Unit, Aircraft Dynamic Model, Integrity Monitoring, Fault Detection.

Abstract

An Approach with Vertical Guidance (APV) is an instrument approach procedure which provides horizontal and vertical guidance to a pilot on approach to landing in reduced visibility conditions. APV approaches can greatly reduce the safety risk to general aviation by improving the pilot's situational awareness. In particular the incidence of Controlled Flight Into Terrain (CFIT) which has occurred in a number of fatal air crashes in general aviation over the past decade in Australia, can be reduced. APV approaches can also improve general aviation operations. If implemented at Australian airports, APV approach procedures are expected to bring a cost saving of millions of dollars to the economy due to fewer missed approaches, diversions and an increased safety benefit.

The provision of accurate horizontal and vertical guidance is achievable using the Global Positioning System (GPS). Because aviation is a safety of life application, an aviation-certified GPS receiver must have integrity monitoring or augmentation to ensure that its navigation solution can be trusted. However, the difficulty with the current GPS satellite constellation alone meeting APV integrity requirements, the susceptibility of GPS to jamming or interference and the potential shortcomings of proposed augmentation solutions for Australia such as the Ground-based Regional Augmentation System (GRAS) justifies the investigation of Aircraft Based Augmentation Systems (ABAS) as an alternative integrity solution for general aviation.

ABAS augments GPS with other sensors at the aircraft to help it meet the integrity requirements. Typical ABAS designs assume high quality inertial sensors to provide an accurate reference trajectory for Kalman filters. Unfortunately high-quality inertial sensors are too expensive for general aviation. In contrast to these approaches the purpose of this research is to investigate fusing GPS with lower-cost Micro-Electro-Mechanical System (MEMS) Inertial Measurement Units (IMU) and a mathematical model of aircraft dynamics, referred to as an Aircraft Dynamic Model (ADM) in this thesis. Using a model of aircraft dynamics in navigation systems has been studied before in the available literature and shown to be useful particularly for aiding inertial coasting or attitude determination. In contrast to these applications,

this thesis investigates its use in ABAS.

This thesis presents an ABAS architecture concept which makes use of a MEMS IMU and ADM, named the General Aviation GPS Integrity System (GAGIS) for convenience. GAGIS includes a GPS, MEMS IMU, ADM, a bank of Extended Kalman Filters (EKF) and uses the Normalized Solution Separation (NSS) method for fault detection. The GPS, IMU and ADM information is fused together in a tightly-coupled configuration, with frequent GPS updates applied to correct the IMU and ADM. The use of both IMU and ADM allows for a number of different possible configurations. Three are investigated in this thesis; a GPS-IMU EKF, a GPS-ADM EKF and a GPS-IMU-ADM EKF. The integrity monitoring performance of the GPS-IMU EKF, GPS-ADM EKF and GPS-IMU-ADM EKF architectures are compared against each other and against a stand-alone GPS architecture in a series of computer simulation tests of an APV approach. Typical GPS, IMU, ADM and environmental errors are simulated.

The simulation results show the GPS integrity monitoring performance achievable by augmenting GPS with an ADM and low-cost IMU for a general aviation aircraft on an APV approach. A contribution to research is made in determining whether a low-cost IMU or ADM can provide improved integrity monitoring performance over stand-alone GPS. It is found that a reduction of approximately 50% in protection levels is possible using the GPS-IMU EKF or GPS-ADM EKF as well as faster detection of a slowly growing ramp fault on a GPS pseudorange measurement.

A second contribution is made in determining how augmenting GPS with an ADM compares to using a low-cost IMU. By comparing the results for the GPS-ADM EKF against the GPS-IMU EKF it is found that protection levels for the GPS-ADM EKF were only approximately 2% higher. This indicates that the GPS-ADM EKF may potentially replace the GPS-IMU EKF for integrity monitoring should the IMU ever fail. In this way the ADM may contribute to the navigation system robustness and redundancy.

To investigate this further, a third contribution is made in determining whether or not the ADM can function as an IMU replacement to improve navigation system

redundancy by investigating the case of three IMU accelerometers failing. It is found that the failed IMU measurements may be supplemented by the ADM and adequate integrity monitoring performance achieved.

Besides treating the IMU and ADM separately as in the GPS-IMU EKF and GPS-ADM EKF, a fourth contribution is made in investigating the possibility of fusing the IMU and ADM information together to achieve greater performance than either alone. This is investigated using the GPS-IMU-ADM EKF. It is found that the GPS-IMU-ADM EKF can achieve protection levels approximately 3% lower in the horizontal and 6% lower in the vertical than a GPS-IMU EKF. However this small improvement may not justify the complexity of fusing the IMU with an ADM in practical systems.

Affordable ABAS in general aviation may enhance existing GPS-only fault detection solutions or help overcome any outages in augmentation systems such as the Ground-based Regional Augmentation System (GRAS). Countries such as Australia which currently do not have an augmentation solution for general aviation could especially benefit from the economic savings and safety benefits of satellite navigation-based APV approaches.

Table of Contents

List of Figures

List of Tables

List of Abbreviations

ABAS – Aircraft Based Augmentation System

ADM – Aircraft Dynamic Model

APV – Approach with Vertical Guidance

CFIT – Controlled Flight Into Terrain

DH – Decision Height

EGNOS - European Geostationary Navigation Overlay Service

FAA – Federal Aviation Administration

FD – Fault Detection

FDE – Fault Detection and Exclusion

GAGAN – GPS Aided Geo Augmentation System

GAGIS – General Aviation GPS Integrity System

GBAS – Ground Based Augmentation System

GM – Gauss-Markov

GNSS – Global Navigation Satellite System

GPS – Global Positioning System

GRAS – Ground-based Regional Augmentation System

HAL – Horizontal Alert Limit

HDOP – Horizontal Dilution of Precision

HPE – Horizontal Position Error

HPL – Horizontal Protection Level

HNSE – Horizontal Navigation System Error

IAF – Initial Approach Fix

ICAO – International Civilian Aviation Organisation

IMU – Inertial Measurement Unit

INS – Inertial Navigation System

LSQ – Least Squares

MAP – Missed Approach Point

MEMS – Micro-machined electromechanical system

MOPS – Minimum Operational Performance Standards

MMF – Multiple Model Fusion

MSAS – MTSAT Satellite Augmentation System

NPA – Non Precision Approach

NSE – Navigation System Error

NSS – Normalized Solution Separation

MSS – Multiple Solution Separation

RAIM – Receiver Autonomous Integrity Monitoring

RTCA – Radio Technical Commission for Aeronautics

SARPS – Standards and Recommended Practices

SBAS – Space Based Augmentation System

TCXO – Temperature Compensated Crystal Oscillator

VAL – Vertical Alert Limit

VDOP – Vertical Dilution of Precision

VHF – Very High Frequency

VPE – Vertical Position Error

VPL – Vertical Protection Level

VNSE – Vertical Navigation System Error

WAAS – Wide Area Augmentation System

Statement of Original Authorship

The work contained in this thesis has not been previously submitted to meet requirements for an award at this or any other higher education institution. To the best of my knowledge and belief, the thesis contains no material previously published or written by another person except where due reference is made.

Signature

Date

Acknowledgements

This research was supported and funded by the Australian Research Council's Linkage Projects with industry funding scheme (project number LP0455566). This research would not have been possible without project industry partners Graeme Hooper and GPSat Systems Pty Ltd. and Keith MacPherson and Airservices Australia.

Thanks to primary supervisor Prof. Rodney Walker for his guidance and Dr Yanming Feng for his role of secondary supervisor and role in the project. Thanks to Duncan Greer in particular for his help, particularly with his knowledge of aviation. Thanks to all fellow members of the Australian Research Centre for Aerospace Automation (ARCAA) who provide an atmosphere of research community, motivation and enthusiasm and each individual who has contributed to this work in some way with helpful ideas, criticisms and insights. Thanks to my family Helen, Leon and David. Without your personal encouragement and support this research would not have been possible.

1 Introduction

1.1 Research Background

An Approach with Vertical Guidance (APV) is an instrument approach procedure which provides horizontal and vertical guidance to a pilot landing in reduced visibility conditions. APV approaches can greatly reduce the safety risk by improving the pilot's situational awareness. In particular the incidence of Controlled Flight Into Terrain (CFIT) which has occurred in a number of fatal air crashes over the past decade in Australia, can be reduced [1]. The general aviation sector made up the greatest proportion of CFIT cases for the period from 1996 to 2005, two-thirds of which occurred during the approach phase of flight [1]. If implemented at Australian airports, APV approach procedures are expected to bring a cost saving of millions of dollars to the economy due to fewer missed approaches, diversions and increased safety [2].

The provision of accurate horizontal and vertical guidance on the approach is achievable by using the Global Positioning System (GPS). However unlike GPS receivers purchased from consumer electronics stores, an aviation-certified GPS receiver must have integrity monitoring to ensure that its navigation solution can be trusted. However the current GPS satellite constellation has been shown to be inadequate for meeting APV integrity requirements [3-7]. This has motivated the development of augmentation systems to help GPS meet integrity requirements.

Space-based and ground-based augmentation systems monitor GPS externally to the aircraft and rely upon a continuous datalink between ground or space-based transmitters and the aircraft. However, augmentation systems may not detect severe atmospheric conditions or multipath for example that may affect the equipment at the user and there is always the potential for the signal to be jammed or blocked. For example with the Ground-based Regional Augmentation System (GRAS) concept which uses ground-based line of sight VHF transmissions to aircraft, the signal may be blocked for short periods of time due to terrain [8]. During these blockages augmentation is required from an alternative source otherwise the GPS cannot be used for navigation according to aviation regulations.

This problem of potential GRAS outages and the need for GPS integrity for APV approaches in Australia justified the formation of a three year ARC linkage project with industry between QUT, Airservices Australia and GPSat Systems Pty Ltd. in 2004, entitled “Development of High Integrity Airborne Navigation Sensor for Aviation Communities”. It is this problem of GRAS outages which enabled and motivated this research in the investigation of low-cost Aircraft Based Augmentation System (ABAS) for general aviation. The following section defines the research problem and explains the purpose of this research.

1.2 Research Problem and Purpose

GPS needs integrity monitoring to meet APV requirements to improve the safety of general aviation aircraft operations. In countries which cannot afford expensive SBAS solutions or are unwilling to adopt them due to sovereignty concerns, cheaper ground-based alternatives such as GRAS may be an option. However augmentation solutions such as GRAS may not be able to provide complete coverage for all general aviation operations. Aircraft Based Augmentation Systems (ABAS) may provide the required integrity monitoring performance by fusing the GPS information with information from other sensors local to the aircraft.

Past ABAS designs [9-11] rely upon an accurate inertially-derived reference trajectory in Kalman Filters. However these high quality inertial sensors are too expensive for general aviation aircraft. As an alternative, augmenting GPS with low quality Micro-Electro-Mechanical System (MEMS) Inertial Measurement Units (IMU) may provide the necessary augmentation in lower-cost ABAS designs for general aviation. It may also be possible to augment GPS with aircraft dynamic information. The purpose of this thesis is to investigate using an Aircraft Dynamic Model (ADM) and low-cost IMU in an ABAS architecture for general aviation. The fundamental research question for this research is:

What GPS integrity monitoring performance can be achieved by augmenting a GPS with an ADM and low-cost IMU for a general aviation aircraft on an APV approach?

The literature review identified a number of sub-questions which this research will

address:

(a) Can augmenting a GPS with a low-cost IMU or ADM provide improved GPS integrity monitoring performance over GPS alone and if so by how much?

(b) How does augmenting a GPS with an ADM compare to using a low-cost IMU in ABAS for general aviation?

(c) Can an ADM be used as an IMU replacement to improve navigation system redundancy?

(d) Is there any benefit to GPS integrity monitoring in fusing an IMU with an ADM?

Justification for investigating these questions is explained next.

1.3 Research Justification

The inadequacy of the current GPS satellite constellation alone to meet APV integrity, the high cost or sovereignty concerns with SBAS, the potential shortcomings of augmentation systems such as GRAS and the high cost of high quality inertial sensors justify the investigation of alternative solutions for general aviation such as low-cost ABAS. This is particularly important for general aviation communities in countries like Australia which do not have an augmentation solution, yet could benefit from improved operations and increased safety that satellite navigation and APV approaches provides.

There is a noticeable gap in the existing literature concerning ABAS designs for general aviation. On the one hand there are ABAS designs assuming high quality (but typically expensive) inertial sensors which are really only suited for commercial airliners and high-end aircraft. On the other hand there is sole-means GPS, where the current satellite constellation may not support APV requirements and GPS is susceptible to jamming and interference. Although GPS has the capability to operate very well as a sole-means sensor and despite the advances made in signal tracking capability, satellite navigation by its very nature of receiving extremely weak signals

on earth transmitted from satellites far away in space is susceptible to jamming and interference. This is not ideal for safety of life applications such as airborne navigation. Clearly, a more robust approach is to fuse GPS with other sensors such as low-cost IMU.

Although the fusion of low-cost IMU with GPS in general is well known in the literature, its APV integrity monitoring performance when fused with GPS has not been well researched. Further to this, there is the possibility of using different information such as an Aircraft Dynamic Model (ADM) in ABAS. The idea of using an ADM in airborne navigation is not new as it has been studied before for aiding inertial coasting or attitude determination [12], [13], [14]. However in the available literature no research was found exploring its use in ABAS. As revealed in the literature review there are a number of potential advantages of the ADM that warrants its investigation:

- The ADM is only an addition of software; the only hardware components required for its use are sensors to measure control inputs.
- It is onboard the aircraft and is immune to jamming or interference as it does not receive or transmit electromagnetic signals. Like an IMU this makes the ADM suitable to consider in ABAS which is self-contained onboard the aircraft.
- It is based upon information which is different to the inertial sensors – the aerodynamic properties of the aircraft. Incorporating this additional information into ABAS may contribute to the navigation system robustness.

The following section highlights the original contributions which this thesis makes.

1.4 Original Contribution

The original contribution that this thesis makes to knowledge is in the investigation and comparison of the integrity monitoring performance of an ADM and low cost MEMS IMU in ABAS for a general aviation aircraft on APV approach.

Specifically, a contribution to research is made in determining whether a low-cost IMU or ADM can provide improved integrity monitoring performance over stand-alone GPS. It is found that a reduction of approximately 50% in protection levels is possible using a GPS-IMU EKF or GPS-ADM EKF as well as faster detection of a slowly growing ramp fault on a GPS pseudorange measurement.

A second contribution is made in determining how augmenting GPS with an ADM compares to using a low-cost IMU. By comparing the results for a GPS-ADM EKF against a GPS-IMU EKF it is found that protection levels for a GPS-ADM EKF were approximately 2% higher. This indicates that a GPS-ADM EKF may potentially replace a GPS-IMU EKF for integrity monitoring should the IMU ever fail. In this way an ADM may contribute to the navigation system robustness and redundancy.

A third contribution is made in determining whether or not an ADM can function as an IMU replacement to improve navigation system redundancy by investigating the case of three IMU accelerometers failing. It is found that failed IMU measurements may be supplemented by the ADM and adequate integrity monitoring performance achieved. However this may be difficult to achieve in practice due to the need for consistent filter tuning, the possibility of filter instability and considering that the ADM is not normally used in general aviation aircraft. It may be better simply to use another IMU.

A fourth contribution is made in investigating the possibility of fusing IMU and ADM information together to achieve greater performance than either alone. This is investigated using a GPS-IMU-ADM EKF. It is found that a GPS-IMU-ADM EKF can achieve protection levels approximately 3% lower in the horizontal and 6% lower in the vertical than a GPS-IMU EKF. However such a small improvement may not justify the complexity of fusing the IMU with an ADM in practical systems.

The following section describes the significance of this research.

1.5 Significance of Research

This research investigates ABAS with an ADM and low-cost IMU and in doing so

makes a step towards affordable low-cost ABAS for general aviation. It may help GPS meet integrity requirements for a general aviation aircraft on an APV approach. This can result in improved safety (particularly less risk of CFIT incidents occurring) and cost savings due to fewer missed approaches, diversions and the increased safety benefit.

Because ABAS relies upon information available at the aircraft itself, ABAS may operate independently or cooperatively where non-aircraft based augmentation solutions exist. Alternatively it may serve as backup augmentation in case other existing augmentations have problems. For example, the Ground-based Regional Augmentation System (GRAS) can provide GPS augmentation for an aircraft on an APV approach. However due to GRAS using ground-based line of sight transmissions to aircraft the signal may be blocked for short periods of time due to terrain for example. During these blockages, alternative augmentation from various sensors onboard the aircraft may be able to provide continuous high-integrity navigation on the approach.

The following section describes the methodology undertaken in this research.

1.6 Methodology

The approach taken to answer the research questions was firstly to research and design a new ABAS architecture concept consisting of a GPS, low-cost IMU and ADM. The approach was to base this concept on existing ABAS designs which typically use high quality inertial sensors and Kalman filters. The existing literature gave some insight as to the design. Instead of using Kalman filters and rely upon an accurate inertially-derived reference trajectory, use an EKF with low-cost IMU and use frequent GPS updates. Instead of a loosely coupled configuration use a tightly coupled configuration and for fault detection, investigate and use the Normalized Solution Separation method.

After the new ABAS architecture concept was developed it was considered what the options were with using the IMU and ADM information. The presence of the IMU and ADM gave a number of possibilities. The ADM may function

independently of the IMU in a GPS-ADM EKF or may be combined with the IMU. It was decided to focus upon three possible architectures, a GPS-IMU-EKF, GPS-ADM EKF and GPS-IMU-ADM EKF where the IMU and ADM is combined using an existing multiple model fusion strategy. For the GPS-ADM EKF, two additional architectures which make wind estimates were also investigated.

A computer simulation environment called GARDSim was used to test the different architectures in simulation. One main advantage of computer simulation environments over flight test experiments is test repeatability. A certain test can be repeated a number of times and full control can be had over each parameter in the simulation to observe its effect. This is particularly important for research in GPS integrity monitoring and ABAS, whose performance in practice depends upon many factors such as the time of day, the current and past states of the aircraft (position, velocity, attitude etc), the current and past environmental conditions (wind, temperature, air density, etc) as well as the performance of the individual sensors. Given the lack of a fully instrumented flight test experiment aircraft being available for this research in time, the use of GARDSim was seen to be the most effective tool to use.

After implementing the architectures in computer simulation, their performance was compared against a stand-alone "snapshot" implementation of the Normalized Solution Separation Method in a "GPS-only" architecture. The simulation tests conducted were of a Navion general aviation aircraft on APV approach. In the tests, particular focus was given to the protection levels and whether or not they met the APV requirements, because they determine the availability of the fault detection function. If the fault detection function is not available on the approach, the aircraft may have to abort, conduct a missed approach or divert to another airfield resulting in wasted time, excess fuel usage and inconvenience to aircraft operations. Other tests compared and investigated the GPS-IMU EKF, GPS-ADM EKF and GPS in accuracy, protection levels and detection of 0.5 m/s and 2.5 m/s ramp faults. Because the ADM does not make estimates of wind, another test investigated the impact of wind shear on the GPS-ADM EKF protection levels. In another test, to see if combining the IMU and ADM together resulted in improved performance, the GPS-IMU-ADM EKF was compared against the GPS-IMU EKF and GPS-ADM EKF. In

another test, to investigate how the changing satellite geometry affects the protection levels in the different architectures, the protection levels over a 24-hour period were compared in 70 simulation runs. Another test was made for a faster approach velocity that could be due to the system being used on a faster aircraft such as a small jet, for example. This was to see if there was any significant difference in results for a faster approach. Finally, a test was made to investigate substituting some IMU measurements with ADM estimates. This was to determine whether or not using partial information from the ADM can improve the redundancy in the navigation system. The scope and key assumptions made in this thesis are listed next.

1.7 Scope and Key Assumptions

The scope of this thesis is restricted to:

- Investigation of ABAS with the existing GPS satellite constellations. This thesis is not concerned with multiple constellation systems (e.g. Galileo) as GPS is currently the only operational system used in aviation, especially in Australia. As such, multiple GNSS performance and faults are not considered.
- This thesis not concerned about system identification processes to identify the ADM for a particular aircraft. Only a simple aircraft dynamic model is considered. The complexities of high angle of attack, high speed or nonlinear aircraft dynamic modeling issues are not considered.
- It is assumed that GPS is the primary navigation system and is always available. That is, this thesis is not concerned with IMU or ADM "coasting" during a GPS outage as it is already studied to some degree in the existing literature.
- Although there are acknowledged to be potential limitations with using low cost IMUs in practical systems due to their reliability, this thesis does not investigate these issues. The failure modes associated with inertial sensors are already researched to some extent in the literature (e.g. [15]).
- Only fault detection performance is investigated in this thesis not fault exclusion.

An outline of the thesis is given next which makes a summary of the content of each chapter.

1.8 Thesis Outline

This thesis is structured in the following way. Chapter 2 introduces and discusses the topic of GPS integrity monitoring and also reviews relevant literature in the topic area. Topics include Approaches with Vertical Guidance (APV), Global Navigation Satellite Systems (GNSS), the GPS navigation performance requirements, fault detection methods, augmentation systems including inertial sensors, aircraft dynamic models and the Wide Area Augmentation System (WAAS) and Ground-based Regional Augmentation System (GRAS).

Chapter 3 presents and discusses the ABAS architecture concept named the General Aviation GPS Integrity System (GAGIS) for convenience. The architecture is described in general terms followed by a description of the GPS, IMU, ADM, EKF and fault detection components. Different configurations being a GPS-IMU EKF, GPS-ADM EKF, GPS-ADM EKF including wind estimates and a GPS-IMU-ADM EKF are discussed.

Chapter 4 presents results of a series of computer simulation tests to investigate the integrity monitoring performance of GAGIS. A simulated test scenario of a Navion general aviation aircraft on APV approach is described. The values of the simulation parameters used in the tests are given, including values of the GPS, IMU, ADM and environmental errors which were modeled. The GPS-IMU EKF and GPS-ADM EKF are compared with a GPS-only implementation in accuracy, protection levels and detection of slowly growing ramp faults. It is investigated whether not including wind estimates in the ADM can allow for lower protection levels over not including them. Results for a simulated APV approach with changing wind conditions (wind shear) over the flight are presented. The GPS-IMU-ADM EKF is then investigated and compared to the GPS-IMU EKF and GPS-ADM EKF. The affect of changing satellite geometry is evaluated by comparing the performance of the different architectures over a 24 hour period. The effect of a faster approach velocity is evaluated by re-running the simulations for a faster approach velocity. Finally,

substituting IMU measurements with ADM estimates is investigated to see if the ADM may contribute to the redundancy in the navigation system.

Chapter 5 draws conclusions and presents limitations and recommendations for further research and a list of publications made during the course of the research. The Appendix contains a description of the computer simulation environment used in this thesis named the GRAS Airborne Receiver Development Simulation Environment (GARDSim) and some relevant notation.

2 GPS Integrity Monitoring and Literature Review

2.1 Introduction

This chapter introduces and discusses the topic of GPS integrity monitoring and also reviews relevant literature in the topic area. Section 2.2 describes and gives the benefits of an instrument approach procedure called an Approach with Vertical Guidance (APV) where a pilot is provided with horizontal and vertical guidance on landing.

Section 2.3 presents the current state of Global Navigation Satellite Systems (GNSS) and describes the Global Positioning System (GPS). Section 2.3.1 describes the common GPS errors and Section 2.3.2 describes the more severe GPS failures which justify the need for GPS integrity monitoring.

Section 2.4 describes the navigation performance requirements which GPS must meet and defines integrity. Section 2.4.1 defines the aviation integrity requirements which GPS must meet for APV approaches.

Section 2.5 describes the method of GPS fault detection followed by a review of GPS fault detection methods in Section 2.5.1, an example fault detection method in 2.5.2 to highlight the processes involved and a review of their ability to meet APV requirements in Section 2.5.3.

Section 2.6 presents the four types of International Civilian Aviation Organisation (ICAO) approved augmentation system standards for GNSS, reviews the Wide Area Augmentation System (WAAS) and the Ground-based Regional Augmentation System (GRAS) and their limitations. The potential problem of GRAS outages is highlighted and how ABAS may help overcome short-term GRAS outages.

Section 2.7 discusses Aircraft Based Augmentation Systems (ABAS). Section 2.7.1 reviews the use of inertial sensors in ABAS and Section 2.7.2 reviews the use

of aircraft dynamic models in ABAS. Section 2.7.3 reviews filtering methods for ABAS and Section 2.7.4 reviews ABAS fault detection methods.

Section 2.8 draws conclusions from the literature review and shows where an original contribution to research can be made. The following section introduces Approaches with Vertical Guidance (APV) and its benefits to general aviation.

2.2 APV Approaches

An Approach with Vertical Guidance (APV) is an instrument approach procedure which provides horizontal and vertical guidance to a pilot on approach to landing [8]. An electronically-stabilized glide slope and course deviation indicator provides greater situational awareness to the pilot on the approach. This can reduce the safety risk for aircraft landing in reduced visibility conditions and particularly reduce the risk of Controlled Flight Into Terrain (CFIT) [1, 8]. General aviation in particular can benefit from this increase in safety as two-thirds of CFIT in Australia were in the general aviation sector [1]. APV approaches may also give a benefit to the Australian economy in the order of millions of dollars per year, due to the cost savings from fewer accidents, missed approaches and diversions [2].

Satellite navigation technology such as GPS can provide accurate horizontal and vertical navigation and enable APV-I approaches. Figure 1 and Figure 2 are diagrams of an APV approach based upon a GPS approach [16], which are intended to be representative only. During poor visibility GPS can guide the pilot both horizontally and vertically to follow the approach path as given in Figure 1 and Figure 2. Figure 1 shows the segment from the Initial Approach Fix (IAF) waypoint to the Missed Approach Point (MAP) assumed to be at the location of the Decision Height (DH) which represents a minimum height above the ground a pilot can descend to without being able to see the runway ahead. Figure 2 shows the glide slope from the Final Approach Fix (FAF) to the DH.

The segment of interest to this research is the Final Approach Segment (FAS) from the FAF to the MAP. It is during this segment where the APV integrity requirements need to be met. If the pilot has not established a visual reference by the

time MAP is reached the pilot should conduct a missed approach procedure.

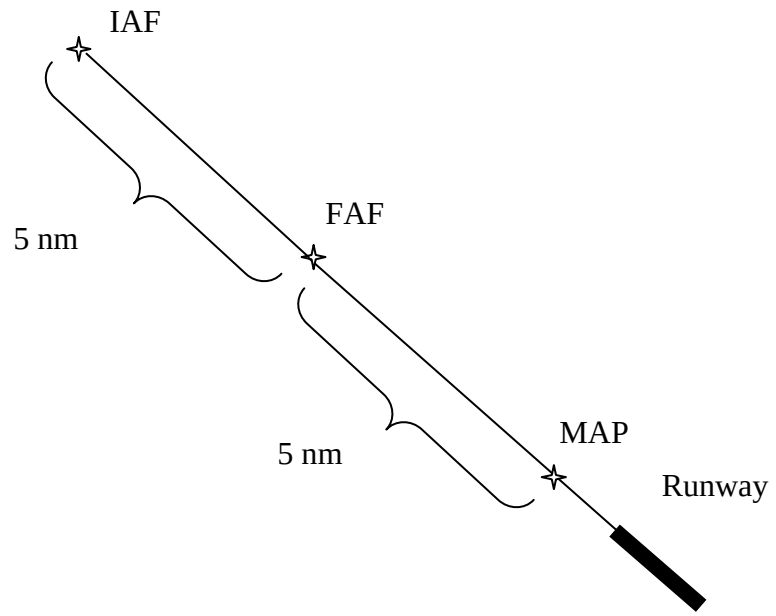

Figure 1 ***APV Approach Description from IAF to MAP, Top View.***

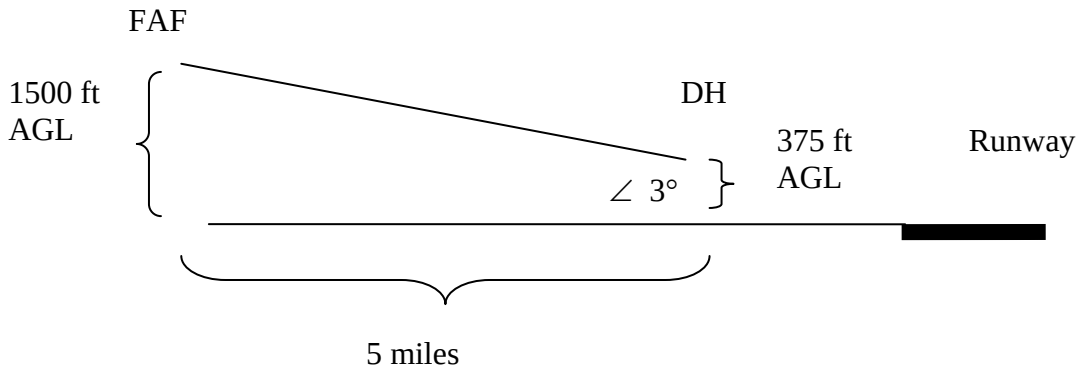

Figure 2 ***APV Approach Description from FAF to DH, Side View.***

Summary

APV approaches can bring an economic benefit as well as increased safety for general aviation. Global Positioning System (GPS) technology which can enable APV approaches will be explained in the following section.

2.3 Global Positioning System (GPS)

GPS, GLONASS, Galileo and Compass are four Global Navigation Satellite Systems (GNSS) currently or soon to be operational [17]. The NAVSTAR Global Positioning System (GPS) was the first global space-based navigation system, conceived in 1973 as a United States Department of Defense program. It consists of a constellation of nominally 24 satellites. Initially intended for military use, GPS has gained widespread use in both military and civilian applications today.

GLONASS is the GNSS developed by the former U.S.S.R and became fully operational in 1996. However in 2003, the number of operational satellites dropped to eight yet Russia appears to be committed to renewing their GNSS program [18].

The European Union has been working towards a GNSS called Galileo since the late 1990's [19]. Galileo is not yet a fully operational system but is expected to be fully deployed within the next 5 years. Compass is China's planned GNSS [20] but it is uncertain as to if and when it will be made available to the global community.

Whilst there are a number of planned GNSS in addition to GPS, only GPS is considered in this thesis because,
(1) GPS is currently the only fully operational GNSS used in aviation.
(2) Other GNSS are unproven systems in aviation, whereas GPS has been used in aviation for a number of years.

Summary

The current state of Global Navigation Satellite Systems (GNSS) has been presented. GPS is the most proven satellite navigation system in aviation and currently the only GNSS fully operational. For these reasons GPS is the only constellation which this research will consider. The following section presents the common error sources in GPS.

2.3.1 GPS Error Sources

GPS operates by the satellites continuously broadcasting signals to Earth which are received by a user's GPS receiver. From these signals, ranges of distance (the raw

measurement called pseudo-range, which is the true range plus errors) can be measured. Four or more measurements are sufficient to provide a user with three-dimensional position, velocity and time information, at any time anywhere on the Earth surface and close to it [21]. But errors on the pseudorange measurements degrade the accuracy of the navigation solution. The typical sources of errors on the pseudorange are due to [22]:

- GPS Satellite
  - Satellite clock – the atomic clocks onboard the GPS satellites have a bias and drift error.
  - Ephemeris – the error in the receiver's estimation of the satellite orbit.
- Signal Propagation Effects
  - Ionospheric delay – caused by the region in the atmosphere where ionized particles and 'free electrons' degrade the signal. Ionospheric scintillation causes signal fading.
  - Tropospheric delay – caused by refraction of the signal due to 'dry atmosphere' and water vapour in the tropospheric region of the Earth's atmosphere.
- Local Receiver Effects
  - Receiver clock – the GPS receiver's clock is typically a crystal oscillator which has an unknown clock bias and drift.
  - Multipath delay – caused by GPS signal reflections off objects or surfaces near to the receiver antenna.
  - Receiver noise – intrinsic receiver noise due to the receiver hardware and software processes, including the error due to measurement precision.

Any of these errors may exceed expected values unknowingly and if so pose a safety risk for an aircraft on an APV approach which requires integrity-checked positions in a matter of seconds. For these reasons if GPS is to be used in aviation there needs to be a way for the user to know whether it can be relied upon or not. This need for integrity is especially important for APV because of tight tolerances in the horizontal and vertical directions which may mean even small errors can have a greater impact on the system. However certain errors such as the ionosphere for

example are more likely to cause a problem than others as it is typically one of the largest, most uncertain and most variable errors on the GPS pseudorange measurement especially in equatorial regions or during solar storm events [8].

To calculate and correct for the ionospheric delay dual frequency measurements may be used to provide better ionospheric error estimates than single frequency ionosphere models. However, until GPS is modernized only the L1 frequency is able to be used in civilian aviation as the second civilian frequency L2 is not in the Aeronautical Radio Navigation System (ARNS) band. As part of the GPS modernization program an additional frequency (L5) in the ARNS band will eventually become available on all GPS satellites. Full capability for the L5 signal is scheduled for 2018 [23] which is expected to bring a number of benefits such as improved ranging accuracy, reduced multipath errors, better carrier phase tracking, enhanced weak-signal acquisition and tracking [24].

Summary

The typical errors on the GPS measurements have been explained which are due to satellite clock, ephemeris, ionospheric, troposopheric, receiver clock, multipath delay and receiver noise. All of these limit the ability of GPS to provide an accuracy position solution. The ionospheric error can be the most problematic error in GPS but may be cancelled through the use of dual frequency (L1/L5) techniques. The L5 signal will be a second signal able to be used in civilian aviation and is expected to be fully available in 2018. Of greater concern to aviation however is not just the accuracy but the amount of trust which can be placed in the system, that is, the integrity. Any of the above mentioned errors may exceed expected tolerances unknowingly which justifies the need for integrity. There are also some possible GPS failures which may be more catastrophic than the typical errors mentioned previously. These and some examples of past GPS failures are discussed in the following section.

2.3.2 GPS Failures

Besides the typical errors on GPS measurements as given in 2.3.1 there are some possible causes of GPS failures [25-27].

Signal blocking/masking errors

These occur when radiated satellite signals are unable to reach the receiver antenna system or signal strengths are too low to be detected. Satellite drop-outs cause a degraded satellite-to-user geometry which increases the uncertainty in the accuracy of the navigation solution.

Signal Interferences

These occur when high or certain electromagnetic conditions exist which prevents satellite signals being acquired or cause frequent loss of lock. This includes unintentional or intentional jamming of the receiver. This may cause GPS to stop navigating completely or cause increased uncertainty in the accuracy of the navigation solution due to satellite drop-outs.

Equipment Failures

GPS satellite hardware or software failures may occur which includes power supply loss, software bugs or physical damage. Slow failures causing performance degradation over a long time can be caused by problems with clocks on the GPS satellite. Sudden 'bit-flips' with digital signals may occur because of the space environment. Satellite failure may cause excessive or insufficient broadcast satellite power. Equipment failures may cause signal in space errors.

Signal in Space errors

Signal in space errors are one of the more subtle and harder to detect errors. Problems with satellite transmission, code generation and space environmental degradation may affect the signal broadcast to users. Propagation-based effects such as electromagnetic and atmospheric disturbances can severely undermine integrity. Ionospheric anomalies are difficult to predict and therefore cause the majority of concern on a day to day basis.

One example of signal in space errors are the so-called "evil waveforms" [13, 14]. These are anomalous satellite signals caused by a failure of the signal generating hardware of a satellite. There are two types: digital failure and analogue failure. Digital failures are seen as errors generated by the Navigation Data Unit (NDU) of the satellite. Analogue failures are caused by signal reflections before broadcast and

signal synthesizer failure in the satellite [14]. Detection of these errors is difficult because the resulting range error is dependent on the spread spectrum receiver discriminator type, correlator spacing and bandwidth of the GPS receiver [13].

Over the years there have been cases of GPS satellites failing, some without being detected. In October 1993 an event occurred where satellite PRN 19 transmitted a so-called ‘evil waveform’. This is known as the ‘SV-19’ event [15]. A problem with satellite hardware caused signal deformation, resulting in non-common range errors across different receiver types. Other cases of satellite failure were found recorded in the literature [16]. It is stated that there have been fourteen GPS satellite failures up until 2003 with the following causes of failure: six examples of reaction wheel (attitude control system), four examples of clock, two examples of power, one example of Telemetry and Control and one example of Navigation Data Unit. Any scheduled satellite outages are announced via the Notice Advisory to Navigation Users (NANU). Unscheduled outages are announced as known. Because of these possible events there is a need for timely integrity in airborne navigation systems as an undetected error could be dangerous to safe operations. For these reasons there are strict performance requirements for any navigation system used in civilian aviation and this will be discussed next.

Summary

Some of the possible GPS failures and some cases which have occurred in the past have been presented. These justify the need for integrity in safety critical applications such as aviation and have partly motivated the development of performance requirements for the use of GPS in aviation. The following section will describe the required navigation performance.

2.4 Required Navigation Performance

Regulations governing the use of GPS in aviation are controlled through the FAA release of Technical Standard Order's (TSO's) based upon RTCA Minimum Operational Performance Standards (MOPS) [28] and ICAO Standards and Recommended Practices (SARPS) [29]. The Required Navigation Performance (RNP) is a statement of the navigational performance necessary for operation within a defined airspace [16]. The four primary performance measures are:

Accuracy: The degree of conformance between the estimated or measured position and/or velocity of a platform and its true position and/or velocity at a given time [30].

Integrity: The ability of a system to provide timely warnings to users when the system should not be used for navigation [31].

Availability: The ability of the system to provide the required function and performance at the initiation of the intended operation. Availability is an indication of the ability of the system to provide usable service within the specified coverage area. Signal availability is the percentage of time that navigational signals transmitted from external sources are available for use. Availability is a function of both the physical characteristics of the environment and the technical capabilities of the transmitter facilities [28].

Continuity: The ability of the total system (comprising all elements necessary to maintain aircraft position within the defined airspace) to perform its function without interruption during the intended operation. More specifically, continuity is the probability that the specified system performance will be maintained for the duration of a phase of operation, presuming that the system was available at the beginning of that phase of operation and was predicted to operate throughout the operation [28].

The quantitative requirements for these performance measures vary according to the phase of flight. The following is a list of the phases of flight. In order from least demanding to most demanding in terms of the required integrity performance [31].

- Enroute (accommodating domestic and oceanic/remote)
- Terminal Area (TAR)
- Non Precision Approach (NPA)
- Approach with Vertical Guidance (APV-I and APV-II)
- Precision Approach (PA)

The scope of thesis is only concerned with meeting the integrity requirements for APV-I.

Summary

The requirements for navigation systems in aviation have been summarized. The focus of this thesis is on meeting the integrity requirements for APV-I. These requirements will be presented next.

2.4.1 Aviation Integrity Requirements

A GPS receiver must meet certain integrity requirements specified in ICAO SARPS and RTCA MOPS [28, 29]. A summary of the most relevant terminology and requirements to this thesis are:

Alert: An indication that is provided by the GPS equipment when the positioning performance achieved by the equipment does not meet the integrity requirements.

Time-To-Alert: The maximum allowable elapsed time from the onset of a positioning failure until the equipment annunciates the alert.

Missed Alert: Positioning failures which are not annunciated as an alert within the time-to-alert. Missed alerts are caused by both missed detection and wrong exclusion conditions after the time-to-alert expires.

False Detection: Detecting a positioning failure when a positioning failure has not occurred. It is internal to the GPS equipment.

False Alert: A false alert is the indication of a positioning failure when a

positioning failure has not occurred (a result of false detection). A false alert would cause a navigation alert.

Horizontal Alert Limit: The Horizontal Alert Limit (HAL) is the radius of a circle in the horizontal plane (the local plane tangent to the WGS-84 ellipsoid), with its centre being at the true position, which describes the region which is *required* to contain the indicated horizontal position with the required probability for a particular navigation mode.

Horizontal Protection Level: The Horizontal Protection Level (HPL) is the radius of a circle in the horizontal plane (the local plane tangent to the WGS-84 ellipsoid), with its centre being at the true position, which describes the region which is *assured* to contain the indicated horizontal position. It is a horizontal region for which the missed alert and false alert requirements are met for the chosen set of satellites when autonomous fault detection is used. It is a function of the satellite and user geometry and the expected error characteristics.

Vertical Protection Level: The Vertical Protection Level (VPL) is half the length of a segment on the vertical axis (perpendicular to the horizontal plane of the WGS-84 ellipsoid), with its centre being at the true position, which describes the region which is *assured* to contain the indicated vertical position when autonomous fault detection is used. It defines the vertical region for which the missed alert and false alert requirements are met for the chosen set of satellites when autonomous fault detection is used. It is a function of the satellite and user geometry and the expected error characteristics.

Availability of Detection: The detection function is defined to be available when the constellation of satellites provides a geometry for which the missed alert and false alert requirements can be met on all satellites being used for the applicable alert limit and time-to-alert. When the constellation is inadequate to meet these requirements the fault detection function is defined to be unavailable. The availability of detection is for a specific location, time, constellation and horizontal alert limit (HAL).

The requirements for the use of GPS in aviation are stringent which is due to the high level of safety and assurance required. For example: 99.9% fault detection probability, 8 second time-to-alert, 10^{-5} false alert probability rate and 0.3 NM (556 m) Horizontal Alert Limit (HAL) is required for the Non Precision Approach (NPA) phase of flight, for which the GPS only provides horizontal guidance [28]. The requirements for the APV approach are given in Table 1 and are even tighter than for NPA, particularly for the accuracy and alert limits. The *Integrity* requirement in Table 1 will be converted to false alert probability and probability of missed detection for APV later in Section 3.7.1 and 3.7.2.

Performance Requirement	***APV-I***
Horizontal Accuracy (95%)	**16 m**
Vertical Accuracy (95%)	**20 m**
Integrity	**1-2 × 10^{-7}/h/approach**
HAL	**40 m**
VAL	**50 m**
Time to Alert	**10 s**
Availability	**99 – 99.999%**

Table 1 ***APV-I Integrity Monitoring Requirements.***

Summary

A summary of the integrity requirements which are relevant to this research have been presented. Also, the APV-I requirements have been presented to show the level of performance which GPS equipment must meet for an approach. The performance of GPS in meeting these requirements will be discussed in the following sections.

2.5 GPS Fault Detection

It is possible that the GPS receiver performance will be degraded beyond the expected level since it is vulnerable to a range of possible errors and failures as previously mentioned in Section 2.3. Should these occur they need to be detected quickly before the error causes the GPS position solution to exceed strict performance requirements. The integrity problem is basically to detect and exclude measurement errors (faults) in the presence of measurement noise and to notify the pilot in a timely manner if the system should not be used for navigation.

The term “fault” means a significantly large error in a range measurement which may potentially cause a Hazardously Misleading Information (HMI) event [28]. Any anomalies which cause HMI to be displayed to the pilot are the major concern and are a significant safety risk. An example of HMI is a sudden error occurring in one GPS satellite causing an undetected fault on a GPS pseudorange measurement, causing a large position error at the user's receiver which has exceeded the HAL or VAL limits. In poor visibility conditions and without integrity-checking (fault detection) the pilot will not know that his or her GPS is in error.

Summary

An introduction to GPS integrity has been provided. The main purpose of integrity monitoring is to prevent hazardously misleading information being reported to the pilot by detecting and excluding (if possible or necessary) any fault. The following section reviews some common fault detection methods found in the literature.

2.5.1 GPS Fault Detection Methods

The main problem is that GPS was not originally designed for use in civilian aviation but for military use. Although it may be used in civilian aviation, there is no guarantee of service. Although GPS has a certain level of integrity checking of its own signals by the control segment, any signal errors found are not reported in a timely manner to the civilian user. This poses a significant safety risk for a pilot on approach to landing who requires the integrity information within seconds. Self-checking methods for GPS receivers were developed as far back as the late 1980's. This is called Receiver Autonomous Integrity Monitoring (RAIM). RAIM uses redundant GPS measurements to check the consistency of the reported GPS position.

At least four GPS pseudoranges are required for the receiver to calculate a position and estimate receiver clock bias. To perform RAIM with a redundant pseudorange measurement it requires at least five pseudoranges to be available. RAIM typically means the capability to detect the presence of malfunctioning satellite(s) only. Another term commonly used, is Fault Detection and Exclusion (FDE). FDE will not only detect the presence of malfunctioning satellite(s) (fault detection) but also identify and exclude the malfunctioning satellite(s) from being included in GPS's navigation solution (fault exclusion). This allows the navigation sensor to continue to output a valid integrity-checked position despite any malfunctioning satellite [28].

GPS fault detection techniques can be categorized into two broad categories: "snapshot" RAIM schemes and filtered RAIM schemes. Snapshot RAIM schemes are among the simplest and use current redundant measurements in the self-consistency check, assuming no correlation in time between measurements. Alternatively, filtered schemes may involve using past and present information along with *a priori* assumptions of vehicle motion [27]. Firstly, "snapshot" schemes will be discussed. Filtered schemes will be discussed in Section 2.7.4.

There are three main "snapshot" RAIM methods to be found in the literature, developed in the late 1980's. One is using the pseudo-range residual presented by Parkinson and Axelrad (1988) [32]. This method calculates a test statistic in the range domain based on statistical theory of the pseudo-range errors. The threshold is determined by Monte Carlo simulation methods and set to meet the false alarm and missed detection requirements.

Another snapshot RAIM method is the range comparison method by Y.C. Lee in 1986 [33]. This performs integrity checking by comparing ranges which are estimated from the position solution derived from a sub-set of measurements, with the remaining measurements that were not included in the sub-set solution. Inconsistency between the estimated and measured ranges indicates a failure to be present.

A third method is the parity space method presented by Sturza and A. Brown (1988) [33, 34]. This procedure is similar to the range comparison method but uses a

linear transformation of the pseudo-range from the range domain into a parity space domain. As presented in [35] it is more useful to transform the information in the range residual vector into what is called the parity vector which has some special properties with respect to the noise. The threshold level is determined using the chi-square probability distribution with the requirement for the probability of false alarm (in a constant-false-alarm-rate algorithm), the number of satellites in view and the expected pseudo-range noise. Brown (1992) [33] showed that the three RAIM methods presented above are mathematically equivalent. The RTCA SC159 Working Group 5 tentatively decided to use the magnitude of the parity vector as the test statistic in its baseline RAIM algorithm [35]. However in the MOPS it does not recommend one particular technique over another [28].

Summary

A description of GPS-only fault detection methods has been presented. These have formed the basis of many fault detection methods in the literature. An example of one fault detection method will be given in the following section.

2.5.2 GPS Fault Detection Method Example

The following presents a brief description of the general method for GPS integrity monitoring based on two papers by Brown [33, 35] to provide an understanding of the process involved.

Fault Detection and Exclusion (FDE) consists of two parts: Detection of a fault and identification and exclusion of the fault. GPS fault detection typically uses statistical hypothesis testing. The key parameters required are a test statistic, a decision threshold and the Horizontal Protection Level. Two key checks are required. Firstly, a check that the detection function is available. This is done by comparing the protection level against the alert limit requirement. If the protection level exceeds the alert limit there is no guarantee that a fault will be detected within the probability of missed detection. This will affect the availability of detection (Section 2.4.1). Secondly, the pseudoranges are checked to determine whether or not a fault exists. The various components required for fault detection are presented:

Test Statistic

The test statistic is normally derived from the pseudo-range residuals vector. This vector is an output of a standard GPS-only position solution which is an over-determined solution of the difference between measured and expected pseudo-range measurements. This approach assumes that any errors on the range measurements will be observable in the residuals.

Detection Threshold

The threshold is set to yield a desired false alert rate. Thresholds are normally selected by Monte Carlo methods or using the chi-square probability distribution to give a desired probability of false alert.

Horizontal Protection Level (HPL)

The HPL is the maximum allowable horizontal position error before an error must be detected. If HPL is exceeded the error should be detected within the probability of detection requirement.

To calculate the HPL a quantity called slope which is a function of satellite geometry is calculated for each satellite in view (see [33, 35] for details). This then relates the test statistic domain with the position error domain. The satellite with the maximum slope value is deemed the satellite which is the most difficult satellite to detect an error on. In other words, an error on this satellite measurement is considered the hardest to detect because it yields the largest position error for the lowest test statistic value.

Figure 3 plots the *Horizontal Position Error* (HPE) against the *Test Statistic*. The oval shape on Figure 3 represents the scatter cloud expected if a bias (fault) was on the *SLOPE_max* satellite, sufficient to push the cloud up the *SLOPE_max line* to the point where the fraction of data to the left of the threshold line is equal to the allowable probability of missed detection (denoted P_{md}). p_{bias} is the critical bias value and is the bias required to yield the desired missed detection probability. Any fault greater than p_{bias} can be detected within the specification for probability of detection.

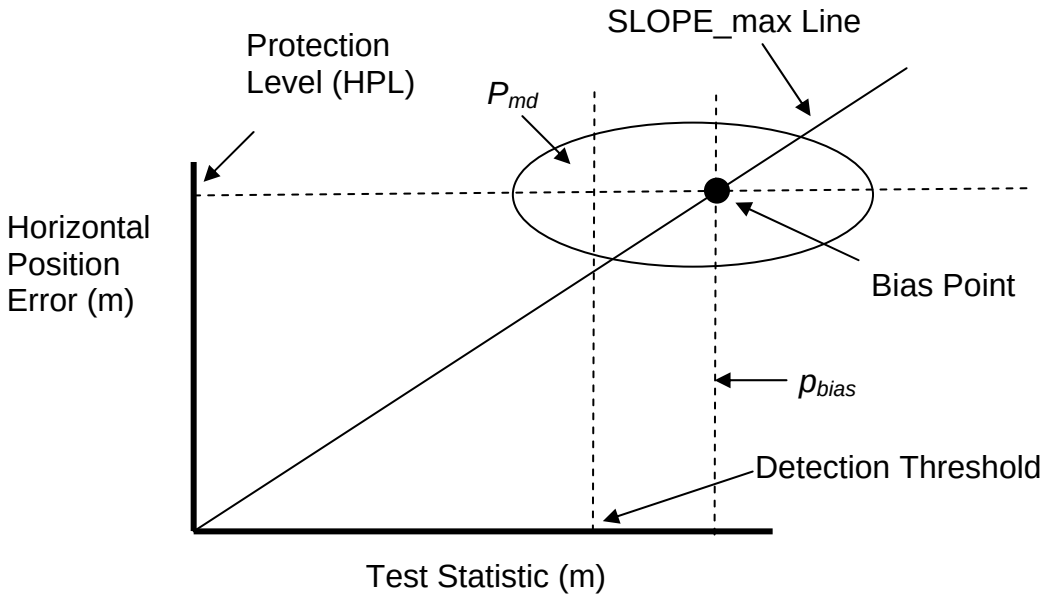

Figure 3 ***Bias Fault on Slope_max Satellite.***

After the above parameters have been calculated, the two key checks can be made for fault detection. The first check is to check the availability of fault detection. The second check is to detect any faults on the measurements.

Availability of Fault Detection

Each phase of flight has a Horizontal Alert Limit (HAL) requirement. Recall that HAL is the radius of a circle in the horizontal plane which describes the region which is *required* to contain the indicated horizontal position. Once the HPL is calculated to yield a desired probability of missed detection, the HPL is compared with the HAL to check if the detection function is available. If the HPL exceeds the HAL then no guarantee can be given that a fault can be detected within the probability of detection requirement. In this case the fault detection function is deemed to be not available.

Detection of a Fault

If the fault detection function is available, a comparison of the test statistic with the threshold determines whether a fault is present on the measurements. If a fault is detected, exclusion (if it is available) can be attempted to try to identify and exclude the fault.

Summary

A general integrity monitoring method has been presented in order to aid understanding of the processes involved. The following section will discuss the performance of GPS fault detection in aviation.

2.5.3 GPS Fault Detection Performance in Aviation

In the past various availability analyses have been conducted to assess the suitability of RAIM to meet the requirements [3, 5]. One investigated the capability of the existing GPS constellation to meet the RAIM requirements for en-route civilian flights over the continental USA [5]. Simulation results showed that a baseline 24 satellite GPS constellation with expected satellite failures will not meet FAA RAIM detection or exclusion availability requirements (99.999%) for civilian users with barometric aiding. It was calculated that the addition of 5 or 6 satellites to the GPS constellation should meet the 99.999% RAIM availability requirement for the en- route phase of flight. Alternatively, it was concluded that the en route availability could be obtained by augmenting the existing GPS constellation with 5 geosynchronous Wide Area Augmentation System (WAAS) satellites.

It must be noted that since these analyses were made, a deliberately introduced error to GPS (for USA security reasons) called selective availability (SA) was turned off in early 2000. This has resulted in a substantial improvement to integrity availability [6]. The FAA standards state that GPS receivers in aviation (TSO C145/C146 receivers [36]) must have FDE for primary means navigation. The requirements to enable this are more stringent than alone since FDE needs at least 6 GPS satellites in view. It was shown that a 30 satellite constellation with SA off is required for FDE availability to approach 100% for all phases of flight. It is stated that "*GPS alone will not be able to satisfy availability requirements for primary means navigation with FDE without additional satellites*" [6]. Although currently there are more operational satellites in the constellation than the baseline 24, the constellation is not optimized for the additional satellites. It is not only the number of satellites which are important but how they are distributed.

Lee et al. [4] studied the ability of single and dual constellation RAIM and WAAS to meet APV-II requirements in the USA. They concluded that RAIM operating with

a single constellation would not be suitable for vertical guidance. They showed that a combined GPS/Galileo constellation with single or dual frequency and WAAS has the potential to achieve a high availability for the USA.

Van Dyke [7] assessed the suitability of the GPS constellation in meeting APV-I and APV-II requirements. It was found that in order to provide high availability for APV-I, a UERE (user equivalent range error) of 2.5 metres or less is required, possibly with a constellation of more than 24 satellites and barometric altimeter aiding.

Limitations in the GPS constellation meeting RAIM requirement justify the need for augmentation. Augmentation is especially needed for meeting the stricter requirements for approaches in APV, particularly if the current GPS constellation is used. These show that it may be difficult to meet APV requirements using RAIM with the current GPS constellation. The use of dual frequency (L1/L5) measurements may make a UERE of 2.5 metres or less possible after the ionospheric error on the pseudorange is reduced, however the limitations of the satellite constellation geometry still remain.

Regarding dual frequency GPS, Tsai et al. (2004) [37] describe algorithms using multiple GPS frequencies in integrity monitoring. By using the L2 and L5 signals the atmospheric errors such as the ionospheric delay can be removed. This results in a lower measurement error variance, more accurate position and the time of detection for errors is improved. It is shown by simulation that when compared with single frequency RAIM, multi-frequency algorithms give a more accurate position, higher performance in detecting small failures and a similar level of performance in detecting large failures. The removal of ionospheric error also results in a cleaner parity vector which makes fault identification and exclusion more reliable. It is shown that the dual-frequency method has a lower incorrect exclusion rate and a triple-frequency method has a lower rate still.

The research on L1/L5 GPS shows promising results for aviation integrity. In this research it will be assumed that the L5 signal is available for the purpose of ionospheric delay corrections which will help achieve the integrity requirements by

reducing the pseuodrange error. Without these corrections, APV performance may not be achieved as the uncertainty on the pseudoranges due to the ionosphere may be too large especially in equatorial regions or solar storm events.

Summary

This section presented the expected GPS fault detection performance with the current satellite constellation. The literature showed that it is expected that GPS alone will not meet APV unless there is a reduction in pseudorange error and changes to the existing satellite constellation. The use of L1/L5 measurements may be able to give the reduction in pseudorange error required. For this reason dual frequency GPS is considered in this thesis. However the existing satellite constellation may not support integrity monitoring for APV without augmentation. Whilst the literature showed that dual constellations may meet the requirements, this thesis considers a single satellite constellation only for reasons stated in Section 2.3. Augmentation is discussed next.

2.6 Augmentation Systems

Because of shortcomings of GPS in supporting integrity monitoring with RAIM methods as shown in 2.5.3, augmentation systems such as WAAS have been developed. There are four types of International Civilian Aviation Organisation (ICAO) approved augmentation system standards for GNSS [29]:

- SBAS – Space Based Augmentation System: broadcasts augmentation information to users by satellites in space. These are useful in providing wide area coverage over a large area.
- GBAS – Ground Based Augmentation System: broadcasts augmentation information to users from ground-based transmitters. It is not intended for wide-area coverage. These are predominantly intended as an ILS replacement for precision approaches.
- GRAS – Ground-based Regional Augmentation System: broadcasts augmentation information to users from ground-based transmitters, but allowing continuous reception over wide areas. In this way it is similar to SBAS, yet also similar to GBAS. Because of the use of ground-based transmitters like GBAS, GRAS can be considered as an extension to GBAS [38].
- ABAS – Aircraft Based Augmentation System: Augment GPS with other information available onboard the aircraft.

The United States of America's SBAS is named the Wide Area Augmentation System (WAAS). WAAS augments GPS with a number of geosynchronous satellites to provide the required availability, accuracy, integrity and continuity for en-route, Non Precision Approach (NPA), Lateral/Vertical Navigation (LNAV/VNAV) and Precision Approach (PA) phases of flight in the US national airspace system. Correction and integrity data is transmitted for the WAAS and GPS and the WAAS satellites also transmit GPS-like ranging signals. This provides additional range measurements for the GPS receiver to use [39] which can improve the GPS navigation solution. The WAAS architecture consists of [39] :

- A network of Wide area Reference Stations (WRS) which collect data from GPS and WAAS satellites.
- Wide area Master Stations (WMS) which collect and process the data from the WRS and generate the WAAS messages to be transmitted to the user via WAAS satellite.
- Ground Communications network between ground stations.
- Infrastructure to support the operation of WAAS satellites and uplink capabilities.
- User equipment to receive and process GPS and WAAS signals.

A disadvantage of this system is that it is expensive to operate and maintain geosynchronous satellites [8]. This makes a cheaper ground-based system such as GRAS (discussed in the next section) an attractive solution for countries such as Australia, which do not wish to have the cost of maintaining geosynchronous satellites [40]. Australia was able to receive signals from at least one WAAS satellite however this cannot be used to improve the accuracy of GPS because Australia is outside of the WAAS service volume and cannot receive broadcast integrity messages for Australian airspace. WAAS is not the only SBAS there is also MSAS (Japan), EGNOS (Europe), GAGAN (India) to name a few which have potential for providing a service to Australia. However it appears that the limiting factor in adopting these systems for Australia is over sovereignty control [8]. With MSAS for example, if there is a network of WRS in Australia, the data may have to be transmitted to Japan for processing and upload to the satellites before re-transmission to Australia. There may be time delays in this approach, as the information needs to be sent to Japan, to the satellite and back to Australia again within time to alert requirements for an aircraft on APV approach. In addition, there may be political or legal issues with processing Australia's GPS integrity data in another country, not to mention any safety and security concerns.

An alternative to SBAS is the Ground-based Regional Augmentation System (GRAS). GRAS consists of multiple ground stations with overlapping coverage. Each station can provide approximately 200 NM radius coverage at 10,000 feet altitude [40]. GRAS can support operations in en-route, terminal, non-precision approach and Approach with Vertical Guidance (APV) phases of flight.

The GRAS architecture consists of [40-43] :

- A network of GRAS Reference Stations (GRS) which collect GPS data.
- A GRAS Master Station (GMS) which processes data from the GRS, determines GPS corrections and integrity status and generates SBAS messages.
- GRAS VHF Stations (GVS) which receive and verify SBAS messages, convert these to GBAS format and broadcast the GRAS messages to the user.
- Ground Communications network between ground stations.
- User equipment to receive and process GPS and GRAS signals.

The modulation scheme used in GRAS is as follows:

- Uses Differential Eight Phase Shift Keying (D8PSK)/Time Division Multiple Access (TDMA) data link technology (accepted by ICAO for use in GBAS).
- Uses a single frequency, using TDMA to separate the signals from the various VHF transmitter sites.
- Adjoining data broadcast sites are separated by using different time-slots. User accepts messages from the time slot with the strongest signal. Up to 16 time slots are available on a single frequency.
- There are no issues with same slot interference.
- Coverage is approximately 200 NM maximum range with D8PSK/TDMA.
- Using a single frequency:
- It avoids the difficulties of frequency spectrum availability issues.
- Uses simpler devices.
- There is no need to retune to different frequencies in-flight.

GRAS is intended to provide enhanced accuracy and integrity for any navigation satellite system (GPS, GLONASS and Galileo) and the ability to accept ranging signals from Space Based Augmentation Systems as well, if available.

There are thought to be a number of benefits of GRAS over SBAS [38, 42]:

1) GRAS is suitable for high latitude regions where signals from

geosynchronous satellites are not available (such as Sweden).

2) GRAS is suitable for areas of the earth where the cost of having and maintaining geosynchronous satellites (such as with the USA's WAAS) is too expensive. The costs for these could be $15 to $20 million per satellite per year, in addition to the costs of facilities and maintenance for the ground segment.
3) A GRAS network consisting of ground based transmitters is easier to deploy, cheaper to maintain and able to provide a faster time for repair in the event of failure than for satellites. For these reasons GRAS may be implemented in a modular way or in stages. For example, GRAS sites may be located in high-demand areas initially and later scaled up or down depending upon the need. In addition, the failure of a single ground based transmitter does not impact the whole network, whereas the failure of a single SBAS satellite can impact a wide area of users.
4) GRAS is suitable for areas where satellite signals are blocked by structures or terrain (e.g. airport surface operations).
5) With GRAS there are less sovereignty issues than if an existing SBAS is shared with another country. Countries can be in control of their own augmentation data broadcast. Some countries may not be able to participate in a regional SBAS solution for legal or political reasons.

Comparatively, GRAS can have as many economic and safety benefits to aviation as the SBAS systems, at a much lower cost [40]. The use of SBAS satellite ranging information is optional because unlike WAAS, GRAS does not transmit additional ranging signals to aircraft. It has been demonstrated that the achievable accuracy is comparable to the accuracy achieved with SBAS [44]. This could therefore be a technically viable low-cost alternative to SBAS, well suited to Australia's economic and aviation environment.

From a technical perspective, ignoring the additional ranging signal which SBAS can provide, the only real difference between SBAS and GRAS is the delivery mechanism to the user; SBAS uses satellites and GRAS uses ground-based transmitters. The related ground infrastructure (the reference stations and master stations) to provide integrity monitoring of the GPS satellites and the atmospheric

(ionosphere and troposphere) is essentially the same – a wide-area differential GPS network However the use of ground-based VHF transmitters may be a limitation, because a clear view of the signal from the ground to the aircraft is required.

Although the GPS system itself is owned and operated by another country to Australia, GRAS allows a service provider to have some level of control over their own system. This may be preferred rather than both the GPS and augmentation system being in another country. Another advantage may be that if two countries each have their own augmentation system for example, as GRAS can allow, it provides the ability for independent analysis and comparison of the GPS signals between the two.

Airservices Australia proposed a Ground-based Regional Augmentation System (GRAS) to provide integrity monitoring service for Australian airspace particularly because of the high cost of developing and operating its own SBAS and sovereignty concerns over sharing an SBAS which belonged to another country [40]. Australia was not the only country interested in such a system. Sweden and Russia were interested in GRAS since existing SBAS did not cover high latitude regions [42]. A number of countries in South-East Asia, the Middle East, Africa, Eastern Europe and South America expressed interest in the GRAS system [8].

However there is a potential limitation of GRAS which is the GRAS signal not always being received at the aircraft. Due to cost or siting constraints such as lack of sufficient communications infrastructure, mountains, forests and large distances to maintenance facilities may mean to GRAS data broadcast stations are not able to be placed at optimal or every location to guarantee complete coverage [8]. For example, GRAS stations may be placed at major airports, but regional airports may not have a transmitter on-site, but rely upon transmissions from another airport within the vicinity. Ground infrastructure is also susceptible to lightning strikes, power outages or communications failures may mean the broadcast integrity message is not available for periods of time [8]. These situations may cause regions in the network where GRAS signals are not available. Since the range of the signal decreases with altitude, there may also be unwanted temporary loss of GRAS signal due to masking by the terrain for aircraft flying at low altitudes, for example. One possible scenario

is that GRAS may be available for the initial stage of an APV approach, but as the aircraft descends in altitude towards the runway it encounters a GRAS outage if the signal is blocked by surrounding terrain.

There is also the possibility that isolated effects may cause severe unmodelled disturbances at the aircraft which GRAS may not account for. One of the most difficult errors to estimate is the ionospheric error. The ionosphere can be the largest source of error for GPS [45, 46]. Ionospheric storm events (in times of solar flares) and other random effects can occur, putting unexpected burdens on the system. Equatorial regions which include the northern parts of Australia and the south-east asian and pacific island regions typically have severe ionospheric effects impacting the performance of GPS. However an adequate number of GRAS ground stations may not be able to be placed in order to give good estimation of the ionospheric delay. Jamming of the augmentation system is also a possibility [47]. The incorporation of ABAS to overcome the limitations could ensure that any errors local to the aircraft have not caused the system to exceed the navigation performance requirements. These checks are important because it is only at the GPS receiver onboard the aircraft where all the information is combined.

For increased safety and reliability, a backup integrity augmentation such as ABAS could provide continuous GPS navigation for short periods of time in the event of a GRAS outage. Furthermore, even when GRAS signals are available it may be advantageous for the user equipment to employ a backup integrity strategy using ABAS in case of severe multipath or ionospheric effects at the aircraft which are not detected or modelled by GRAS.

Summary

Four types of International Civilian Aviation Organisation (ICAO) approved augmentation system standards for GNSS have been listed which are SBAS, GBAS, GRAS and ABAS. GPS is integrated with other sensors onboard the aircraft and may provide improved accuracy and integrity performance because of the additional information available to the system. A description of an SBAS named WAAS has been provided and it has been shown that these have limitations such as cost and sovereignty control concerns for countries such as Australia to adopt them.

The GRAS system has been reviewed, which may be a viable alternative to the more expensive SBAS and allow countries to retain sovereignty control. However GRAS may be vulnerable to short-term outages due to siting constraints or the signal being blocked by terrain for example. These justify the investigation of ABAS for general aviation which is discussed next.

2.7 Aircraft Based Augmentation Systems (ABAS)

The type of augmentation this thesis considers is ABAS. GPS is integrated with other sensors onboard the aircraft and this can provide improved accuracy and integrity performance because of the additional information available to the system. It can also improve the overall robustness of the navigation solution since the additional sensors do not suffer from the same types of errors as GPS. In integrity monitoring it is an advantage to have augmentation systems as local to the aircraft as possible since only at the user's equipment is all the information combined. GRAS for example may not be able to detect a GPS receiver fault or severe localized ionospheric or tropospheric effects at the aircraft. Other advantages of ABAS is that being self-contained on the aircraft there is no need for communication links to satellites or ground based receivers. Also there is no need for regular maintenance as with ground stations which can have issues with rodents, lightning strikes, earth movement, water damage etc. ABAS operation is also not limited by extreme latitudes or difficult terrain as may limit the reception of satellite signals in SBAS or placement of ground stations as with GRAS. The following section discusses augmenting GPS with inertial sensors.

2.7.1 ABAS with Inertial Sensors

Integrating GPS with Inertial Navigation Sensors (INS) [22, 27, 48] is common. Both can complement each other to give improved navigation performance. Inertial sensors consist of accelerometers and gyroscopes and can provide position, velocity and attitude of an aircraft by processing measured accelerations and angular rotation rates with respect to the inertial frame. In general GPS alone provides poor short term accuracy and better long term accuracy whereas INS alone has poor long term accuracy but good short term accuracy. INS can also typically output at a much faster rate than GPS can and combining both together can result in a more stable robust navigation system than either alone. Provision is made in the RTCA MOPS for GPS/inertial systems to be used for FDE, provided such a system meets the requirements in Appendix R [28].

Bhatti, Ochieng and Feng (2007) [49] [50] conducted a review of the performance of GPS/INS in integrity monitoring, particularly with detecting slowly growing

errors. Firstly, they promote the benefits of fusing GPS with INS. The benefits of fusing GPS with INS are:

- Integrated systems are more accurate.
- The additional information provided by the addition sensors means more trust can be placed in the output, due to the redundancy.
- The integrated output can be provided at a higher rate than GPS because of the higher data rate of INS.
- The integrated system will be available even during a GPS outage. The time of availability is limited by the quality of the INS.

This applies to both loosely and more tightly coupled systems. However [49] recommends tightly coupled methods. An advantage of tightly coupled is that even with less than four satellites available the navigation solution can be maintained by the filter. There is also greater access to pseudorange measurements which can provide a benefit for detecting slowly growing errors. A stated disadvantage is that it responds more slowly to INS errors than loosely coupled systems.

Low-quality MEMS inertial sensors have difficulty meeting the required accuracy in stand-alone operation except for short periods of time. The main limitation of low-quality MEMS sensors is that their noise is too large to fulfill the typical assumption associated with inertial sensors – the ability to provide an unbounded yet accurate navigation solution during periods of GPS outage [51]. Therefore, whilst they can provide an accurate estimate of trajectory in between frequent GPS updates, they cannot “coast” without aiding for very long while maintaining the accuracy required for APV [52-55].

Despite limitations of MEMS sensors, Bhatti [15] who researched the performance and failure modes of INS with respect to aircraft integrity states "in future, MEMS based INS are expected to be used in aviation mainly because of relatively low cost". This warrants the investigation of MEMS INS in ABAS. However there are some reliability issues with MEMS sensors as highlighted in [15] and as stated by Bhatti, it will take time before MEMS based INS can be used in commercial aircraft. An approach taken in [15] was a "piggy back" architecture where the low cost INS

position is combined with GPS satellite positions derived from broadcast ephemeris to derive a fictitious range measurements. Treating the INS as an additional pseudorange measurement allows for isolating an INS fault which is an advantage of this architecture.

Summary

This section described inertial navigation sensors and the benefits for fusing them with GPS in ABAS. Provision is made for the use of inertial sensors in the RTCA requirements. However these assume a high grade inertial sensor which would be unsuitable for use in general aviation due to the high cost. For this reason this research will consider low-quality MEMS inertial sensors in ABAS.

2.7.2 ABAS with Aircraft Dynamic Models

Besides inertial sensors the use of aircraft dynamics has been considered before for use in navigation systems. Koifman and Bar-Itzhack (1999) [12] investigated the feasibility of using an aerodynamic motion model to aid an inertial navigation system. A computer simulation was made for the investigation. It contained a strap-down inertial navigation system computing aircraft position, velocity and orientation. This was run in parallel to a navigation system where position, velocity and orientation are calculated from the aircraft's dynamic motion model. The position, velocity and orientation outputs from both systems are fed into an extended Kalman filter (EKF). The output of the EKF is the estimated navigation errors of the INS and aerodynamic model systems. This output is used to update and calibrate both systems.

The two main causes of navigation error in the aerodynamic model is the lack of knowledge of the wind velocity and errors in the aircraft dynamic model coefficients. With both systems integrated, the INS estimates the constant wind velocity and errors in the dynamic model coefficients. Likewise, the aerodynamic model estimates the INS errors such as the gyro drift and accelerometer bias. Through simulation of flight paths, this research showed that a perfectly known aerodynamic model gave considerable improvement to the inertial navigation system. This was with appropriate calibration manoeuvres and accurate knowledge of aircraft dynamic

model parameters. Analysis was also conducted with inaccurate knowledge of parameters. It was mentioned that in practice the aerodynamic parameters can vary up to +/- 10% of their true values. When the aircraft coefficients are varied +/- 10% of their nominal values, one at a time, it was shown that this degraded the system performance considerably. It was discovered that not all varied coefficients degraded the performance because not all coefficients were observable during certain manoeuvres. To try and improve the performance, the errors in the coefficients were added as additional states to the Kalman filter for estimation. This gave an improved navigation performance. However the coefficient errors were not estimated individually but as groups of coefficients. There was no attempt to identify individual aerodynamic coefficients since the goal was to provide continuous navigation.

In summary it was found that it is possible to improve the accuracy of an INS using an aerodynamic model with an addition of software and no added instrumentation. It was shown that with estimation of aerodynamic model errors, the navigation performance of the system is satisfactory even when the parameters of the aircraft model are not perfectly known.

They also suggest that it may be useful in a system with a GPS and INS, although no further work by the authors has been found of this implementation in the existing literature. Despite the advantages shown by including an aerodynamic model with an INS for "inertial coasting", if the aerodynamic model is to be used in a navigation system for civilian aviation it must meet the integrity requirements for the particular phase of flight.

Estimation of the errors in the aircraft coefficients which are observable during appropriate calibration manoeuvres was attempted. Although Koifman and Bar-Itzhack achieved satisfactory navigation by attempting to estimate the parameter errors, it was not explored in detail. An aircraft on APV approach however, cannot perform calibration manouvres unless they are somehow incorporated into the specified approach procedures, or performed prior to commencement of the approach.

Lievens et al. (2005) [14] proposes using an aerodynamic model with GPS as a

low-cost system for single-antenna attitude determination. The Euler angles, angle of attack and side slip angle are estimated using only a single-antenna GPS and aerodynamic model of the aircraft. The aircraft is required to fly a turn at constant airspeed from time to time to be able to estimate wind and true airspeed from GPS ground speed measurements. Controllability and observability analysis was conducted. Unstable states that are controllable are not expected to cause a problem, yet a problem is expected with the wind which is both uncontrollable and unobservable. This shows the capability of using an aerodynamic model and single GPS receiver.

Eck, Geering and Bose [13, 56], incorporated a mathematical model in the navigation process for improving autonomous helicopter navigation during GPS outage. They state that it can increase the robustness and reliability of the navigation data if low-cost inertial sensors are used, or during periods of GPS outage. This paper is similar in nature to the previously discussed papers which consider aiding inertial coasting with an ADM during GPS outages.

Cork and Walker [57] used a nonlinear dynamic model to replace the inertial navigation equations in an Interacting Multiple Model (IMM) and Unscented Kalman Filter (UKF) architecture to provide improved state estimation in the presence of inertial sensor faults for fault-tolerant control of Unmanned Aerial Vehicles (UAVs).

From the available literature on the use of aircraft dynamic models in navigation the benefits are:

- The ADM is an addition of software, the only hardware components are sensors for measuring control inputs.
- Like an IMU the ADM is onboard the aircraft and is immune to jamming or interference, as it does not receive or transmit electromagnetic signals.
- It can be used to estimate the full state of the vehicle (position, velocity attitude) in a similar manner to an IMU.
- It is based upon existing and typically unused information – the aerodynamic properties of the aircraft. Incorporating this additional

information may contribute to navigation system robustness and reliability.

The disadvantages of the ADM are the uncertainties due to inaccurately known aerodynamic coefficients, surrounding environment (e.g. wind) and how to measure pilot control inputs. Although it is not difficult to add sensors such as potentiometers to measure aircraft control surface movements, measurement of these is not normally made for most general aviation aircraft and therefore there will be additional costs involved. Another disadvantage is that an ADM is valid only for a particular aircraft type.

Summary

This section reviewed past literature where the aircraft dynamic model has been studied for use in navigation systems. Applications previously considered included aiding or replacing inertial sensors during GPS outages or backup attitude determination and it was found to be useful or provide a benefit. However there was no literature found on its use in ABAS. The usefulness of an ADM in ABAS will be evaluated in this thesis.

2.7.3 ABAS Filtering Methods

There are a number of ways in which GPS and other information such as inertial measurements can be combined. Nikiforov (2002) [58] states that multi-sensor integrated navigation systems can be divided into two groups. There are those which include navigation error equations which can be reduced to a static regression model such as the case with barometric altimeters. Others involve stochastic dynamical error equations which is the case for combining GPS and inertial systems.

The most commonly used method for ABAS is the Kalman Filter. A Kalman filter is a set of equations that provides a recursive method to estimate the state of a dynamic system from a series of noisy measurements [48, 59]. It minimizes the mean square error in its estimates of modeled state variables. For a problem which is nonlinear in both the states and measurements, which is the case for low cost IMU fused with GPS, a better solution linearizing around the current estimate leads to the Extended Kalman Filter where nonlinearities are approximated by linear functions. A disadvantage of the EKF is that the distributions of the random variables are no

longer normal after undergoing nonlinear transformations and the estimated covariances may not be equal to the true covariance. This has led to the development of the unscented transform which is presented in the following.

Julier and Uhlmann (1997) [60] presents the Unscented Kalman Filter. The Unscented Kalman filter is a variation on the traditional Kalman filtering methods as it uses the Unscented Transform. The Unscented Transform uses a set of appropriately chosen weighted points to parameterise the means and covariances of probability distributions. The difference between the Unscented Transform and Monte-Carlo methods are that the samples are not drawn at random but according to a specific, deterministic algorithm. It is stated that the UKF can predict the state of a system more accurately than the EKF.

The particle filter is a nonlinear filtering method which uses Monte Carlo simulation to evolve a distribution of random state estimates as determined by the model state [61, 62]. Particles are independent samples of the probability distribution which are generated by Monte Carlo simulation. These represent the likelihood that a particle corresponds to the true system state. It is stated that particle filtering provides a very accurate estimation of position for an integrated GPS/INS when the number of satellites is less than a critical number. For a low number of satellites the linearization methods such as the EKF may provide an unacceptable estimate of position [61]. A disadvantage is that many particles are generated (normally thousands) which makes particle filtering a very computationally intensive method. In addition, for an ABAS for general aviation aircraft on APV approach, the degree of accuracy required may not justify a particle filter.

Wendel et al. [63] compares the EKF and SPKF for tightly coupled GPS/INS systems. The study showed that there is no accuracy improvement in using SPKF over EKF unless initial errors are large (greater than 30 km in the study), which has no practical relevance when accuracy of GPS itself is typically a few metres. In addition the study states the computational load of the SPKF is significantly greater than the EKF. If used in ABAS this would be compounded further for GPS integrity monitoring algorithms which use multiple filters for fault detection. The UKF not giving any great advantage in accuracy was also confirmed in [64]. However if the

UKF estimates the covariances more accurately than the EKF and it is significant enough, it may justify the investigation of nonlinear filters such as the UKF.

Summary

Different filtering methods have been reviewed. The most commonly used method for ABAS is the Kalman Filter. UKF, SPKF and Particle Filters are thought to be unnecessary for ABAS. For a low cost MEMS IMU and ADM in ABAS the EKF may be the most suitable common extension of the KF to the nonlinear system.

2.7.4 ABAS Fault Detection Methods

The principles of GPS-only FD methods can be applied to an ABAS, where GPS is integrated with other sensors onboard the aircraft. As the following review of the literature will show, most of the methods for ABAS integrate GPS and high quality (but expensive) Inertial Reference Systems (IRS).

Diesel (1994) [10] discusses Autonomous Integrity Monitored Extrapolation (AIME) for providing sole means GPS availability without WAAS. It is stated that an approach and landing system based on position information alone is inherently unstable making it vulnerable to time lags, gaps due to masking or jamming, noise, interference, multipath and wind shear. A method where the GPS is augmented by other systems onboard the aircraft is desirable. This method involves storing averaged GPS measurements at 2.5 minute intervals in a circular buffer for 30 minutes or more. High quality inertial sensors can provide the ability to coast through outages of GPS integrity. However an inertial system alone cannot provide this ability without proper calibration, otherwise un-calibrated errors can cause the system to exceed integrity limits.

A way to reduce errors and improve the ability to coast through integrity outages is to calibrate the solution from the inertial system using GPS when the GPS integrity can be assured, using a Kalman filter. However a drawback of Kalman filters with inertial systems is that it can be difficult to detect slowly growing errors, which may occur when a satellite clock slowly drifts away for example. Since a slowly drifting measurement error can cause a position error before it is detected in a Kalman filter, this extrapolation approach allows satellite clock drifts to be detected with only a

minimal number of satellites for long periods. This is because it observes the GPS measurements over a long period of up to 30 minutes. All valid past and present GPS measurements can then be used to estimate present position by extrapolation. This is an advantage over the 'snapshot' RAIM algorithms which assume that measurements are not correlated in time. The test statistic of this method is a normalized sum of squares residual, which is calculated from the Kalman filter innovations process residual vector. Unlike the parity method test statistic, this statistic depends on the entire past history of measurements. This means that AIME can detect failures with one, two or three satellites in view depending on past history.

In flight tests and simulation, drifts were deliberately inserted of between 0.05 to 0.1 m/s and allowing only 3 or 4 satellites in view. It was shown that NPA world-wide availability of 0.99999 based on 21 to 24 satellite constellations without WAAS is achievable. In addition, the conditional probability of detecting a failure is increased from 0.999 to 0.99999.

Diesel and Gunn (1996) [65] states that AIME has been certified for primary means navigation on an Airbus A330/340 aircraft. It is stated that although availability is improved by augmenting GPS with WAAS, complete reliance on satellite navigation alone results in vulnerability to unintentional radio frequency interference and intentional interference such as jamming or spoofing. They show that the availability required for sole means can be achieved by integrating GPS with an IRS using AIME.

Brenner (1995) [9] presents a method of fault detection called the Multiple Solution Separation (MSS) method. The parity space methods commonly adopted in RAIM snapshot approaches monitor the measurement or parity space domain. This algorithm is based on solution separation in the horizontal position domain. A bank of Kalman filters are used where one filter processes the full set of N GPS measurements and the others process sets of $N-1$ GPS measurements. The test statistic is the horizontal separation between the full-set and subset solutions. Decision thresholds for the solution separation between full-set and subset solutions are calculated from the Kalman filter covariance matrix for each subset solution.

Young and McGraw (2003) [11] present an approach for GPS/inertial sensors that combines a normalized solution separation for fault detection and a residual monitoring scheme for fault exclusion. Similar to the methods discussed previously, the filtered FDE algorithm uses a full Kalman filter, a number of sub-filters and a least squares navigation method. The full filter and the least squares method process all available measurements while the sub-filters each exclude one of the available measurements. Since the fault detection and fault exclusion functions are in different domains, for some failure types the fault exclusion function may detect a failure sooner than the fault detection function. To take advantage of this the fault detection and fault exclusion functions are treated as two independent processes running in parallel. Simulation results for NPA show that the filtered algorithm outperforms the snapshot method. It is shown that the filtered FDE algorithm has an availability performance equivalent to other filtered algorithms.

Two FDE algorithms are presented using this method; a snapshot and a filtered algorithm. For the snapshot scheme it is shown that the normalized solution separation method is equivalent to the parity method. It is shown that with proper normalization the normalized solution separation test statistic is a consistent estimator of a faulty measurement. It is also shown that computing sub-solutions is not necessary for fault isolation, as it is with other snapshot FDE algorithms.

This algorithm uses the Circular Error Probable (CEP) distribution which is claimed to provide a more accurate estimate of HPL. This is because the horizontal position error is a two-dimensional Gaussian distribution, whereas the use of one-dimensional Gaussian distribution may not be as accurate. A benefit of this algorithm over the MSS method is a faster processing time since a dual covariance matrix is not propagated as with the MSS method. However the disadvantage of this approach is a possible rank deficiency issue.

For snapshot algorithms, range domain methods are equivalent to position domain methods. However for filtered algorithms the relationship between test statistics in the range domain and their corresponding position errors cannot be clearly defined. This is because past measurements and statistics of the system model also influence the current navigation solution. Therefore since the test statistic for a filtered solution

separation method is in the position domain, HPL can be analytically derived which is an advantage. However despite the fault detection function being in the position domain, the fault exclusion function is in the range domain. The Horizontal Exclusion Limit (HEL) cannot be analytically derived. It is stated that this is not a problem since HEL is only required for off-line availability analysis and not a real-time output from aviation equipment.

No other literature was found that studies the performance of the NSS algorithm. However, a number of studies have been made on the performance GPS/inertial systems comparing the AIME and MSS methods. Lee and O'Laughlin (1999) [54] investigated how well a tightly coupled GPS/inertial system can detect slowly growing errors for two integrity monitoring methods. It was stated that the general consensus among RTCA SC-159 Working Group members was that ramps in the range of 0.2 to 2 m/s are the worst case. This paper investigated whether a slowly growing error smaller than 2 m/s but larger than 0.2 m/s can be detected with a required detection probability of 0.999 in the absence of redundant GPS satellites. This is significant because Kalman filters used with an inertial system tend to adapt to and include any slowly varying drift as a dynamic state. It is a challenge to detect slowly growing errors with a high probability of 0.999. The two methods compared were the Solution Separation Method and the Extrapolation Method as mentioned above.

Both methods successfully detected the ramp error fault and identified and excluded the faulty satellite. However the extrapolation method had an advantage over the solution separation method in terms of HPL. The extrapolation method HPL was generally larger than the Solution Separation method's HPL. This means that the extrapolation method may provide greater availability. Therefore in certain cases the integrity monitoring function will be available for a GPS/INS system using the extrapolation method but not for the solution separation method.

The results showed that both methods suffer in the ability to detect failed satellites during periods of fewer than four satellite visibility. For coasting capability, it was shown that an aircraft with a tightly coupled GPS/inertial system using a navigation-grade inertial unit can coast for 20 to 30 minutes and maintain an accuracy of 0.3 nm.

The coasting time is also depending upon the type of turning manoeuvre made. Although the extrapolation method can achieve a lower HPL, the main disadvantage of the extrapolation method is that the integrity performance (whether the HPL meets the probability of detection requirement) must be verified by use of Monte Carlo simulation. A subsequent paper [66] presents the use of covariance matching to reduce the effort required in verifying the AIME method. The solution separation method on the other hand can be verified analytically, despite the protection levels typically being higher than those calculated by the extrapolation method.

Bhatti, Ochieng and Feng (2007) [49] [50] conducted a review of the performance of GPS/INS in integrity monitoring, particularly in detecting slowly growing errors. It is stated that tightly coupled GPS/INS systems have the highest potential for detecting slowly growing errors rather than snapshot RAIM. The performance the MSS and AIME methods and a new rate detector algorithm was compared. The rate detector algorithm is proposed for implementation alongside the AIME method and is based upon detecting the rate of the test statistic to provide early detection of slowly growing errors. Although they stated the NSS method is credible, they stated that the assumption of position error being a Gaussian variable is not resolved fully and there may not be any advantage in choosing it as a one or two dimensional and that the calculation of the test statistics using a rank deficient matrix may create numerical instabilities. For these reasons they chose the MSS as representative of solution separation methods. In their results it was found that the AIME is able to detect a slowly growing error of 0.1 m/s sooner than the MSS method. It was shown that the rate detection algorithm can significantly reduce the detection time of slowly growing errors.

For an APV approach as considered in this thesis, the question must be asked whether or not it is necessary to detect an error of 0.1 m/s or less on the approach itself. An error of this magnitude or smaller may not grow enough in the two minute approach for the position error to exceed the threshold before the approach is complete. The error could however start to grow some time prior to the approach and only breach the position error on the approach itself. However as stated in [54] very slowly growing errors are unlikely to be missed by the GPS control segment.

Summary

A number of fault detection methods have been presented for ABAS. The extrapolation method can achieve lower HPL than the solution separation method. But unlike the solution separation method, the method cannot be verified analytically but requires Monte Carlo simulation. The normalized solution separation method which is a normalized version of the solution separation method has faster processing time than other methods.

2.8 Conclusion

The main points from the literature review are summarised here, showing the areas where further research can be made and motivating the topic of this thesis.

APV approaches can bring an economic benefit as well as increased safety for general aviation (Section 2.2). APV approaches are achievable with GNSS. GPS is the most proven satellite navigation system in aviation and currently the only GNSS fully operational. For these reasons GPS is the only constellation which this research will consider (Section 2.3).

There are various GPS error sources and anomalies which make integrity important for safety of life applications like aviation. The ionospheric error can be the most problematic error in GPS but may be cancelled through the use of dual frequency (L1/L5) techniques. The L5 signal will be a second signal able to be used in civilian aviation and is expected to be fully available in 2018 (Section 2.3).

APV requirements are more stringent than NPA, requiring integrity in both horizontal and vertical directions. The APV-I requirements were presented to show the level of performance which GPS equipment must meet for an approach (Section 2.4).

The main purpose of integrity monitoring is to prevent hazardously misleading information being reported to the pilot by detecting and excluding (if possible) any fault. However the existing satellite constellation may not support integrity monitoring for APV without augmentation (Section 2.5).

Four types of International Civilian Aviation Organisation (ICAO) approved augmentation system standards for GNSS are SBAS, GBAS, GRAS and ABAS. The limitations of SBAS for small countries such as Australia are excessive costs and sovereignty concerns. The limitations of SBAS alternatives such as GRAS are the problem of potential outages or siting constraints. An advantage of ABAS is that it is onboard the aircraft and does not require links to ground stations or satellites (Section 2.6).

With ABAS, GPS is integrated with other sensors onboard the aircraft and may provide improved accuracy and integrity performance because of the additional information available to the system. The advantage of Aircraft Based Augmentation Systems (ABAS) is that all information is combined at the aircraft rather than externally to the aircraft in ground processing stations or in another country (Section 2.7). ABAS could operate independently of other augmentation systems or seamlessly with them for backup integrity monitoring as an additional level of safety.

However, typical ABAS designs assume a high grade inertial sensor which would be unsuitable for use in general aviation because of their high cost. For this reason this research will consider low-quality MEMS inertial sensors. As revealed in the literature review, there is little research about the use of low-cost IMU in aviation. The only research to be found in this area was a "piggy-back" architecture which used the IMU to make virtual pseudorange measurements (Section 2.7.1). Further investigation could be made into the use of low-cost IMU in ABAS, particularly for APV approaches. Also, the literature showed that tightly coupled GPS/INS systems have the highest potential for detecting slowly growing errors.

Aircraft dynamic models have been studied for use in navigation systems before. Applications previously considered included aiding or replacing inertial sensors during GPS outages or backup attitude determination. However there was no literature found exploring its use in ABAS (Section 2.7.2).

Different filtering methods were reviewed. The most commonly used method for ABAS is the Kalman Filter. The UKF, SPKF and Particle Filters are thought to be

unnecessary for ABAS. For a low cost MEMS IMU and ADM in ABAS, the EKF may be the most suitable (Section 2.7.3).

A number of fault detection methods for ABAS were presented (Section 2.7.4). The extrapolation method can achieve lower HPL than the solution separation method. But unlike the solution separation method, the method cannot be verified analytically but requires Monte Carlo simulation. A third algorithm which is a normalized version of the solution separation method called the Normalized Solution Separation method was reviewed and may have faster processing time than the other methods.

As has been shown from the literature review, further research can be made in researching the use of low cost MEMS IMU or aircraft dynamics in ABAS designs for general aviation. An ABAS design concept incorporating MEMS IMU and aircraft dynamics is discussed in the next chapter.

3 General Aviation GPS Integrity System (GAGIS) Concept

3.1 Introduction

This chapter presents and discusses the ABAS architecture concept named the General Aviation GPS Integrity System (GAGIS) for convenience. Section 3.2 describes the GAGIS architecture in general terms where the subsequent sections describe the different components of GAGIS. Section 3.3 describes the GPS component of GAGIS. Section 3.4 describes the IMU component of GAGIS and Section 3.4.1 describes the IMU errors. Section 3.5 describes the ADM, Section 3.5.1 describes the aerodynamic model and Section 3.5.2 describes the ADM errors.

Section 3.6 describes the generic Extended Kalman Filter equations used in GAGIS. Section 3.6.1 describes the role of the process model in GAGIS and how it influences the integrity performance. Section 3.6.2 describes the filter consistency and tuning of GAGIS.

Section 3.7 describes the Normalized Solution Separation algorithm which is used for fault detection. The calculation of the probability of missed detection for APV-I is given in Section 3.7.1 and likewise the calculation of the probability of false detection is given in Section 3.7.2.

The calculation of the accuracy requirements is given in Section 3.7.3. Calculation of test statistics and thresholds is given in Section 3.7.4. The calculation of protection levels is given in Section 3.7.5. A discussion on the use of the NSS method in GAGIS is given in Section 3.7.6.

There are different configurations possible with GAGIS. A GPS-IMU EKF is described in Section 3.8 and a GPS-ADM EKF described in Section 3.9. Section 3.10 describes the GPS-ADM EKF with wind estimation architecture. Section 3.10.1 describes estimating the wind in the EKF with no additional sensors. Alternatively, 3.10.2 describes estimating the wind with the addition of air data sensors to the GPS-ADM EKF architecture. Section 3.11 describes a GPS-IMU-ADM EKF architecture

where the IMU and ADM information is fused together. Section 3.12 describes the stand-alone GPS architecture with the Normalized Solution Separation method, which is used for comparison with GAGIS.

3.2 General Aviation GPS Integrity System (GAGIS) Architecture Concept

For an ABAS design for general aviation incorporating MEMS IMU and an ADM, the literature provided some insight to the design. This was to fuse GPS with a low cost IMU and ADM in a tightly coupled, rather than a loosely coupled configuration (Section 2.7.1). Frequent GPS updates would be required to correct the IMU rather than rely upon inertial coasting and the Normalized Solution Separation (NSS) method was chosen for the fault detection method (Section 2.7.4).

A new ABAS architecture concept which uses these features is presented in Figure 4 named GAGIS. It consists of a GPS, IMU, ADM, a bank of EKFs and NSS Fault Detection (FD) scheme. As stated in Section 2.7.1, typical approaches for ABAS use a high-grade (but expensive) IMU in an open-loop configuration with Kalman filter where the IMU provides an accurate reference trajectory and frequent GPS updates are not necessary. Because these systems are too expensive for most general aviation aircraft, a similar yet lower cost solution could be provided by using a lower cost (yet less accurate) MEMS IMU. Besides the use of a MEMS IMU, the inclusion of an Aircraft Dynamic Model (ADM) is investigated in this thesis and may contribute to navigation system robustness as an IMU supplement or replacement. However, as indicated on Figure 4, measured control inputs are required to the ADM. In this thesis they are assumed to be measured control surface deflections (elevator, aileron, rudder) and throttle setting.

The inclusion of both the IMU and ADM allows a number of possibilities. Fault detection may be performed by

a) Combined GPS and IMU, where a GPS-IMU EKF architecture will be presented in Section 3.8,
b) Combined GPS and ADM, where a GPS-ADM EKF architecture will be presented in Section 3.9,
c) Combined GPS, IMU and ADM, where a GPS-IMU-ADM EKF architecture will be presented in Section 3.11.

The integrity monitoring performance of each of these configurations will be evaluated by computer simulation in Chapter 4.

The IMU and ADM information is blended in the Extended Kalman Filter (EKF) with the GPS measurements. Due to the poor accuracy of the MEMS IMU and ADM considered in this research, the MEMS IMU or ADM will not be able to “coast” for very long before the integrity requirements are exceeded (Section 2.7.1). Therefore a closed-loop (feedback) configuration and frequent (1 Hz) GPS update rate is used. In this way rather than use a "piggy back" architecture as in [15] (Section 2.7.1), the use of the EKF and feedback retains the IMU as a provider of a dynamic reference trajectory in the filters, making predictions of the aircraft position at a high rate between GPS updates.

As indicated on Figure 4 there are one full and *N* Sub EKFs. This because the Normalized Solution Separation (NSS) method relies on one filter using all *N* satellites in view termed the “full-filter” and *N* “sub-filters” which use *N*-1 satellites. Each sub-filter has a different pseudorange measurement omitted from its solution than the others, allowing for detection of one satellite fault at a time. The solutions from the full-filter and sub-filters are used by the FD algorithm to determine whether there is a position fault or not. If no fault is detected, the corrections are applied to the IMU and GPS state estimates as shown by the “corrections” block in Figure 4. Each filter is corrected with corrections from its own filter, so there are a total of *N+1* filter corrections fed-back to the *N+1* filters in the system. This means that if one GPS satellite is faulty, there will be one sub-filter which is not corrupted by this faulty satellite measurement.

If a fault is detected normally a fault exclusion process would run, however this thesis does not consider fault exclusion but focuses on the fault detection. The approach taken by [11] was to treat the fault exclusion as a separate process. Alternatively instead of excluding the failed measurement the MOPS [28] also allow compensation of the failures using models of satellite failure, as long as the HPL continues to bound the horizontal position error. The consideration and design of any fault exclusion algorithm for GAGIS is left for further work.

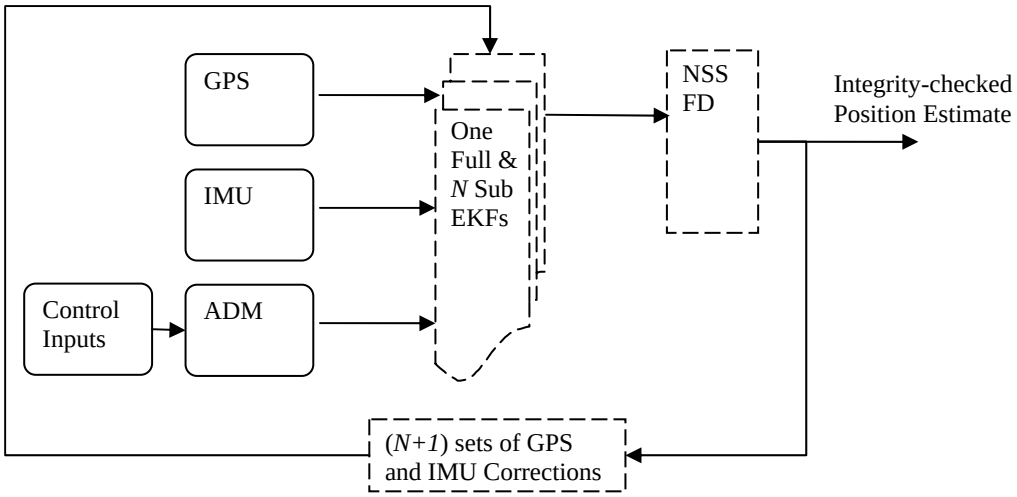

Figure 4 ***GAGIS Architecture Concept***

Whilst fault detection can be accomplished by GPS alone with sufficient satellites in view it is difficult to meet APV-I requirements with the current GPS constellation as explained in Section 2.5.3. For this reason, there are benefits in using Kalman filtering to fuse the IMU or ADM information with GPS to help achieve APV-I requirements. This filters the GPS solution, enables greater integrity monitoring performance through better state estimates and the additional measurements provided by the IMU or ADM means that the fault detection performance is less dependant upon satellite geometry than without them. This may be important for times when good satellite geometry is not assured. The following sections will describe the components of GAGIS.

3.3 Global Positioning System (GPS) Description

The GPS measures the absolute position and velocity of the vehicle from pseudorange and pseudorange rate measurements. Four or more pseudorange measurements are required to estimate the position of the vehicle. A model for the GPS pseudorange measurement (m) is [48, 67] :

$$\tilde{\rho} = \rho + c(dt - dT) + \varepsilon_{eph} + d_{ion} + d_{trop} + \varepsilon_{mp} + v_{rcvr} + \Delta PR_{\dot{\Omega}} \quad (1)$$

Where ρ is the geometric range between satellite and user, c is the speed of light, dt is the receiver clock bias, dT is the satellite clock bias, ε_{eph} is ephemeris error, d_{ion} is ionospheric delay, d_{trop} is tropospheric delay, ε_{mp} is multipath, v_{rcvr} is C/A code measurement noise, $\Delta PR_{\dot{\Omega}}$ is relativistic error due to earth rotation. Each of these will contribute to the GPS receiver position error, however some of them can be corrected for or neglected. The pseudorange and pseudorange-rate models used in GAGIS are

$$\tilde{\rho} = \rho + c(dt - dT) + d_{ion} + d_{trop} + \Delta PR_{\dot{\Omega}} + v_{rcvr} \quad (2)$$

$$\tilde{\dot{\rho}} = \dot{\rho} + c(d\dot{t} - d\dot{T}) + v_{rcvr} \quad (3)$$

Receiver clock biases dt and $d\dot{t}$ are estimated in the EKFs and the satellite clock biases dT and $d\dot{T}$ can be calculated based upon correction parameters provided in the broadcast ephemeris. Earth rotation error $\Delta PR_{\dot{\Omega}}$ can be corrected by a simple earth rotation correction term. v_{rcvr} is modeled in the Kalman filter by white Gaussian noise. Because atmospheric errors are typically the dominant error on the GPS range measurements, ionospheric delay d_{ion} is assumed to be calculated by using dual frequency GPS with L1 and L5 signals and the tropospheric delay d_{trop} is assumed to be calculated by using a tropospheric delay model such as given in [28]. The remaining errors will play a part in influencing the integrity monitoring performance of GAGIS, which will be discussed further in Section 3.6.1. The following section will describe the MEMS IMU component of GAGIS.

3.4 MEMS Inertial Measurement Unit (IMU) Description

Micro-machined electromechanical systems (MEMS) accelerometers and angular rate sensors (gyroscopes) are manufactured from silicon chips. The advantages of MEMS sensors are their ease of manufacture, small size, low weight, negligible power consumption, short start-up time, ruggedness construction, low maintenance and reliability [51]. These properties make MEMS IMU sensors an attractive choice for use in ABAS for general aviation. One example is the ADXRS150 angular rate sensor shown in Figure 5.

Figure 5 ***ADXRS150 Angular Rate Sensors.***

As shown in Figure 6 the strap-down MEMS Inertial Measurement Unit (IMU) considered in GAGIS consists of three orthogonally-mounted MEMS accelerometers and three orthogonally-mounted MEMS gyroscopes which measure the accelerations and angular rates of the vehicle in three dimensions.

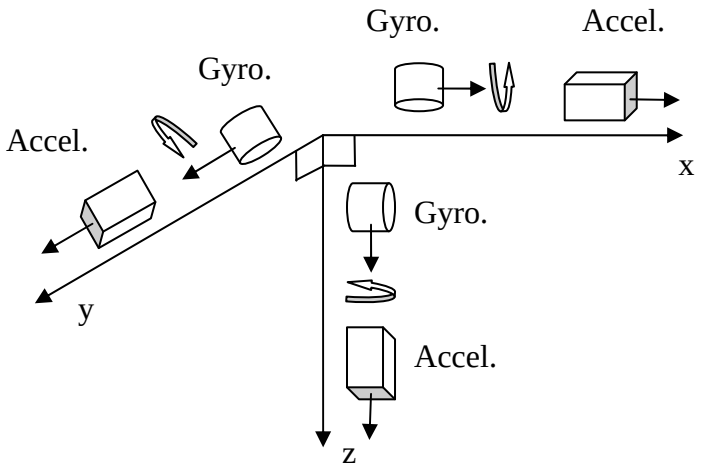

Figure 6 ***MEMS IMU Configuration.***

The raw acceleration and angular rate measurements are in the body frame and need mechanizing to estimate the attitude, velocity and position of the vehicle. The frame chosen for the mechanization is the North, East, Down (NED) local frame. Quaternions are used for the attitude representation. For the attitude dynamics, the quaternion propagation in discrete time *k* is [68]

$$\overline{q}_k = e^{-0.5\tilde{\Omega}_k \Delta T}\overline{q}_{k-1} \tag{4}$$

Where

$$\overline{q}_k = \begin{bmatrix} q_0 & q_1 & q_2 & q_3 \end{bmatrix} \tag{5}$$

Is a vector of four quaternion variables and

$$\tilde{\Omega}_k = \begin{bmatrix} 0 & p & q & r \\ -p & 0 & -r & q \\ -q & r & 0 & -p \\ -r & -q & p & 0 \end{bmatrix} \tag{6}$$

where *p, q, r* are the gyroscope measurements of angular rate and ΔT is the sample time.

For the linear dynamics [51]

$$\dot{v}^n = f^n - (2\omega_{ie}^n + \omega_{en}^n) \times v^n + g_l^n \tag{7}$$

where v^n is the velocity vector.

f^n is the specific force vector which is the body-axis accelerometer measurements transformed into the navigation frame,

$$f^n = T_b^n f^b . \tag{8}$$

Where T_b^n is the body to navigation frame transformation matrix.
ω_{ie}^n is the inertial angular velocity of the earth with respect to the earth fixed frame.
ω_{en}^n is the transport rate, the turn rate (angular velocity) of the navigation frame with respect to the earth-fixed frame.
g_l^n is the local gravity vector.

(7) is integrated to yield the velocity in the navigation frame.

To calculate the position of the vehicle, the transformation of the velocity in the local frame to the geodetic frame is

$$\dot{l} = \frac{v_n}{R_n + h} \tag{9}$$

$$\dot{\Lambda} = \frac{v_e}{(R_e + h)\cos(l)} \tag{10}$$

$$\dot{h} = -v_d . \tag{11}$$

Where l is latitude, Λ is longitude, h is height, R_n is the Meridian radius of curvature, R_e is the normal radius of curvature, v_n, v_e, v_d are North, East and Down velocities. (9-11) is integrated to yield latitude longitude and height in the Geodetic frame (WGS-84).

A description of the MEMS IMU considered for use in GAGIS has been provided. The following section will discuss the errors on the MEMS IMU measurements.

3.4.1 MEMS IMU Errors

Inertial sensor error characterization is well known. This section will only provide a summary of the most common errors. The total error on the IMU measurements of acceleration and angular rate will consist of [51, 69]:

- Axis misalignment
    - The axes of the sensors are not mounted perfectly orthogonally with each other. Signals couple onto sensors on different axes resulting in errors. This can be due to the sensor die not being perfectly aligned on the chip and also misalignment of the chip on the circuit board.

- Temperature-dependent biases
    - These are biases which vary with temperature and look like a time-varying additive noise source, driven by external or internal temperature variations.
- Alignment errors
    - This is the error in determination of initial attitude.
- Scale-factor errors
    - These are errors relating to the change in output signal to the change in the input signal which is being measured.
- Gravity errors
    - The errors between the true gravity and the assumed gravity model.
- Sensor noise
    - Random noise (which can be effectively modeled as white noise) is due to the semiconductors intrinsic noise, power supply noise and quantization error.

Deterministic errors such as axis misalignment and temperature dependent biases may be corrected by applying pre-determined models such as from manufacturer's datasheets for example, but random error will still exist which needs to be accounted for. Random biases are accounted for in the Extended Kalman Filters by modelling them as a first-order Gauss Markov process [70] (see B. Definitions).

Low quality MEMS sensors can be very noisy compared to navigation grade ones as explained in Section 2.7.1. Because of this these devices cannot maintain the required accuracy in stand-alone operation (inertial coast) for much longer than tens of seconds. GPS aiding via frequent GPS updates are necessary to compensate. The MEMS errors will play a part in the achievable integrity monitoring performance of GAGIS and this will be discussed in Section 3.6.1. MEMS sensor errors can also vary widely from switch on to switch on and also vary from sensor to sensor, i.e. two different sensors of the same type may have different noise characteristics. Manufacturers often only provide a typical performance value for these devices, but cannot guarantee that its performance will not be worse than specified. The reliability of MEMS sensors may have implications for the practical use of MEMS IMU in

ABAS. However it is not the aim of this thesis to research this as it is an active area of research such as [71], [72]. The following section will describe the Aircraft Dynamic Model (ADM) component of GAGIS.

3.5 Aircraft Dynamic Model (ADM) Description

The Aircraft Dynamic Model (ADM) chosen for GAGIS consists of a set of coupled, nonlinear ordinary differential equations by which the aerodynamic forces and moments acting on the aircraft can be estimated. These equations are a function of nondimensional aerodynamic coefficients, measured control surface deflections and aircraft states. From this aerodynamic knowledge, the accelerations and angular rates of the vehicle are derived. The references [73-75] were used for development of the ADM in this thesis. Fig. 1 shows the body axes of the aircraft, x_b, y_b, z_b with origin at the centre of gravity. p, q, r are the angular rates, u, v, w are the body velocities, X, Y, Z are the aerodynamic forces and L, M, N are the aerodynamic moments as per standard nomenclature [76].

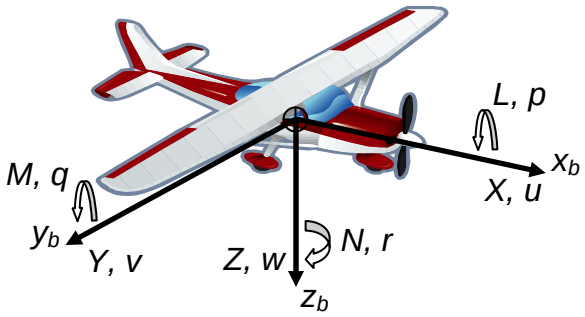

Figure 7 ***Aircraft body axes.***

Aerodynamic forces and moments are due to the relative motion of the aircraft with respect to the air and depend on the orientation of the aircraft with respect to the airflow. Two angles with respect to the relative wind are needed to specify the aerodynamic forces and moments. Referring to Figure 8, the angle of attack is the angle between the x-axis in the body axes, x_b (assumed aligned with respect to the fuselage reference line) [75] and the stability x-axis, x_s. The angle of sideslip is the angle between the fuselage reference line and x-axis in wind axes, x_w which is aligned with the relative wind.

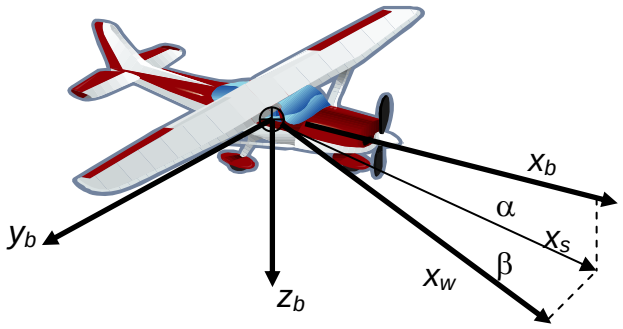

Figure 8 ***Aircraft wind axes.***

The angular accelerations in rad/s^2 are

$$\dot{p} = (c_1 r + c_2 p)q + c_3 L_{cg} + c_4 N_{cg} \tag{12}$$

$$\dot{q} = c_5 pr - c_6 (p^2 - r^2) + c_7 M_{cg} \tag{13}$$

$$\dot{r} = (c_8 p - c_2 r)q + c_4 L_{cg} + c_9 N_{cg} \tag{14}$$

where c_1 to c_9 are inertial coefficients as given in [9].

The body-axis accelerations in m/s^2 are

$$\dot{u} = rv - qw - g\sin(\theta) + X_{cg} / m \tag{15}$$

$$\dot{v} = pw - ru + g\sin(\phi)\cos(\theta) + Y_{cg} / m \tag{16}$$

$$\dot{w} = qu - pv + g\cos(\phi)\cos(\theta) + Z_{cg} / m \tag{17}$$

where ϕ, θ are roll and pitch, g is gravity and m is the mass of the aircraft.

The assumptions associated with this model are [74, 75]:

- The aircraft is a rigid body (there are no wing bending effects) with fixed mass distribution and constant mass (dynamics due to fuel slosh, structural deformation is assumed negligible).
- The air is at rest relative to the earth (no wind, gusts, turbulence etc).
- Earth's surface is flat, having negligible curvature (because the aircraft flies close to the earth surface).
- Gravity is uniform and the aircraft centre of gravity and centre of mass are coincidental (no gravity moment acts on the aircraft), gravity does not change with altitude.
- The aircraft is symmetrical about the x_b-z_b plane. There is no cross-coupling between longitudinal and lateral motion.
- The earth is fixed in inertial space (i.e. earth axes are in an inertial

reference frame).

Using the angular rates, obtained from integrating (12-14) and body-axis accelerations obtained from (15-17), the equations (9-11) are used to derive attitude, velocity and position. The estimation of the aerodynamic forces (*X*, *Y*, *Z*) and moments (*L*, *M*, *N*) is discussed next.

A description of the ADM has been given. The following section will describe the aerodynamic model component of the ADM.

3.5.1 Aerodynamic Model Description

Mathematical expressions are needed to relate the aerodynamics of the aircraft to the forces and moments. This is the purpose of the aerodynamic model. A linear model is built up by a linear Taylor series expansion of the forces and moments about a reference condition. A flight condition which is not steady can be mathematically thought of as having been perturbed away from some steady state [74, 77]. The equilibrium condition, or steady state (otherwise known as the "trim"), is specified by a set of reference parameters. A reference flight condition for steady descending flight is specified by reference angle of attack α_0, Mach number M_0, airspeed V_0, altitude h_0, mass m_0, inertia properties I_0 and path angle γ_0. It is also assumed that $\beta_0 = v_0 = p_0 = q_0 = r_0 = 0$.

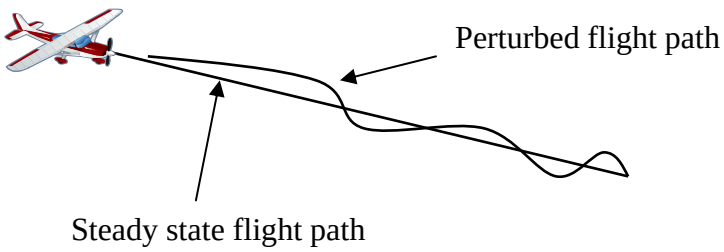

Figure 9 ***Steady State Descending Flight Path with Perturbation.***

The following equations are the linear aerodynamic model for quasi-steady flow. Each variable comprises of a steady value (e.g. α_0) associated with the steady reference condition plus a perturbation (e.g. $\Delta\alpha$),

$$\Delta\alpha = \alpha - \alpha_0 \tag{18}$$

where $\Delta\alpha$ is the perturbation of α relative to its trim value α_0. The components of the aerodynamic forces and moments are typically expressed in terms of non-dimensional coefficients for convenience as the known dependence on air speed and air density is removed [74]. The equations from the aerodyanmic model are given (19-24) where the left-hand side terms C_L etc are the nondimensional coefficients and the right hand side terms are the nondimensional stability and control derivatives. For example C_{L_α} is the contribution of angle of attack to lift. The values for the stability and control derivatives may be obtained from theoretical calculations or experimental methods such as wind-tunnel or flight testing. See B. for the notation in the following equations.

$$C_L = C_{L_0} + C_{L_\alpha}\Delta\alpha + (C_{L_q}\Delta q + C_{L_{\dot\alpha}}\Delta\dot\alpha)\frac{\bar c}{2V_a} + C_{L_M}\Delta M + C_{L_{\delta_e}}\Delta\delta_e + C_{L_{\delta_f}} \tag{19}$$

$$\begin{aligned} C_D &= C_{D_0} + (C_L - C_{L_{D0}})^2 k + C_{D_M}\Delta M + C_{D_{\delta_e}}\Delta\delta_e \\ &\quad + C_{D_{\delta_a}}\Delta\delta_a + C_{D_{\delta_r}}\Delta\delta_r + C_{D_{\delta f}} \end{aligned} \tag{20}$$

$$C_Y = C_{Y_\beta}\Delta\beta + (C_{Y_p}\Delta p + C_{Y_r}\Delta r)\frac{b}{2V_a} + C_{Y_{\delta_a}}\Delta\delta_a + C_{Y_{\delta_r}}\Delta\delta_r \tag{21}$$

$$C_l = C_{l_\beta}\Delta\beta + (C_{l_p}\Delta p + C_{l_r}\Delta r)\frac{b}{2V_a} + C_{l_{\delta_a}}\Delta\delta_a + C_{l_{\delta_r}}\Delta\delta_r \tag{22}$$

$$C_m = C_{m_0} + C_{m_\alpha}\Delta\alpha + (C_{m_q}\Delta q + C_{m_{\dot\alpha}}\Delta\dot\alpha)\frac{\bar c}{2V_a} + C_{m_M}\Delta M + C_{m_{\delta_e}}\Delta\delta_e + C_{m_{\delta_f}} \tag{23}$$

$$C_n = C_{n_\beta}\Delta\beta + (C_{n_p}\Delta p + C_{n_r}\Delta r)\frac{b}{2V_a} + C_{n_{\delta_a}}\Delta\delta_a + C_{n_{\delta_r}}\Delta\delta_r \tag{24}$$

The assumptions associated with this aerodynamic model are [74]:

- The atmosphere is constant density.
- The airflow is quasi-steady (i.e. the flow field adjusts instantaneously to change).
- Fluid properties change slowly.
- Froude number effects are small.
- The airplane mass and inertia are significantly larger than the surrounding air mass and inertia.

Only linear aerodynamic models were considered in this research for the following

reasons:

- Linear models are simple.
- A linear model is adequate for many practical purposes [74].
- For this application a general aviation aircraft on an APV approach is assumed to be flying with low dynamics. That is, flying at low speed, small angle of attack on a steady descent profile with no large or rapid excursions from the reference flight condition. This research does not consider spinning, stalling or high angle of attack flight.

[74] states that in many practical situations he linear model is a good representation of the aerodynamic forces and moments. However the linear model is valid provided the perturbations from the reference condition are small [74]. If there are large or rapid excursions from the reference condition, nonlinear terms may need to be added to the linear model or alternatively nonlinear models can be implemented in the form of a lookup-table [74].

After the nondimensional coefficients are calculated (19-24), they are dimensionalized into aerodynamic force and moment contributions in the wind axes as:

$$L = QSC_L \tag{25}$$

$$D = QSC_D \tag{26}$$

$$Y = QSC_Y \tag{27}$$

Where L is aerodynamic lift, D is aerodynamic drag, Y is aerodynamic sideforce, Q is dynamic pressure,

$$Q = 0.5\rho V^2 \tag{28}$$

where ρ is air density and V is airspeed.

$$L = QSbC_l \tag{29}$$

$$M = QS\bar{c}C_m \tag{30}$$

$$N = QSbC_n \tag{31}$$

Where L, M, N are the aerodynamic roll, pitch and yaw moments, S is wing area, b is wing span and $\bar{c}$ is mean aerodynamic chord.

(25-27) are transformed into aerodynamic force and moments in the body axes:

$$F_a = T_w^b \begin{bmatrix} -D & Y & -L \end{bmatrix}^T \tag{32}$$

T_w^b is the wind to body axes transformation matrix.

$$M_a = \begin{bmatrix} L & M & N \end{bmatrix}. \tag{33}$$

Accounting for the propulsion and the centre of gravity location [73],

$$F_{cg} = F_a + F_T \tag{34}$$

$$M_{cg} = M_a + M_T + (r_{aero} - r_{cg}) \times F_a + (r_T - r_{cg}) \times F_T \tag{35}$$

Where F_T and M_T is the force and moment due to the propulsion system, r_{aero} is the aerodynamic force and moment application point r_{cg} is the centre of gravity location and r_T is propulsion force and moment application point in the body axes. The aerodynamic model component of the ADM has been described. The following section will discuss the errors of the ADM.

3.5.2 ADM Errors

The main errors in the ADM acceleration and angular rate estimates (12-17) will consist of:

- Aircraft modelling errors including aerodynamic parameter uncertainty, centre of gravity centre of mass error and moment of inertia error.
- Measurement errors including measuring control surface deflections (pilot inputs).
- State errors which will add uncertainty in the reference condition upon which linearization is performed in (19-24).
- Uncertainties in the surrounding environment such as wind, temperature, dynamic pressure and gravity error.
- Alignment error (error in determination of initial attitude).

Whilst all the errors considered above contribute error to the acceleration and rotation rate estimates from the ADM, the most significant ones are the aerodynamic coefficient uncertainty and wind (Section 2.7.2). The net effect of these errors will affect the fault detection algorithm's ability to meet APV requirements, as process model noise will need to be increased to accommodate them. If the errors are

significant enough they may result in a false detection on the GPS fault detection test statistics due to filter divergence or large ADM error. The ADM errors will play a part in the achievable integrity monitoring performance of GAGIS and this will be discussed in Section 3.6.1. The most significant errors which are parameter uncertainty and wind are discussed next.

Aerodynamic Parameter Uncertainty

Obtaining the aerodynamic parameters (19-24) and equations is a system identification problem. As such, the accuracy with which these parameters are estimated will depend upon the system identification procedure used. For example, the parameters may initially be estimated based on theoretical calculations. These parameters may be further refined by wind tunnel testing or flight tests for example if greater accuracy is required. Once the parameters are known, they may be modeled as constants or slowly varying parameters with time. The more accurate these parameters are known the less uncertainty there will be in the ADM, contributing to greater GPS fault detection performance.It is stated in [12] that aerodynamic parameters can vary up to +/- 10% of their true value. Parameter identification results given in [74] show that parameters may be determined with a reasonable accuracy.

Wind Turbulence and Shear

Turbulence (random gusts) is the main effect of wind on an aircraft. The wind is non-uniform, that is the velocity changes in space and time and can be thought of as having a mean value with variations from it. Near the ground there are rapid changes in turbulence with altitude. A velocity gradient in the mean wind is called wind shear, or wind gradient [78]. They may extend to hundreds of feet above the earth's surface, depending upon the underlying terrain. Because of wind shear an aircraft on an approach may encounter severe variations in wind magnitude and direction in the horizontal and vertical directions. The effect of unknown wind is seen as an error (uncertainty) on the estimates of angular rates and body axis velocities. The effect it will have on the aircraft will depend upon the aircraft type, for example a high aspect ratio wind will perform differently to a low aspect ratio wing [77]. In severe cases turbulence may induce a stall on the aircraft, as it continuously induces an angle of attack on the airplane.

Because wind is both uncontrollable and unobservable, it may be the largest source of uncertainty in the ADM. If wind is uniform and steady, standard aerodynamic equations may be used. But because of the assumption that the linear aerodynamic model is based on small disturbances from a reference condition, the presence of severe turbulence and shear may violate this assumption. In this case a nonlinear aerodynamic model may be required for the ADM which takes the turbulence and shear effects into account. Wind may be estimated as an unknown in the Kalman Filter as in [12, 14], or a model of low-altitude turbulence may be used [78] or it may be estimated from measurements from onboard sensors. To include the effect of wind on fault detection performance, wind with Von Karman wind turbulence model will be considered in the simulations in Chapter 4. Also, a GPS-ADM EKF architecture with wind estimates will be presented in Section 3.10.

Mass, Inertia and Centre of Gravity Uncertainty

Error in the knowledge of the centre of gravity location, mass and inertia contributes error on the ADM acceleration and angular rate estimates. However these can typically be known or measured to a reasonable accuracy.

Flaps and Landing Gear

The purpose of deploying flaps during an approach is to decrease the angle of descent without increasing airspeed. When flaps and or landing gear and deployed for landing, it will have an effect on aircraft dynamics which should be accounted for in the filters. The effect when they are deployed will depend upon the aircraft type but this is typically seen as an increase in lift and drag and a downward pitching moment which is anticipated and corrected for by the pilot. If it is assumed that flaps and landing gear are deployed prior to the APV approach and the configuration is not changed during the APV approach, this is no concern. However if they are deployed during the 2 min APV segment they will need to be accounted for in the ADM, otherwise the unexpected dynamics, if severe enough, may cause a false alarm in the GPS integrity monitoring method.

Control Input Error

If control surface deflections are measured using low-noise potentiometers the expected measurement noise on these will be small and contribute minimal error to

the ADM estimates. The effect of errors in a thrust or propulsion system model will also contribute error to the ADM.

Environmental Errors

The ADM needs estimates of gravity, temperature, air density and viscosity. Errors in knowledge of these will contribute some error to the ADM estimates. These parameters may be calculated from standard atmosphere and gravity models, or could be measured by additional sensors on the aircraft. In this research only standard atmosphere models are assumed.

The errors on the ADM estimates have been presented. The following section describes the Extended Kalman Filter (EKF) component of GAGIS.

3.6 Extended Kalman Filter (EKF) Description

In GAGIS the processes (IMU and ADM equations given in sections 3.4 and 3.5) and measurements (GPS pseudoranges and pseudo-range rates) are nonlinear. The Extended Kalman Filter (EKF) is the most common application of Kalman filtering to nonlinear systems. The following description of the EKF is based upon [24, 48, 70].

A continuous-time nonlinear process is represented by the equation

$$\dot{x}(t) = f(x(t),t) + v(t) \tag{36}$$

Where *x(t)* is the state and *v(t)* is process noise which is assumed Gaussian, white, uncorrelated. Nonlinear measurements (such as pseudoranges) can be represented as a function of the state *x(t)* by:

$$y(t) = h(x(t),t) + w(t) \tag{37}$$

where *y(t)* is the measurements and *w(t)* is measurement noise assumed Gaussian, white, uncorrelated.

The dynamics matrix (Jacobian) is

$$F(t) = \frac{\partial f(x(t),t)}{\partial t} \tag{38}$$

and input matrix is,

$$G(t) = \frac{\partial f(v(t),t)}{\partial t} \quad . \tag{39}$$

The measurements matrix is

$$H(t) = \frac{\partial h(x(t),t)}{\partial t} \quad . \tag{40}$$

For implementation in software the discrete-time equations are more relevant. The nonlinear process and measurement equations with discrete time *k* are

$$x_{k+1} = f(x_{k,}k) + v_k \tag{41}$$

$$z_k = h(x_{k,}k) + w_k \tag{42}$$

A prediction of the future state is made by the process model

$$\bar{x}_k = f(x_{k-1}, k-1) \tag{43}$$

With associated state error covariance

$$P_k^- = \Phi_{k-1} P_{k-1} \Phi_{k-1}^T + Q_{k-1} \quad (44)$$

Where Φ_{k-1} is the state transition matrix from *k-1* to *k*.

When *F(t)* is known, Φ_{k-1} can be determined by

$$\Phi = e^{F\Delta t} \quad (45)$$

Q is a process noise covariance matrix where,

$$E(v \cdot v^T) \sim N(0, Q). \quad (46)$$

The measurements matrix is

$$H_k = \frac{\partial h(x_k^-, k)}{\partial t} \quad (47)$$

The weighting matrix between process and measurements is

$$K_k = P_k^- H_k^T (H_k P_k^- H_k^T + R_k)^{-1} \quad (48)$$

R is a measurement noise covariance matrix where,

$$E(w \cdot w^T) \sim N(0, R). \quad (49)$$

The state is updated by the measurements as:

$$x_k = x_k^- + K_k (z_k - h(x_k^-, k)). \quad (50)$$

The state covariance is updated as:

$$P_k = (I - K_k H_k) P_k^- (I - K_k H_k)^T + K_k R_k K_k^T. \quad (51)$$

Whilst the EKF may perform better than the KF for nonlinear applications [24, 48, 70], the EKF is an approximate filter. It can result in biased filter estimates because it assumes the error is linear on the scale of the error, when it may not be [79]. With the EKF the estimation error is *approximately* zero mean and strictly speaking the covariance matrix of the EKF is a pseudo-covariance matrix, that is, it is really a mean-squared error (MSE) matrix because the state estimate is not the exact conditional mean [79]. However as mentioned in Section 2.7.3 GPS-IMU fusion is not nonlinear enough to warrant considering a nonlinear filtering algorithm like the UKF.

The EKF has been explained in generic terms. The following section discusses the role of the IMU and ADM process models in GAGIS and how they will influence the integrity monitoring performance.

3.6.1 Role of the IMU and ADM Process Models in GAGIS

In this section, firstly, the role of the process model in the EKF will be discussed in general terms and then the IMU and ADM process models will be discussed. Julier [79] studied the role of the process model in Kalman filtering. His work will be referred to here but discussed in the context of GAGIS integrity monitoring performance.

A process model is a mathematical description of the physical process of the system and how the system states develop over time. It provides a prediction of the states of the vehicle based on past measurements. Julier states, “Process models perform an important role by facilitating temporal fusion of data. States can be estimated with greater accuracy than the sensors can measure them” [79]. There is a trade-off between the measurements and the process model. As the model becomes more accurate, the same performance can be achieved with less accurate measurements.

In GAGIS there are two process models, one for the IMU and one for the ADM. In the case of a GPS-IMU EKF, the process model is the IMU mechanization equations (2)-(9). Although the IMU itself is a sensor, it functions as the provider of angular rate and acceleration measurements to the mechanization equations (4)-(7) which themselves are an approximation to the dynamics of the true system. The process model in a GPS-ADM EKF is the ADM equations as given in Section 3.5.

The process models predict the state of the vehicle at a high rate (100 Hz) after which the GPS measurements are used to update their prediction at a slower rate (1 Hz). In between GPS updates, the position state is unobservable and its covariance increases rapidly, because of the poor stand-alone accuracy of the IMU and ADM. The covariance is reduced when new GPS measurements arrive. After the measurement update the covariance (51) may be lower than the covariance estimated by a standard GPS solution, that is, without the process model. This can result in lower protection levels which contributes to greater availability of the fault detection function. This may be useful particularly in times of poor satellite geometry when GPS alone cannot meet the APV requirements.

The process model should maximize the information in the prediction [79]. However this does not mean that the filter should use the same state space and process model as the actual physical system. This is because a complex physical system such as an aircraft requires many states to describe it and would not be practical to implement. Furthermore, a very detailed model may only work over a narrow range of operating conditions. For these reasons the model should be the least complex process model which is capable of describing the most significant features of the true system [79].

There is also the "bias/variance tradeoff problem" [79]. As a model becomes more complex, it describes the true system better and the errors become smaller. However a more complex model includes more parameters and states which have to be estimated. The result is that the finite amount of measurement data has to be spread more thinly between the states and the result is that the variance on the estimates of all the states increases.

These considerations were taken into account in the design of the ADM in this thesis. Firstly, as given in Section 3.5.1 a linear aerodynamic model is used rather than a more complex nonlinear model or lookup table. Whilst a nonlinear model is used for the ADM this is still only an approximation to the real physical system as given in Section 3.5 with the list of assumptions made in the model. There are possibly hundreds of other physical processes that could have been modeled. For example, distortion of wings/structures, dynamics due to the motion of onboard cargo, fuel or passengers and many others.

The process noise accounts for all the discrepancies between the process model and the actual behaviour of the vehicle [79]. The process noise can be classified into three types [79]:

- Control input disturbances including measurement noise and unexpected or unmodelled inputs.
- Noises which act on vehicle parameters where the actual values are unknown or changing with time.
- Stabilizing noises which are used to compensate for other unmodelled error sources. These often have no clear physical basis but are required to ensure

successful filter operation.

With the MEMS IMU, the process noise is largely dependent upon the type and accuracy of the sensors. The process noise can be estimated from the known characteristics of the sensor, such as from a manufacturer's datasheet or laboratory or flight tests. The process noise for the MEMS IMU will account mostly for sensor noise and may also include extra stabilizing noise to account for any uncertainty or variability in the IMU behavior. The ADM process noise will account for all including control input measurement noise, the uncertainty on the aircraft parameters and stabilizing noise to compensate for unmodelled error sources.

Both the IMU and the ADM process models are approximations to the true dynamics of the system and the source of the acceleration and angular rate information presented to each process is different. For example, the IMU measurements of acceleration and angular rate contain random noises and biases due to the internal workings of the MEMS sensors. In contrast, the ADM process has errors due to the assumptions made about the aircraft and the surrounding environment, imperfect knowledge of aerodynamic coefficients and noisy control surface measurements for example. It is the presence of this similar but different information that may contribute to the GAGIS integrity monitoring performance. This is investigated further in Section 3.11 where the IMU and ADM process model information is fused together.

It should be noted that the ADM is not expected or required to provide the most accurate source of dynamic information possible or be as accurate as the MEMS IMU. It is well known that the GPS carrier phase for example may provide a very good source of dynamic information [80], however GPS carrier phase is still susceptible to interference, jamming and carrier phase cycle slips [21]. A possible benefit of using the ADM as a provider of dynamic information to the system is that it contributes different information and is not as susceptible to the same sources of errors as the GPS and IMU. Therefore the ADM may contribute to the navigation system robustness.

It is important to note that assessing the performance of the ADM in GAGIS is not

a simple matter of comparing its stand-alone performance with an IMU. This is because the process model performance is not only dependant upon the process noise statistics *Q* but also upon the measurements noise statistics *R* [79]. Therefore its performance cannot be tested independently of the GPS. For this reason, the way to assess it is in the navigation system after it is tuned consistently. Filter tuning will be discussed next in Section 3.6.2.

3.6.2 Filter Consistency and Tuning

The following discussions on consistency and tuning is based upon [70, 79]. Filter consistency for a filter estimating the states of a dynamic system can be defined as the estimation errors being *consistent* with their theoretical statistical properties [70]. It is important for the EKF to undergo consistency testing because " Only if the bias is negligible with respect to the filter-calculated error variances and the mean square errors are consistent with these variances is the filter consistent and its results can be trusted" [70].

Consistency is necessary for the filter to be optimal. Any wrong covariances mean wrong gain leading to suboptimal filter performance. When a filter is not consistent (otherwise known as divergence), the filter's state estimation errors are too large and the filter thinks it estimates the state more accurately than it actually does.

The consistency criteria are [70]:

(1) State errors should be acceptable as zero mean with magnitude matching the state covariance as yielded by the filter,

(2) The innovations have the same property as (1),

(3) The innovations should be acceptable as white.

In other words the estimates:

a) Have zero mean (unbiased estimates),

b) Have a covariance matrix as calculated by the filter.

As to what estimation error is "acceptable", there are two requirements [70]:

(1) The condition that the estimates are unbiased (i.e. estimation error is zero-

mean)

$$E(\bar{x}_k - x_k) = E(\delta x_k) = 0 \tag{52}$$

Where $\bar{x}_k$ is the true state, x_k is the estimated state, δx_k is the state error.

(2) The 'covariance matching' requirement, that is, the actual MSE (Mean Square Error) equals the filter–calculated covariance.

$$E(\delta x_k \cdot \delta x_k{}^T) = P_k \tag{53}$$

Where the state error vector is

$$\delta x_k = \bar{x}_k - x_k \tag{54}$$

If there is a bias, it will increase the level of MSE. In terms of integrity monitoring performance, a large increase in covariance due to a suboptimal filter is not desirable because this may mean fault detection performance requirements are not met. There are upper limits (such as the protection levels and alert limits) which have to be met. Therefore the filters cannot be tuned too conservatively. On the other hand, they cannot be tuned too optimistically otherwise it may result in false alarms should the errors exceed the expected bounds and the protection levels may not bound the error.

There are formal tests for filter consistency to test the consistency criteria (1)-(3) above. The first criterion is the most important one but can only be tested in simulations. To test it, the Normalized (state) Estimation Error Squared (NEES) is

$$\varepsilon_k = \tilde{x}_k^T P_k^{-1} \tilde{x}_k \tag{55}$$

And is χ^2 distributed with *n* degrees of freedom, under the linear and Gaussian assumption. If the filter is consistent, due to the properties of the distribution

$$E\{\varepsilon_k\} = n \tag{56}$$

This test is based on the principle that the average of the squared norm of the estimation error has to be equal to the dimension of the corresponding vector since it is chi-square distributed.

To test the second criterion, which can be tested in real-time operation, the Normalized Innovation Squared (NIS) is

$$\varepsilon_{vk} = v_k^T V^{-1}{}_k v_k \tag{57}$$

Where v is the innovations vector, V is the innovations covariance and ε_{vk} is χ^2 distributed with n degrees of freedom. If the filter is consistent, due to the properties of the distribution

$$E\{\varepsilon_{vk}\} = n \tag{58}$$

For the third criterion, a whiteness test can be performed and the reader is referred to [70] for this.

Tuning is the procedure to match process noise variances to model the disturbances and ensure consistent filter operation. In practice the exact R and Q statistics are rarely known precisely [48]. This is particularly true for the ADM whose performance is affected by an unknown, nondeterministic and uncontrollable environment, of which a large component is the unknown wind conditions. Incorrect R or Q results in suboptimal gains and estimates. An inexact filter model will degrade the filter performance or even cause the filter to diverge. Filter divergence will cause a false alarm to be detected by the fault detection algorithm. For these reasons filter tuning is required and is accomplished by adjusting R and Q until the estimator is consistent, based upon the results of testing with real data. In practice, unmodelled disturbances such as unexpected aircraft dynamics are modeled by injecting additional process noise, termed ‘pseudo-noise’ or artificial noise in the filters. After filter tuning the state errors should lie within two standard deviation bounds 95% of the time. Employing a conservative tuning policy ensures that the filter is robust and consistent [79]. With GPS integrity monitoring however, the system cannot be tuned too conservatively otherwise a corresponding increase in protection levels may be no benefit in fusing the GPS with the IMU or ADM.

It has been seen that filter tuning is important to ensure consistent estimates. The EKF is not an optimal filter and therefore needs to be tuned appropriately. The filter tuning will impact integrity monitoring performance because as will be seen in Section 3.7 the fault detection algorithm uses the calculated covariances from the filter to determine whether a fault exists or not, and whether the integrity monitoring performance requirements can be met. The following section will describe the fault detection component of GAGIS.

3.7 Fault Detection Algorithm Description

A fault detection algorithm must meet the ICAO requirements shown in Table 2 [29].

Performance Requirement	***APV-I***
Horizontal Accuracy (95%)	**16 m**
Vertical Accuracy (95%)	**20 m**
Integrity	**1-2 × 10^{-7}/h/approach**
HAL	**40 m**
VAL	**50 m**
Time to Alert	**10 s**
Availability	**99 – 99.999%**

Table 2 ***APV-I Integrity Monitoring Requirements***

Two probabilities contribute to meeting the Integrity requirement in Table 2; P_{md}, which is the probability of missed detection and P_{fd}, which is the probability of false detection. P_{md} is the probability that a fault will not be detected given that it has occurred. P_{fd} is the probability that a fault has been detected given that it has not occurred.

For FD to be functioning nominally, the following conditions must be satisfied [4],

$$HNSE_k \le HPL_k \le HAL \tag{59}$$

$$VNSE_k \le VPL_k \le VAL \tag{60}$$

Where HNSE is Horizontal Navigation System Error (accuracy) and VNSE is Vertical Navigation System Error (accuracy). If the HPL exceeds the HAL, then the integrity monitoring function is deemed to be unavailable (in other words, it cannot be guaranteed that a fault can be detected within the P_{md}) and the navigation system cannot be used for navigation at that time. For this reason, it is desirable for the protection levels to be as small as possible to avoid exceeding the alert limits, yet large enough to exceed *HNSE*. Similarly for the vertical. The calculation of P_{md} is given next.

3.7.1 Calculation of the Probability of Missed Detection (P_{md})

From Table 2, the integrity risk requirement which is the probability of an undetected failure causing Hazardously Misleading Information (HMI) is $P_{HMI} = 2 \times 10^{-7}$/h/approach. The calculation of P_{md} is shown in Figure 10. From [81] the

probability of a GPS major service failure (defined as pseudorange error in excess of 150 metres) is 10^{-4}/hour, assuming three failure events per year and an average of 8 visible satellites. Therefore the probability of a GPS major service failure occuring during the approach, $P_{Failure}$, is 4.167×10^{-6} assuming the average time for an approach is 150 seconds [7].

For the fault free case H0, the approach by Lee [4] is followed where 1% of the integrity risk requirement is allocated to the fault-free case. This covers causes of HMI that are due to large random errors that can occur with small probability in the normal operation of the system, such as those due to noise and multipath, atmospheric error and inertial sensor errors [4], [28].

For APV the integrity risk is divided into a horizontal and vertical contribution. It was chosen to use a 5% contribution for the horizontal and 95% contribution for the vertical. Due to the nature of GPS, where vertical performance is typically worse than horizontal, greater allocation is attributed to the vertical to make it easier to achieve the requirement [4].

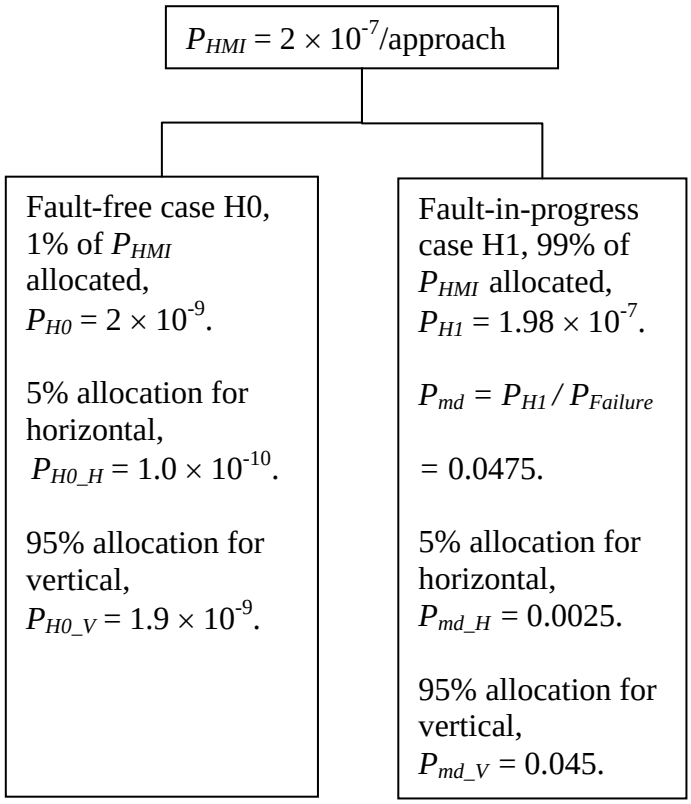

Figure 10 ***Fault Tree Showing P_{md} Derivation***

The calculation of P_{md} has been given, the following section will give the calculation of $P_{fd.}$

3.7.2 Calculation of the Probability of False Detection (P_{fd})

The requirement for the false detection probability is 1.6×10^{-5} per sample [28]. If the worst case scenario is assumed that there is only one independent sample per approach with an average approach time of 150 seconds, $P_{fa} = 1.06 \times 10^{-7}$.

According to [4], conversion of the false alert rate P_{fa} to P_{fd} requires knowledge of the fraction of time that exclusion of a false detection is possible, which in turn requires knowledge about the operating satellite constellation. A conservative approach is taken by assuming that $P_{fd} = P_{fa}$. So $P_{fd} = 1.06 \times 10^{-7}$.

The following section gives the calculation of the accuracy requirements.

3.7.3 Determination of Accuracy Requirements

For the accuracy requirement, that HNSE must be less than HPL and HAL, it is formulated as follows based upon [4]. The 95th percentile NSE bound for the horizontal and vertical directions is 1.96 d_{major} and 1.96 σ_V , where 1.96 is the 95th percentile in the Gaussian distribution, σ_V is the standard deviation of the vertical position, d_{major} is the standard deviation of the position error along the major axis of the assumed Gaussian bivariate error ellipse in the horizontal plane.

The accuracy limits for the horizontal and vertical directions can be determined as:

$$d_{major-max} = min(H_{acc} / 1.96, HAL / K_{H0}) \quad (61)$$

$$\sigma_{V-max} = min(V_{acc} / 1.96, VAL / K_{V0}) \quad (62)$$

Where H_{acc} and V_{acc} are the Horizontal and Vertical accuracy requirements from Table 2 and K_{H0} is function of 1-P_{H0_H} probability, K_{V0} is a function of 1-P_{H0_V} probability.

Finally, if

$$\sigma_V \le \sigma_{V-max} \quad (63)$$

and

$$d_{major} \leq d_{major-max} \tag{64}$$

the accuracy requirements are satisfied.

The following section presents the calculation of the test statistic and threshold with the Normalized Solution Separation method.

3.7.4 Calculation of Test Statistic and Threshold

Fault detection with the Normalized Solution Separation (NSS) method [11] is performed by comparing calculated test statistics against a threshold which are in the solution (position) domain. Note that the following calculations were performed for both the IMU and ADM position estimates, resulting in a HPL for each. The test statistic is in the position domain. It is the separation in the horizontal position domain between full-set and sub-set solutions. For each sub-filter, the test statistic is

$$\lambda_{n_k} = \beta_{n_k}^T (B_{n_k}{}^{+}) \beta_{n_k} \tag{65}$$

where + indicates the Moore- Penrose generalized inverse. The solution separation vector between the full-filter solution and n^{th} sub-filter solution is:

$$\beta_{n_k} = \chi_{0_k} - \chi_{n_k} \tag{66}$$

where χ_{0_k} is the horizontal position vector from the full-filter and χ_{n_k} is the horizontal position vector of the sub-filter. The separation between the sub-filter and full-filter covariance estimates is:

$$B_{n_k} = P_{n_k} - P_{0_k} \tag{67}$$

where P_{n_k} is the horizontal component of $P_k{}^c$ of the n^{th} sub-filter and P_{0_k} is the horizontal component of $P_k{}^c$ of the full-filter.

The detection threshold is determined using chi square statistics to meet the required probability of false alert.

$$TD_n = f(\chi^2, P_{FA} / N) \tag{68}$$

Where N is the number of available GPS measurements.

A fault is detected if

$$\sqrt{\lambda_n} > TD_n \tag{69}$$

for any sub-filter solution.

A potential limitation with this algorithm is the possibility that B is rank deficient. If so, an alternate formulation of the test statistic and threshold is used given in [11].

If a fault is detected, fault exclusion may be performed where an attempt is made to exclude the faulty measurement from contributing to the navigation solution. A fault exclusion function in the measurement domain may be used as was recommended in [11]. However in this thesis, fault exclusion performance is not considered but left for possible further research.

The following section presents the calculation of the protection levels.

3.7.5 Calculation of Protection Levels

Before fault detection takes place there must be confidence that the fault detection can be performed to satisfy the probability of missed detection (P_{md}) requirement. If not, the integrity function is deemed to not be available and the system cannot be used for navigation in accordance with the requirements [41].

P_{md} is ensured by calculating a Horizontal Protection Level (HPL) which is the radius of a circle which bounds the true error in the fault-free condition with a probability of 1-P_{md} [28]. The HPL is calculated as follows.

HPL_{H0} is for the fault free hypothesis H0 and calculated as

$$HPL_{H0k} = K_{H0}\sqrt{\sigma_{1,0}} \tag{70}$$

where K_{H0} is function of 1-P_{H0_H} probability, $\sigma_{1,0}$ is the maximum eigenvalue ($\sigma_{1,0} > \sigma_{2,0}$) of the full-filter covariance P_{0_k} and $(\sigma_{2,0}/\sigma_{1,0})^{1/2}$ from the Circular Error Probable (CEP) distribution [82]. HPL_{H1} is for the fault-in-progress hypothesis H1 and is calculated as:

$$HPL_{H1k} = (HPE_k^n)_{MAX} \tag{71}$$

where the total estimated horizontal position error for the n^{th} sub-filter is

$$HPE_k^n = HPE\_B_k^n + HPE\_NP_k^n - HPE\_NB_k^n \quad (72)$$

where $HPE\_B_k^n$ is the horizontal position error due to bias and uncorrelated noise

$$HPE\_B_k^n = Pbias\sqrt{\sigma_{1,Bn}} \quad (73)$$

where $\sigma_{1,Bn}$ is the maximum eigenvalue of the separation covariance B_{n_k}. *Pbias* is the magnitude of the critical bias vector.

$$Pbias = \sqrt{\lambda} \quad (74)$$

where λ is the noncentrality parameter of the noncentral χ^2 distribution which is determined to meet P_{md_H} and P_{fd}.

$HPE\_NP_k^n$ and $HPE\_NB_k^n$ are the Horizontal Position Errors due to noise only.

$$HPE\_NP_k^n = K_k^n\sqrt{\sigma_{1,n}} \quad (75)$$

where K_k^n is function of 1-P_{md_H} probability and $(\sigma_{2,n}/\sigma_{1,n})^{1/2}$ from the CEP distribution. $\sigma_{1,n}$ is the maximum eigenvalue of the sub-filter covariance P_{n_k}.

$$HPE\_NB_k^n = K_{Bk}^{\ n}\sqrt{\sigma_{1,Bn}} \quad (76)$$

where $K_{Bk}^{\ n}$ is a function of 1-P_{md_H} probability and $(\sigma_{2,Bn}/\sigma_{1,Bn})^{1/2}$ from the CEP distribution.

The HPE can exceed the HPL due either to a GPS measurement fault in the navigation solution or the fault-free event which may be due to IMU errors for example. HPL is therefore the maximum of the two. HPL_{H0} is based on the fault-free hypothesis and HPL_{H1} is based on the fault-in-progress hypothesis. Finally,

$$HPL_k = (HPL_{H0k}, HPL_{H1k})_{MAX} \quad (77)$$

and a similar procedure is followed for calculating VPL.

Now that the method of calculating the protection levels has been described, the following section presents some considerations with using the NSS method in GAGIS.

3.7.6 Considerations when using the NSS Method in GAGIS

Applying the NSS method to the EKF requires some consideration since the EKF is typically a biased estimator as it is an approximate filter. Assuming a biased estimate with bias ε_{bias0} in the full filter solution, then

$$\beta_{n_k} = \chi_{0_k} - \chi_{n_k} + \varepsilon_{bias0} \tag{78}$$

contributing to a larger test statistic in (65). Therefore biased estimates in the full or sub filters may be interpreted by the fault detection algorithm as a GPS fault if the test statistic is greater than the threshold. This highlights the importance of filter tuning (Section 3.6.2). The EKFs should be tuned so that $E(\beta_{n_k}) \approx E(\chi_{0_k} - \chi_{n_k}) \approx 0$ in the fault-free condition. Otherwise there is a risk that the false alarm requirement will not be met. If the threshold is exceeded, the algorithm will be unable to distinguish filter divergence from a true GPS fault and so a false alarm will be generated.

Another factor to consider is how to implement the sub-filters. Unlike [11] where the sub-filter solutions use a high-grade inertial reference trajectory in open loop configuration, GAGIS is in closed loop configuration and incorporates feedback due to the low IMU and ADM accuracy. If the one full-filter mechanization is used by all sub-filters, the sub-filter solutions will not be completely independent of the full-filter or each other since the full-filter estimates have been updated with IMU and ADM bias estimates from all *N* satellites in view. To overcome this, each filter is corrected with corrections from its own filter, therefore there are *N+1* filter corrections fed-back to the *N+1* filters in the system. This means that if one GPS satellite is faulty, there will be one sub-filter which is not corrupted by this faulty satellite measurement.

The following section will describe a GPS-IMU EKF architecture for the one full and *N* sub EKFs.

3.8 GPS-IMU EKF Architecture

In this section the GPS-IMU EKF design is discussed, where it is assumed that the ADM is not used as indicated by the ADM component blanked out in Figure 11.

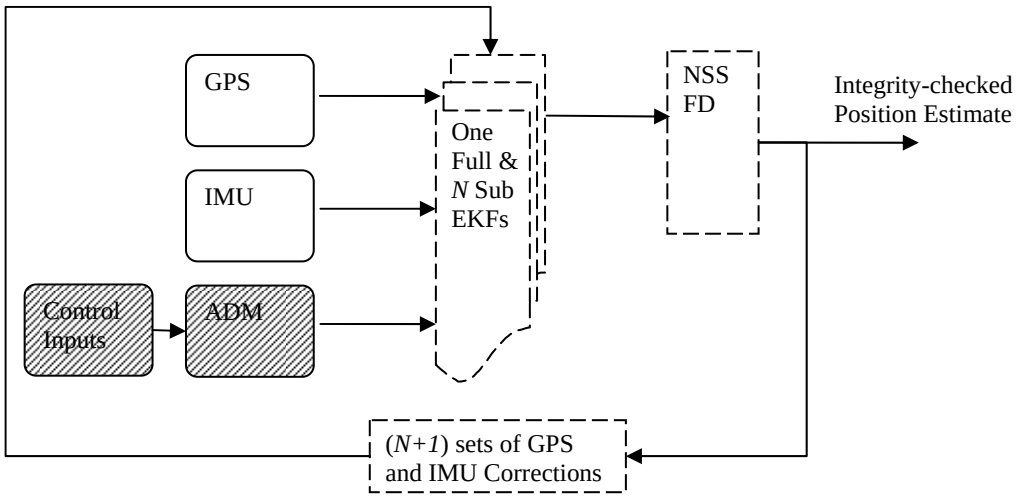

Figure 11 ***The GPS-IMU EKF.***

The form of the IMU state vector at discrete time *k* is

$$\chi_k^I = [\, q_0, q_1, q_2, q_3, v_N, v_E, v_D, l, \Lambda, h\,]^T \tag{79}$$

consisting of four attitude states q_0, q_1, q_2, q_3 (in quaternion representation), three velocity states v_N, v_E, v_D, (in North, East, Down coordinate frame), latitude, longitude and height, l, Λ, h.

A system driven by correlated (colored) process noise can be modeled as a linear stochastic process driven by white process noise [24, 70]. This can be performed in practice by augmenting the state vector with additional states. The state vector is augmented with a vector of error terms to account for GPS receiver clock and IMU biases. These are the corrections applied to the GPS and IMU as indicated by the "corrections" block in Fig. 2.

$$\chi_{A_k}^I = [\Delta t, \Delta \dot{t}, \nabla a_x, \nabla a_y, \nabla a_z, \nabla p, \nabla q, \nabla r]^T \tag{80}$$

where Δt is GPS receiver clock bias, $\Delta \dot{t}$ is GPS receiver clock drift, ∇a_x, ∇a_y, ∇a_z are IMU acceleration biases and ∇p, ∇q, ∇r are IMU angular rate biases. The IMU biases are modeled as first order Gauss Markov processes [70] and the GPS clock terms are modeled by the typical crystal oscillator model from [48].

The EKF operates on the state errors. Whilst a quaternion representation has been used for the attitude component of the state vector (79), the attitude component of the state errors is represented by attitude tilt errors. The state error vector structure is

$$x_k^I = [\delta\Phi_N, \delta\Phi_E, \delta\Phi_D, \delta v_N, \delta v_E, \delta v_D, \delta l, \delta\Lambda, \delta h, \delta\chi_{Ak}^I]^T \quad (81)$$

Where $\delta\Phi_N, \delta\Phi_E$ are tilt errors with respect to the vertical and $\delta\Phi_D$ is azimuth (heading) error. $\delta v_N, \delta v_E, \delta v_D$ are velocity errors and $\delta l, \delta\Lambda, \delta h$ are latitude, longitude and height errors and $\delta\chi_{Ak}^I$ is the vector of augmented state errors.

Two state estimates are calculated by propagating the previous state using the IMU mechanization equations as given in Chapter 4,

$$\chi_k^{I^-} = f(\chi_{k-1}^I, u_{k-1}^I, w_{k-1}^I) \quad (82)$$

where u^I is the IMU measurements (accelerations, angular rates) and w^I is white noise. (82) is calculated at 100 Hz in between GPS measurement updates at 1 Hz.

The state error covariance of x_k^I is

$$P_k^{I^-} = \Phi_{k-1}^I P_{k-1}^I \Phi_{k-1}^{I^T} + Q_{k-1}^I \quad (83)$$

The process noise covariance matrix can be approximated by [48],

$$Q_{k-1}^I = G_{k-1}^I W_{k-1}^I G_{k-1}^{I^T} \Delta t^I \quad (84)$$

Where G^I is a design matrix and W^I is a power spectral density matrix whose diagonal elements are the IMU acceleration and angular rate noise variances. Δt is the sample period.

For measurements a tightly coupled (pseudorange and pseudorange-rate) approach was taken. The measurements supplied to the filter are the difference between the GPS pseudorange and pseudorange-rates $\rho^G, \dot{\rho}^G$ and IMU state estimate-derived pseudorange and pseudorange-rates ρ^I, $\dot{\rho}^I$ (2)-(3).

The measurement vectors of pseudoranges and pseudorange-rates are

$$z_k^I = \bar{\rho}_k^G - \bar{\rho}_k^I \quad (85)$$

where

$$\bar{\rho}_k^G = \left[\rho_k^G, \dot{\rho}_k^G\right]^T \tag{86}$$

and similarly for $\bar{\rho}_k^I$.

The measurement noise covariance matrix R_k^I diagonal elements contain the variances of the expected GPS pseudorange and pseudorange-rate noises.

The state and augmented state errors x_k^I are estimated as

$$x_k^I = K_k^I z_k^I \tag{87}$$

where the Kalman gain is

$$K_k^I = P_k^{I^-} H_k^{I^T} (H_k^I P_k^{I^-} H_k^{I^T} + R_k^I)^{-1} \tag{88}$$

and H_k^I is the measurements matrix.

The state update is

$$\chi_k^I = \chi_k^{I^-} + \hat{x}_k^I \tag{89}$$

Where $\hat{x}_k^I$ is the attitude, velocity and position error components of (81). Note that the three attitude tilt errors of x_k^I are transformed to four quaternion errors before adding to $\chi_k^{I^-}$ in (89).

The augmented state update is

$$\chi_{A\,k+1}^I = \chi_{A\,k}^{I^-} + \delta\chi_{A\,k}^I \tag{90}$$

Finally, the corresponding state error covariance update is

$$P_k^I = (I - K_k^I H_k^I) P_k^{I^-} (I - K_k^I H_k^I)^T + K_k^I R_k^I K_k^{I^T}. \tag{91}$$

Each of the full and N sub filters use the same form of (79)-(91), the only difference being that with the N sub filters there is one less GPS measurement passed to the filter in (85)-(86) than for the full filter.

As shown in [83], with low quality gyroscopes attitude errors are not completely observable when there is only position and velocity measurements. This is because the low quality gyroscopes cannot sense the earth rotation because of their poor accuracy and so the misalignments are not connected to each other through the earth

rotation. The observability can be improved by using external attitude aiding on any single axis. Therefore the alignment process may also be assisted by heading information (e.g. magnetic compass) for example.

A benefit of this architecture is that fusing GPS with the IMU may provide greater confidence in the estimated position and thereby improve the fault detection performance. This improvement in confidence may be an advantage in times of poor GPS satellite geometry and improve fault detection availability because integrity monitoring performance with GPS alone is strongly dependant upon good geometry.

The GPS-IMU EKF architecture has been presented. The following section presents a GPS-ADM EKF architecture.

3.9 GPS-ADM EKF Architecture

In this section the GPS-ADM EKF design is discussed, where it is assumed that the IMU is not used as indicated by the IMU component blanked out in Figure 12.

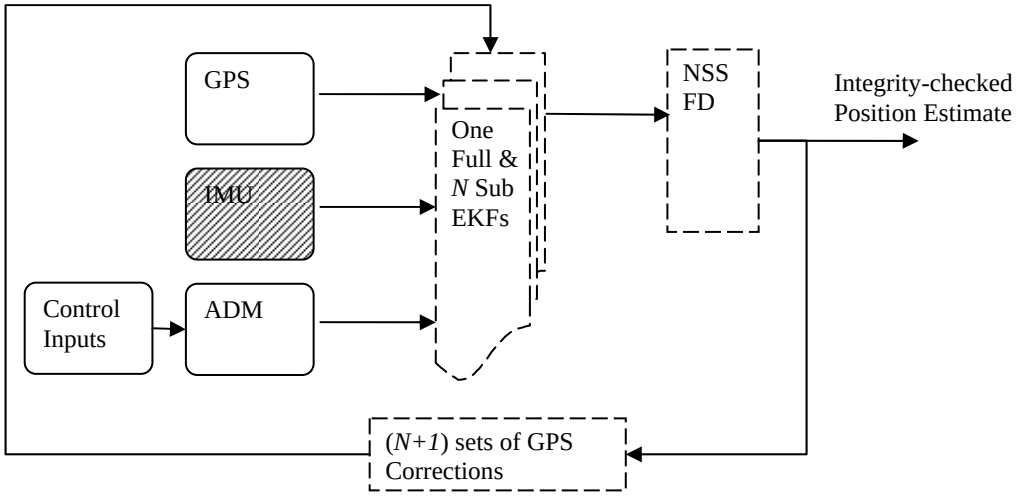

Figure 12 ***The GPS-ADM EKF*****.**

The design of the GPS-ADM EKF is similar to the GPS-IMU EKF presented in Section 3.8. The form of the ADM state vector at discrete time *k* is

$$\chi_k^D = [\, q_0, q_1, q_2, q_3, v_N, v_E, v_D, l, \Lambda, h \,]^T \tag{92}$$

consisting of four attitude states q_0, q_1, q_2, q_3 (in quaternion representation), 3 velocity states v_N, v_E, v_D, (in North, East, Down coordinate frame), latitude, longitude and height, l, Λ, h.

The state vectors are augmented (denoted by subscript A) with error terms to account for GPS errors. These are the corrections applied to the GPS, as indicated by the "corrections" block in Fig. 2. In this GPS-ADM EKF design, there are no augmented states for ADM errors. The ADM state, could be augmented with aerodynamic coefficients or wind estimates as in [12], however this will also have an associated observability penalty. So it was preferred to not augment the ADM state with any extra states in this architecture but augmenting with wind estimates will be investigated in Section 3.10.

$$\chi_{A\,k}^D = [\, \Delta t, \Delta \dot{t} \,]^T \tag{93}$$

where Δt is GPS receiver clock bias and $\Delta \dot{t}$ is GPS receiver clock drift. The GPS clock terms are modeled using the typical crystal oscillator model in [48].

The state error vector structure is

$$x_k^D = [\delta\Phi_N, \delta\Phi_E, \delta\Phi_D, \delta v_N, \delta v_E, \delta v_D, \delta l, \delta\Lambda, \delta h, \delta\chi_{Ak}^D]^T \quad (94)$$

Where $\delta\Phi_N, \delta\Phi_E$ are tilt errors with respect to the vertical and $\delta\Phi_D$ is azimuth (heading) error. $\delta v_N, \delta v_E, \delta v_D$ are velocity errors and $\delta l, \delta\Lambda, \delta h$ are latitude, longitude and height errors and $\delta\chi_{Ak}^D$ is the vector of augmented state errors.

Two state estimates are calculated by propagating the previous state using the ADM equations (Section 3.5),

$$\chi_k^{D^-} = f(\chi_{k-1}^D, u_{k-1}^D) \quad (95)$$

where u^D is the ADM control inputs.

The ADM state error covariance is

$$P_k^{D^-} = \Phi_{k-1}^D P_{k-1}^D \Phi_{k-1}^{D^T} + Q_{k-1}^D \quad (96)$$

The process noise covariance matrix for the filter is approximated by

$$Q_{k-1}^D = G_{k-1}^D W_{k-1}^D G_{k-1}^{D^T} \Delta t^D \quad (97)$$

Where G^D is a design matrix and W^D contains the expected noise statistics for the ADM as determined by filter tuning and based upon experience or empirical data (Section 3.6). Δt is the sample period.

For the GPS measurements a tightly coupled (pseudorange and pseudorange-rate) approach was taken. The measurements supplied to the filter are the difference between the GPS pseudorange and pseudorange-rates $\rho^G, \dot{\rho}^G$ and ADM state estimate-derived pseudorange and pseudorange-rates ρ^D, $\dot{\rho}^D$ (2)-(3).

The measurement vector of pseudoranges and pseudorange-rates is

$$z_k^D = \bar{\rho}_k^G - \bar{\rho}_k^D . \quad (98)$$

where

$$\bar{\rho}_k^G = \left[\rho_k^G, \dot{\rho}_k^G\right]^T \tag{99}$$

and similarly for $\bar{\rho}_k^D$.

The measurement noise covariance matrix is R_k^D whose diagonal elements are the variances of the expected GPS pseudorange and pseudorange-rate noises.

The state and augmented state errors errors x_k^D are estimated as

$$x_k^D = K_k^D z_k^D \tag{100}$$

where the Kalman gain is

$$K_k^D = P_k^{D^-} H_k^{D^T} (H_k^D P_k^{D^-} H_k^{D^T} + R_k^D)^{-1} \tag{101}$$

and H_k^D is the measurements matrix.

The state update is

$$\chi_k^D = \chi_k^{D^-} + \hat{x}_k^D \tag{102}$$

Where $\hat{x}_k^D$ is the attitude, velocity and position error components of (100). Note that the three attitude tilt errors of x_k^D are transformed to four quaternion errors before adding to $\chi_k^{D^-}$ in (102).

The augmented state update is

$$\chi_{A}{}_{k+1}^D = \chi_{A}{}_k^{D^-} + \delta\chi_{A}{}_k^D \tag{103}$$

Finally, the corresponding state error covariance update is

$$P_k^D = (I - K_k^D H_k^D) P_k^{D^-} (I - K_k^D H_k^D)^T + K_k^D R_k^D K_k^{D^T}. \tag{104}$$

The benefits of this architecture are that the ADM is independent of the IMU yet functions in a similar way. The disadvantages of the ADM are the uncertainties due to inaccurately known aerodynamic coefficients, surrounding environment (e.g. wind) and need to measure pilot control inputs. Although it is not difficult to add sensors such as potentiometers to measure aircraft control surface movements,

measurement of these is not normally made for most general aviation aircraft and therefore there will be additional costs involved. Another disadvantage is that the ADM is valid only for a particular aircraft type.

The question might be asked as to how to check the quality of the ADM? For a given aircraft type, the quality of the ADM itself may have been originally known by system identification processes involving flight testing with an appropriately instrumented aircraft, for example. Also, hardware components such as control input sensors will need to be checked during maintenance procedures. Yet obviously, non-deterministic and uncontrollable error sources such as wind remain, and may cause the ADM performance to degrade. But it should be noted, that if the performance of the ADM degrades beyond acceptable limits, any fault from the ADM may also be detected (see [84] for example).

The GPS-ADM EKF architecture has been presented. The following section will present an extension to the GPS-ADM EKF architecture where estimates of wind are made and used to correct the ADM.

3.10 GPS-ADM EKF with Wind Estimation Architecture

The architecture described in this section is an extension of the GPS-ADM EKF where wind velocities are attempted to be estimated at 1 Hz and used to correct the ADM. The state vector is identical to the GPS-ADM EKF except for the angular rate estimates, *p, q, r*, where the form of the state vectors at discrete time *k* is

$$\chi_k^D = [\, q_0, q_1, q_2, q_3, v_N, v_E, v_D, l, \Lambda, h, p, q, r \,]^T . \tag{105}$$

The augmented state vector of the GPS-ADM EKF was also modified to include three states for the wind velocity estimates (North, East, Down wind velocities):

$$\chi_{A_k}^D = [\, \Delta t, \dot{\Delta t}, W_N, W_E, W_D \,]^T \tag{106}$$

These wind estimates are used to correct the ADM estimates of position in between GPS updates. Unlike [12] where manouvres are performed to achieve observability in estimating the wind, for GAGIS an APV approach is only of short duration (approximately 2 minutes) and is a "straight-in" approach. This means flying any manouvres to achieve observability in the wind estimates would be impractical. Keeping this in mind there were two methods considered for estimating the wind,

(1) Estimate the wind in the EKF by modelling it as a random walk. This is presented in 3.10.1.

(2) Estimate the wind based on air data sensor measurements and low-cost GPS/IMU navigation solution. This is presented in 3.10.2.

The following section will describe wind estimation in the EKF as per method (1).

3.10.1 Wind Estimation in the EKF

In this approach no attempt is made to measure the wind directly, but rather to estimate it within the GPS-ADM EKF by modelling it as a random walk and correcting these wind estimates with the GPS measurements every update. The Kalman filter navigation state (attitude, velocity, position) is augmented with three states to account for Wind in the North, East and Down direction as per (106). The

wind velocity vector in North, East, Down frame V_{wind} is modeled as a random walk

$$V_{wind_{k+1}} = V_{wind_k} + v_v \tag{107}$$

where v_v is white Gaussian noise. Although atmospheric turbulence is not necessarily Gaussian, it can be considered Gaussian for practical purposes [78]. An advantage of this approach is that wind can be attempted to be estimated and no additional sensors are required. A disadvantage of this approach is that there is likely to an observability issue with the wind and (107) requires the magnitude of the driving noise to be known apriori or estimated which may present problems with filter tuning in a practical system. If v_v is too small the wind may be poorly estimated or if v_v is too large the covariances of the state estimates may be too large. This may result in worse rather than better integrity monitoring performance since the protection level calculations are based upon the state covariances. Wind estimation results using this method will be presented in Section 4.4. The following section will describe the method of wind estimation in the GPS-ADM EKF with air data sensors and IMU.

3.10.2 Wind Estimation with Air Data Sensors and IMU

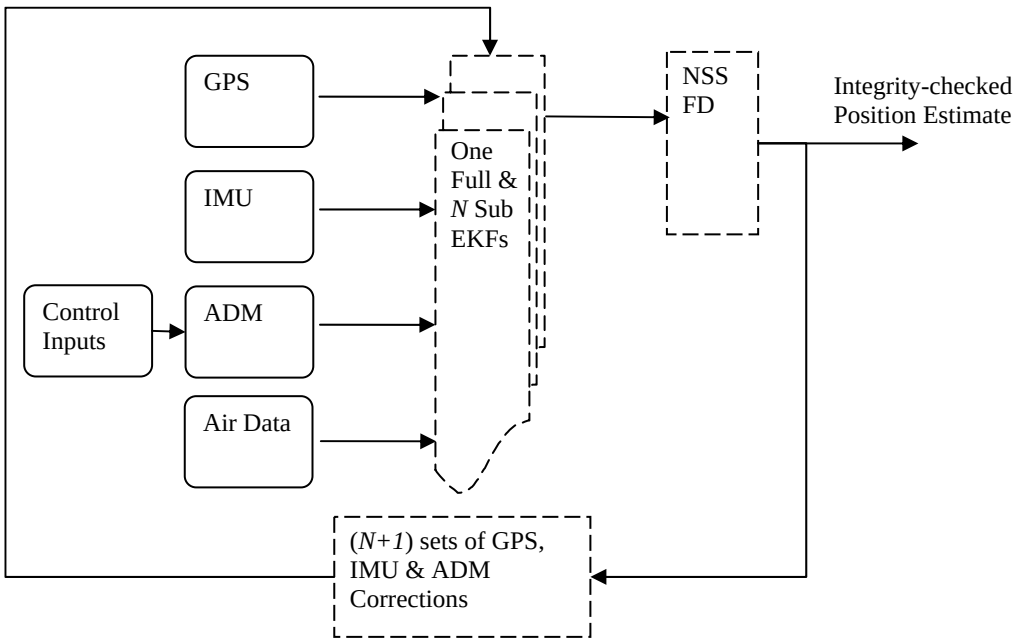

Figure 13 ***The GPS-ADM EKF with Air Data.***

In this approach, the magnitude of the wind in the North, East, Down local navigation frame is measured using air data sensor measurements (airspeed, angle of attack, sideslip) and attitude estimates provided from the GPS-IMU EKF navigation solution. The attitude estimates are provided from the GPS-IMU EKF because the stand-alone IMU attitude estimates are unbounded and uncorrected for bias. The wind estimates are modeled as a random walk as in the previous section and are corrected with the air data and GPS-IMU EKF wind measurements at 1 Hz. The North, East, Down wind vector is estimated as:

$$V_{wind\,k} = V_{nav\,k} - V_{aero\,k} \tag{108}$$

V_{nav} is the aircraft velocity vector in the inertial navigation frame. V_{nav} is estimated from the tightly coupled GPS-IMU EKF.

V_{aero} is the aircraft aerodynamic velocity vector (i.e. velocity of aircraft with respect to the surrounding air) transformed to the inertial navigation frame.

It is assumed that V_{aero} is calculated from an air data system which measures true airspeed, V_{TAS}.

V_{aero} is then the true transformed from the wind axes into the body frame and then from the body frame into the navigation frame,

$$V_{aero} = T_b^n T_\alpha^b V_{TAS} \tag{109}$$

where,

T_α^b is the wind to body axes transform, (depends on angle of attack and sideslip knowledge) [75], T_b^n is the body to navigation transform, (depends on attitude knowledge) [75].

In these results the estimate of angle of attack and sideslip is assumed to be provided by air data measurements (e.g. an air data boom with angle of attack and sideslip vanes). The estimates of attitude are provided by the GPS-IMU EKF, as these estimates are expected to be more accurate than the GPS-ADM EKF attitude estimates. The advantage of this method is that observability in the wind magnitudes and directions may be achieved with the inclusion of the air data sensor and IMU measurements, however a disadvantage is that the GPS-ADM EKF is no longer

independent of the GPS-IMU EKF and air data sensors are required to be fitted to the aircraft. Wind estimation results using this method will be presented in Section 4.4 where it will be shown how accurately the wind may be estimated and how it compares to the method in Section 3.10.1 and GPS-ADM EKF with no wind estimates. The following section describes the GPS-IMU-ADM EKF architecture where the IMU and ADM information are fused together.

3.11 GPS-IMU-ADM EKF Architecture

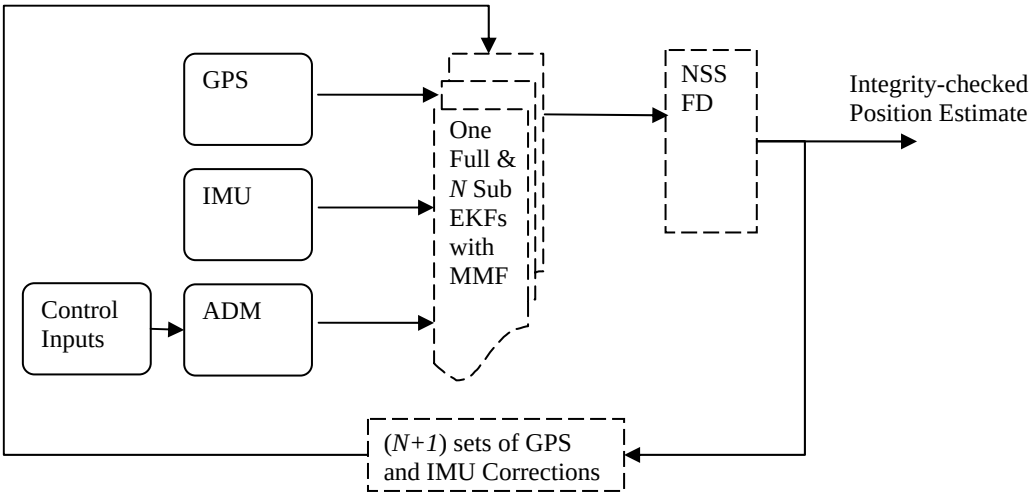

Figure 14 ***The GPS-IMU-ADM EKF with Multiple-Model Fusion.***

In GAGIS there are two process models, one for the IMU and one for the ADM. Therefore, it is possible for each to run separately and independently as given in previous sections with the GPS-IMU EKF and GPS-ADM EKF architectures. Alternatively, in this approach the IMU and ADM process models are fused together with Multiple Model Fusion (MMF) [79].

In contrast to other multiple model strategies that switch between models by selecting which one is most valid to use at the time, the MMF approach assumes the models all contain useful information which can be exploited synergistically. Because the Kalman filter update does not distinguish between predictions and observations, the predictions from each model can be treated as a sensor. MMF exploits the cross correlation information between the different models. In this way their respective strengths can be exploited and their weaknesses complemented. According to [79] the Kalman update rule can be used to consistently fuse the predictions of multiple process models together. It can exploit information about the differences in behavior of each model. As a result, the performance of the fused system can be better than that of any individual model by itself.

The accuracy of the estimates provided by the ADM considered in this study are of lower accuracy than what the low-cost MEMS IMU can measure. This was

established by comparing their angular rate and acceleration estimates in simulation. However despite this, the ADM may still yield useful information about the system which may be exploited by MMF.

To achieve MMF and maintain cross correlation information, the IMU, ADM and GPS are combined in a single "combined filter". This can be thought of as the GPS-IMU EKF of Section 3.8 and the GPS-ADM EKF of Section 3.9 stacked on top of one another.

In the following equations the IMU will be denoted by superscript *I*, the ADM by *D* and the GPS by *G*. Two state vectors are formed. One for the IMU-derived estimates and one for the ADM-derived estimates. The structure of the state vectors at discrete time *k* is

$$\chi_k^I = [\, q_0, q_1, q_2, q_3, v_N, v_E, v_D, l, \Lambda, h \,]^T \tag{110}$$

$$\chi_k^D = [\, q_0, q_1, q_2, q_3, v_N, v_E, v_D, l, \Lambda, h \,]^T \tag{111}$$

consisting of four attitude states q_0, q_1, q_2, q_3 (in quaternion representation), three velocity states v_N, v_E, v_D, (in North, East, Down coordinate frame), latitude, longitude and height, l, Λ, h.

The state vectors are augmented (denoted by subscript A) with error terms to account for GPS, IMU and ADM errors. These are the corrections applied to the GPS, IMU and ADM as indicated by the "corrections" block in Fig. 2.

$$\chi_{Ak}^I = [\, \Delta t, \Delta \dot{t}, \nabla a_x, \nabla a_y, \nabla a_z, \nabla p, \nabla q, \nabla r \,]^T \tag{112}$$

$$\chi_{Ak}^D = [\, \Delta t, \Delta \dot{t} \,]^T \tag{113}$$

where Δt is GPS receiver clock bias, $\Delta \dot{t}$ is GPS receiver clock drift, ∇a_x, ∇a_y, ∇a_z are acceleration biases and ∇p, ∇q, ∇r are angular rate biases.

The EKF operates on the state errors. Whilst a quaternion representation has been used for the attitude component of the state vector, the attitude component of the state errors is represented by attitude tilt errors. The state error vector structure is

$$x_k^C = [x_k^I, x_k^D]^T \tag{114}$$

Where x_k^I is the IMU state error vector (81) and x_k^D is the ADM state error vector

(94).

Two state estimates are calculated by propagating the previous state using the IMU and ADM process models,

$$\chi_k^{I^-} = f(\chi_{k-1}^I, u_{k-1}^I, w_{k-1}^I) \tag{115}$$

$$\chi_k^{D^-} = f(\chi_{k-1}^D, u_{k-1}^D, w_{k-1}^D) \tag{116}$$

where u^I is the IMU measurements (accelerations, angular rates), u^D is the ADM control input measurements, w^I and w^D are white noises. The combined state estimate vector is formed as

$$\chi_k^{C^-} = \left[\chi_k^{I^-}, \chi_{A}^{I^-}{}_{k-1}, \chi_k^{D^-}, \chi_{A}^{D^-}{}_{k-1} \right]^T . \tag{117}$$

The combined state error covariance is

$$P_k^{C^-} = \Phi_{k-1}^C P_{k-1}^C \Phi_{k-1}^{C^T} + Q_{k-1}^C \tag{117}$$

where ϕ is the state transition matrix

$$\Phi_{k-1}^C = \begin{bmatrix} \Phi_{k-1}^I & 0 \\ 0 & \Phi_{k-1}^D \end{bmatrix}. \tag{119}$$

The process noise covariance matrix for the combined filter is

$$Q_{k-1}^C = \begin{bmatrix} Q_{k-1}^I & Q_{k-1}^{I-D} \\ Q_{k-1}^{D-I} & Q_{k-1}^D \end{bmatrix} \tag{120}$$

where

$$Q_{k-1}^I = G_{k-1}^I W_{k-1}^I G_{k-1}^{I^T} \Delta t^I \tag{121}$$

$$Q_{k-1}^D = G_{k-1}^D W_{k-1}^D G_{k-1}^{D^T} \Delta t^D . \tag{122}$$

G^I and G^D are design matrices for the IMU and ADM. W^I contains the expected noise statistics for the IMU and is a power spectral density matrix whose diagonal elements are the acceleration and angular rate noise variances of the IMU. W^D is a power spectral density matrix describing the magnitude of the process noise applied to the ADM attitude and velocity estimates to accommodate ADM uncertainties. W^I and W^D are tuned until the filters are consistent. Δt^I and Δt^D are the sample periods for the IMU and ADM.

$Q^{I\text{-}D}$ and $Q^{D\text{-}I}$ in (118) are the cross correlations between the IMU and ADM process noise. The IMU and ADM process noises will not be independent of each other due to the common assumptions and errors they share and that they are both updated by the same GPS measurements. As it is difficult to determine what the true correlation is, it is treated as a tuning parameter for the filters, where it is tuned based on empirical data or experience.

With the GPS measurements a tightly coupled (pseudorange and pseudorange-rate) approach was taken. The measurements supplied to the filter are the difference between the GPS pseudorange and pseudorange-rates ρ^G , $\dot{\rho}^G$ and IMU and ADM state estimate-derived pseudorange and pseudorange-rates ρ^I , $\dot{\rho}^I$ and ρ^D , $\dot{\rho}^D$ (2)-(3).

The measurement vectors of pseudoranges and pseudorange-rates are

$$z_k^I = \overline{\rho}_k^G - \overline{\rho}_k^I \tag{123}$$

$$z_k^D = \overline{\rho}_k^G - \overline{\rho}_k^D . \tag{124}$$

where

$$\overline{\rho}_k^G = \left[\rho_k^G, \dot{\rho}_k^G\right]^T \tag{125}$$

and similarly for $\overline{\rho}_k^I$ and $\overline{\rho}_k^D$.

In MMF, the IMU and ADM process models can be thought of as virtual sensors whose output is a virtual measurement of the state of the vehicle based on all past time history [79], [85]. States which are common to both systems may be fused together. In GAGIS the logical choice is the position estimates as these are most relevant to the integrity monitoring problem. The difference between the process model's position estimates are presented to the combined filter as measurements,

$$z_k^{I-D} = \chi_{k\ (l,\Lambda,h)}^{\bar{I}} - \chi_{k\ (l,\Lambda,h)}^{\bar{D}} . \tag{126}$$

The measurements vector for the full-filter is

$$z_k^C = \left[z_k^I, z_k^{I-D}, z_k^D\right]^T . \tag{127}$$

The measurement noise covariance matrix is

$$R_k^C = \begin{bmatrix} R_k^G & 0 & R_k^G \\ 0 & R_k^{I-D} & 0 \\ R_k^G & 0 & R_k^G \end{bmatrix} \tag{128}$$

where R^C is a diagonal sub-matrix whose diagonal elements are the variances of the expected GPS pseudorange and pseudorange-rate noises. Because both IMU and ADM process models (114), (115), estimate the same state (position), the expected value of the difference of these (126) is zero with no uncertainty, so $R^{I\text{-}D} = 0$ in (128). This effectively applies hard constraints on the system [79]. In (128), note that R^C is singular. This is due to $R^{I\text{-}D}$ being zero and the off-diagonal sub-matrices R^G which exist because the same GPS measurements are used to update the IMU and ADM state estimates. In this study the singularity of R^C was overcome by applying the Moore-Penrose generalized inverse (pseudo-inverse) denoted as + in (130).

The state errors ${x_k}^C$ are estimated as

$$x_k^C = K_k^C z_k^C \tag{129}$$

where the Kalman gain is

$$K_k^C = P_k^{C^-} H_k^{C^T} (H_k^C P_k^{C^-} H_k^{C^T} + R_k^C)^+ \tag{130}$$

and ${H_k}^C$ is the measurements matrix.

The state update is

$$\chi_k^C = \chi_k^{C^-} + x_k^C \tag{131}$$

where the form of the state vector is

$$\chi_k^C = \left[\chi_k^I, \chi_{Ak}^I, \chi_k^D, \chi_{Ak}^D\right]^T. \tag{132}$$

The corresponding state error covariance update is

$$P_k^C = (I - K_k^C H_k^C) P_k^{C^-} (I - K_k^C H_k^C)^T + K_k^C R_k^C K_k^{C^T}. \tag{133}$$

After the update (130), (133) the state estimates χ_k^I and χ_k^D and their respective covariances in P_k^C are the same [79] and so either state estimates can be used for the fault detection. The state estimates ${\chi_k}^C$ and ${P_k}^C$ for the full-filter and sub-filters are then used by the FD algorithm. The position error covariances of ${P_k}^I$ and ${P_k}^D$ are expected to be reduced due to the fusing of the ADM and IMU process models together by the EKF update equation (133). This is because (133) it includes the

cross-correlations between the IMU and ADM process models, which serves to exploit the information which is different about each process model.

As shown in [79], [85], only the information which is independent between the process models is used to update the predictions. If both the IMU and ADM were identical, no benefit could be gained by fusing them together. Note that the resulting position and covariance estimate for both the IMU and ADM states will be the same after the GPS update.

As mentioned in Section 3.6.1 both the IMU and the ADM process models are approximations to the true dynamics of the system and the source of the acceleration and angular rate information presented to each process is different. For example, the IMU measurements of acceleration and angular rate contain random noises and biases due to the internal workings of the MEMS sensors. In contrast, the ADM process has errors due to the assumptions made about the aircraft and the surrounding environment, imperfect knowledge of aerodynamic coefficients and noisy control surface measurements for example. Fusing this different information together by MMF is expected to result in a reduction in covariances. It can be seen from (70)-(77) that HPL and VPL are dependant upon the state covariance of the full and sub-filters. This is where the MMF with an ADM and IMU can provide a lower state covariance leading to lower protection levels, than the same IMU alone. As will be seen in the results chapter, this reduction has an effect in reducing protection levels in the GPS fault detection.

[79] has shown that the technique of MMF is consistent even if the noises are known imperfectly. However MMF will be consistent only if each approximate system is consistent [79]. This will be when the combined system is consistent. The consistency of MMF as applied to the GPS integrity monitoring problem is important. One foreseen issue with using MMF in GAGIS is that the system overall may be less robust against IMU or ADM errors. This is because the IMU and ADM are not independent, if either the IMU or ADM has a fault, or the IMU or ADM is not tuned properly and the filter diverges, this will propagate through the system. Any unresolved ADM biases will corrupt the IMU estimates causing them to also be biased and vice versa. For this reason, even more care is required in tuning the

system to make sure it is consistent.

Based upon the approach for tuning the combined system in [79], the tuning approach to the GPS-IMU-ADM EKF is such that the GPS-IMU EKF and GPS-ADM EKF are tuned independently first and then finally the combined system is tuned and noises adjusted as required. Additional stabilising noise may need to be added.

The benefit of the GPS-IMU-ADM EKF is that the combining of the IMU and ADM may achieve lower protection levels than GPS-IMU EKF or GPS-ADM EKF. The amount of lowering (if any) will be investigated in Section 4.5. Disadvantages are that it is more complex than GPS-IMU EKF or GPS-ADM EKF and possibly more susceptible to IMU or ADM faults. Because the IMU and ADM are fused together and are not independent in the system, there is greater risk of failure or filter divergence because an error in the IMU or the ADM will affect the whole system.

The following section describes the stand-alone GPS architecture which is compared with GAGIS in the results of Chapter 4.

3.12 Stand-alone GPS Architecture

This architecture is the GPS without any other sensors and is given here because its integrity monitoring performance will be compared with GAGIS in the results of Chapter 4. As shown in Figure 15 this is a "snapshot" least squares (LSQ) implementation of the NSS method [11]. The GPS pseudorange measurements are processed in full and sub-least squares navigation solutions rather than EKFs. The estimates are the aircraft's position and GPS receiver clock bias. The clock bias estimates are fed back to correct the GPS measurements.

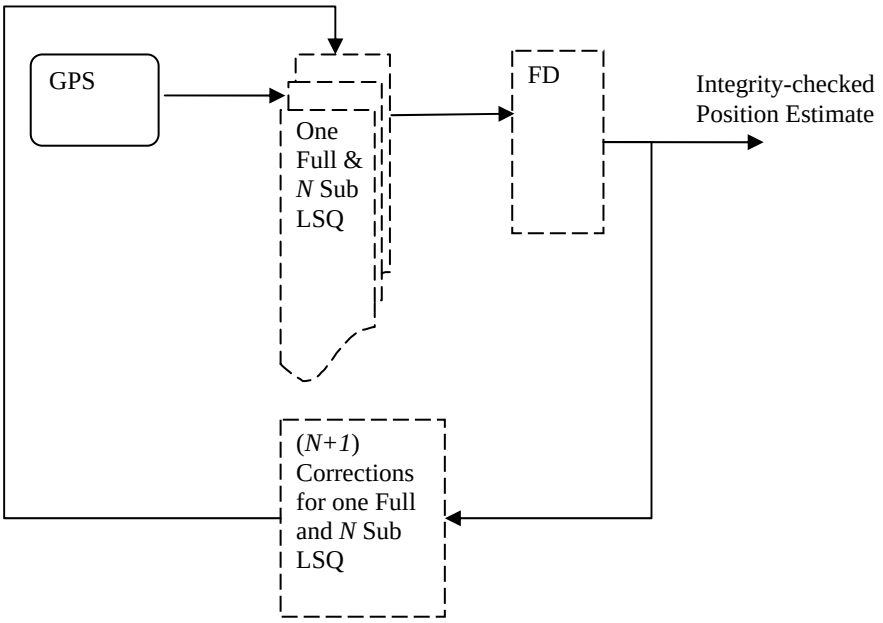

Figure 15 *Stand-alone GPS Architecture*

The main benefit of this architecture is that it is simple – there are no Extended Kalman Filters and no additional measurements from IMU or ADM. However the main drawback of this architecture is that there is no augmentation and the current GPS constellation alone does not support APV integrity requirements (Section 2.5.3).

3.13 Conclusion

A new ABAS architecture concept named the General Aviation GPS Integrity System (GAGIS) has been presented. Each of the components of GAGIS including the GPS, MEMS IMU, ADM, EKF and FD was discussed and calculations given for the integrity monitoring performance requirements.

A GPS-IMU EKF design was presented. The performance of this architecture is expected to be better than GPS alone and will be evaluated in the results in Chapter 4. A GPS-ADM EKF design was presented and discussed which was similar to the GPS-IMU EKF. With the GPS-IMU EKF, the dynamic information comes from measured accelerations and angular rates whereas with the GPS-ADM EKF the dynamic information comes from estimates derived from the aircraft's aerodynamics. It is expected that with the ADM as the process model in the EKF, it has the potential to perform better integrity monitoring than GPS alone. Another two GPS-ADM EKF designs were presented which attempt to estimate the wind at a high rate (1 Hz). It will be seen in the results of Chapter 4 whether or not there is any advantage in attempting to correct the ADM with wind estimates.

An EKF design using a GPS, IMU and ADM was presented where the IMU and ADM is fused together using Multiple Model Fusion. This was called the GPS-IMU-ADM EKF. It is expected that the fusion of the IMU and ADM can result in a performance greater than either the GPS-IMU EKF or GPS-ADM EKF.

To evaluate the performance of these architectures in GPS integrity monitoring, results will be presented in the next chapter where the GPS-IMU EKF, GPS-ADM EKF and GPS-IMU-ADM EKF are implemented and tested in a computer simulation environment. They are compared against each other and a GPS-only implementation.

4 GAGIS Integrity Monitoring Results

4.1 Introduction

This chapter presents results of a series of computer simulation tests to investigate the integrity monitoring performance of GAGIS. The results in this chapter were generated using a simulation environment called the GRAS Airborne Receiver Development Simulator (GARDSim) which was developed for the purposes of this research.

Section 4.2 describes the simulated test scenario of a Navion general aviation aircraft on APV approach. The values of the simulation parameters used in the tests are given, including values of the GPS, IMU, ADM and environmental errors which were modeled.

The aim of Section 4.3 is to compare and investigate the GPS-IMU EKF of Section 3.8, the GPS-ADM EKF of Section 3.9 and the stand-alone GPS architecture of Section 3.12 in accuracy, protection levels and detection of 0.5 m/s and 2.5 m/s ramp faults.

The aim of Section 4.4 is to investigate whether or not including wind estimates in the ADM can allow for lower protection levels over not including them. Results for a simulated APV approach with changing wind conditions (wind shear) over the flight are presented. The wind estimation accuracy of the GPS-ADM EKF with Wind Estimation architecture of Section 3.10 is investigated first. The protection levels are then compared against the GPS-ADM EKF of Section 3.9.

The aim of Section 4.5 is to investigate whether or not a reduction in protection levels is possible by combining the ADM and IMU estimates together using MMF. The protection levels of the GPS-IMU-ADM EKF of Section 3.11 are compared with the GPS-IMU EKF of Section 3.8.

The aim of Section 4.6 is to investigate how the changing satellite geometry affects the protection level by comparing the performance of the different architectures over

a 24 hour period. The average protection levels over the 24 hour period of the GPS-only fault detection architecture, GPS-IMU EKF, GPS-ADM EKF and GPS-IMU-ADM EKF are compared.

The aim of Section 4.7 is to determine whether or not the integrity performance of GAGIS changes significantly with a faster approach velocity. This may be due to the system being used on a fast aircraft such as a small jet, for example. The protection levels and ramp fault detection times will be compared with the GPS-only fault detection architecture, GPS-IMU EKF and GPS-ADM EKF. The GPS-IMU EKF of and GPS-IMU-ADM EKF will also be compared.

The aim of Section 4.8 is to investigate substituting some of the IMU measurements with the ADM estimates. This is to determine whether or not using partial information from the ADM can improve the redundancy in the navigation system. Protection levels of the GPS-IMU EKF architecture where the accelerometer estimates are provided by the ADM are compared with the GPS-IMU EKF.

4.2 Navion General Aviation Aircraft Simulation Test Scenario Details

Results were generated using a simulation environment called the GRAS Airborne Receiver Development Simulator (GARDSim) which was developed for the purposes of this research. Please refer to A. Appendix for more information about GARDSim. The aircraft model used for this study was of a Navion general aviation aircraft. Table 3 gives the parameters and noise values for the GPS, IMU, ADM, air data sensor models, environmental errors and the initialization error used in the simulations. In Table 3 a white noise process is denoted as $WN(\sigma)$ and a first-order Gauss-Markov process will be referred to as $GM(\sigma, \tau)$ where σ is the standard deviation and τ is the correlation time. Please refer to A. Appendix for information of how these values were chosen.

Parameter	***Value***
GPS	
Ephemeris	*GM* (2.4 m, 1800 s)
Ionosphere (L1-L5)	*GM* (0.4 m, 1800 s)
Troposphere (L1-L5)	*GM* (0.4 m, 3600 s)
Multipath (Code)	*GM* (0.25 m, 600 s)
Receiver Noise (Code)	*WN* (0.1 m)
Multipath (Carrier)	*GM* (0.048 m, 600 s)
Receiver Noise (Carrier)	*WN* (0.0019 m)
Total L1-L5 1σ Pseudorange Noise	2.47 m
GPS Receiver Clock	Typical Crystal Oscillator [86]
GPS Antenna Elevation Mask	5°
IMU	
p gyro Noise	*WN* (0.53 °/s)
q gyro Noise	*WN* (0.45 °/s)
r gyro Noise	*WN* (0.44 °/s)
x accel Noise	*WN* (0.013 m/s^2)
y accel Noise	*WN* (0.018 m/s^2)
z accel Noise	*WN* (0.010 m/s^2)
p gyro Bias	*GM*(0.0552 °/s, 300 s)
q gyro Bias	*GM*(0.0552 °/s, 300 s)
r gyro Bias	*GM*(0.0552 °/s, 300 s)
x accel Bias	*GM*(0.0124 m/s^2, 300 s)
y accel Bias	*GM*(0.0124 m/s^2, 300 s)
z accel Bias	*GM*(0.0124 m/s^2, 300 s)
ADM	
Coefficients (on all except the flap coefficients)	*GM* (10 %, 120 s)
Control Inputs	*WN* (0.02 °) aileron, rudder, elevator.

Centre of Gravity Error [x, y, z]	constant [0.03, 0.03, 0.03] m
Mass Error	2% of true
Moment of Inertia Error, [J_x, J_y, J_z, J_{xz}]	2% of true
Thrust Error	Force, 5% of true, Moment 5% of true
Environmental	
Wind [North, East, Down]	[10 kn, 10 kn, 2 kn]
Gravity Error 1σ	36 μg
Air Density Error	5% of true
Speed of sound Error	5% of true
Air Data	
Airspeed Measurement Noise	*WN* (2.5 m/s)
Airspeed Measurement Bias	3 m/s
Angle of Attack Measurement Noise	*WN* (0.25 °)
Angle of Attack Measurement Bias	2 °
Angle of Sideslip Measurement Noise	*WN* (0.25 °)
Angle of Sideslip Measurement Bias	2 °
Initialisation Error	
Attitude (Roll, Pitch, Yaw)	5 °
Velocity (North, East, Down)	2 m/s
Position (North, East, Down)	3 m

Table 3 ***Simulation Parameters used for Simulated Flight.***

The “initialization error” in Table 3 is the accuracies to which the Kalman filters were initialized at the start of the approach for the position, velocity and attitude states. The estimates for IMU biases and GPS receiver clock biases were all initialized to zero.

An APV approach was simulated starting from 1500 feet altitude and descending at a rate of between 350-500 ft/min in the vicinity of Brisbane airport, Australia. This is shown in Figure 16. This segment is from an arbitrarily chosen Final Approach Fix (FAF) waypoint to an arbitrary Decision Height (DH) at 375 ft. The average approach speed was approximately 70 knots.

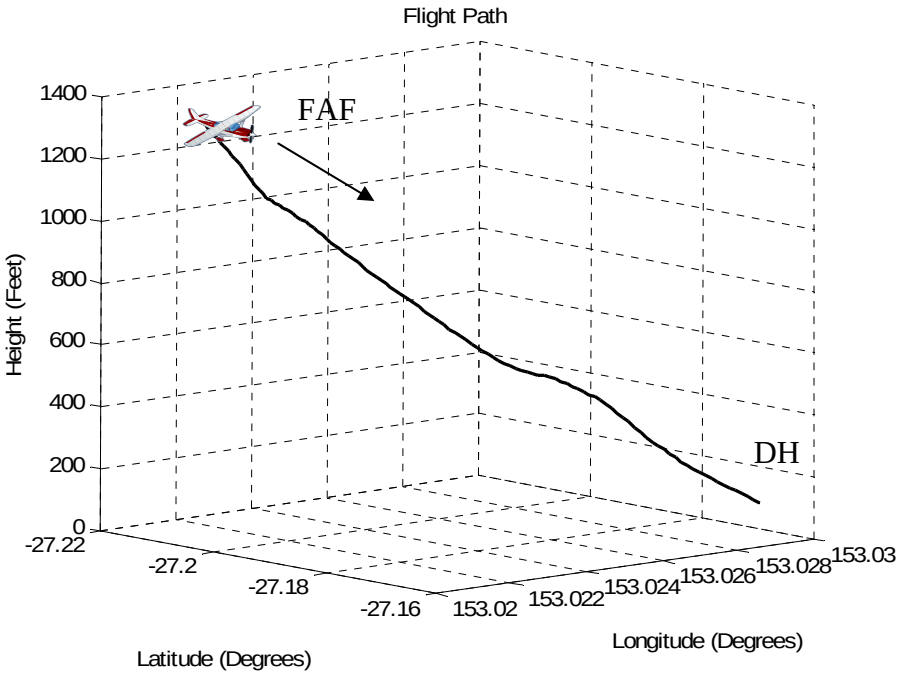

Figure 16 ***The Simulated APV Approach.***

An average of 8 satellites was visible above the elevation mask during the approach as shown in Figure 17. As seen, satellites occasionally dropped in and out and this is due to the satellites dropping below the antenna elevation mask angle due to aircraft motion.

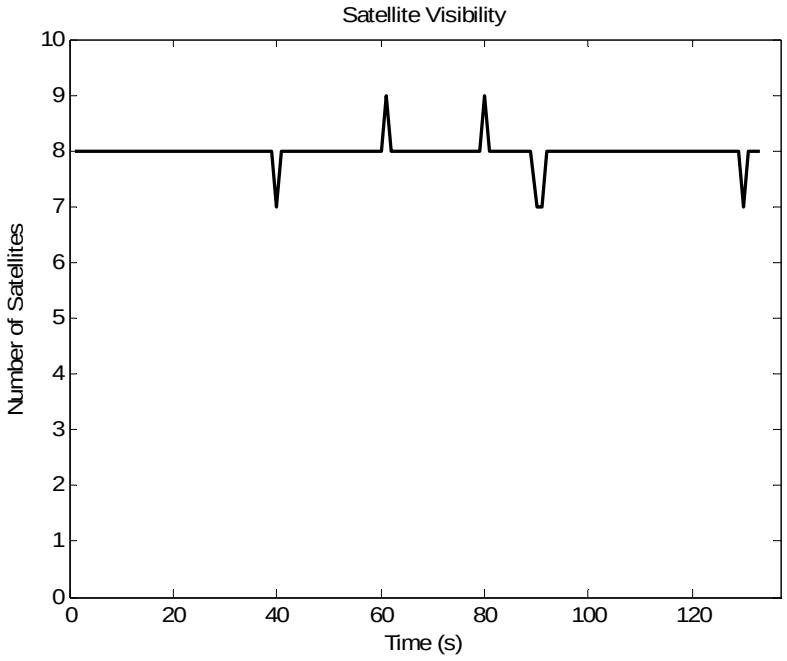

Figure 17 ***Satellite Visibility.***

The next section will compare the GPS-only fault detection, GPS-IMU EKF and GPS-ADM EKF in accuracy, protection levels and detection of ramp faults.

4.3 Comparison Between Stand-alone GPS, GPS-IMU EKF and GPS-ADM EKF Architectures

4.3.1 Accuracy Comparison

The aim of this section is to compare the accuracy of the GPS-only fault detection architecture of Section 3.12, the GPS-IMU EKF of Section 3.8 and the GPS-ADM EKF of Section 3.9.

As stated in Section 3.7.5, the protection levels partly depend upon the position state covariance estimates from both the full and sub-filters. For this reason a comparison between the horizontal and vertical position covariances will be made first before the accuracy results are shown. Figure 18 shows the trace of the position component (north, east, down) of the apriori error covariance of the GPS-ADM EKF (*P^- ADM* in the legend of the figure) and GPS-IMU EKF (*P^- IMU* in the legend of the figure). The calculated position covariance from the GPS-only architecture of Section 3.12 is also given for comparison *(P GPS* in the legend of the figure), which is a function of the satellite geometry and expected pseudorange noise.

In Figure 18 the covariance of the GPS-IMU EKF was approximately 9 m smaller than the GPS-ADM EKF and 6 m smaller than the GPS covariance for the entire simulated approach. However the GPS-ADM EKF covariance was approximately 4 m higher than the GPS covariance. This indicates that with the noise values considered on the ADM in this scenario (Table 3) the uncertainty on the ADM grew more rapidly between GPS updates than for the IMU. In other words, the ADM estimates are not as accurate as the IMU which can be expected considering that the ADM cannot measure unknowns such as wind whereas the IMU can.

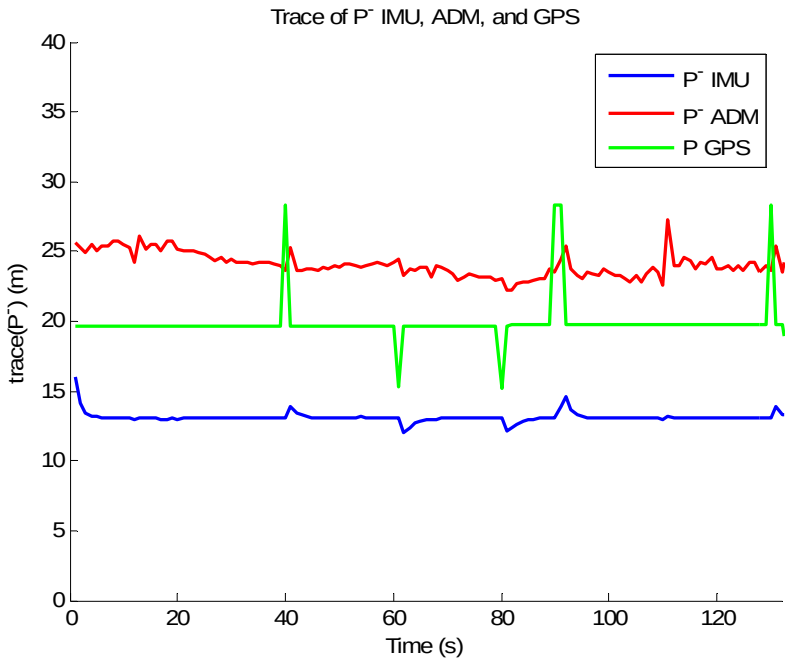

Figure 18 ***Comparison between apriori error covariances of GPS-IMU EKF, GPS-ADM EKF and GPS.***

Figure 19 shows the trace of the position component (north, east, down) of the error covariance of the GPS-ADM EKF *(P ADM*) and GPS-IMU EKF (*P IMU*) after the GPS measurement update. In this case, the covariance of the GPS-IMU EKF was approximately 14 m and the covariance of the GPS-ADM EKF was approximately 16 m smaller than the GPS covariance (*P GPS*) of approximately 20 m. This reduction in covariance is a benefit of fusing the GPS with an IMU or ADM in an Extended Kalman Filter. It can also be observed by comparing Figure 17 with Figure 19 that the changing satellite constellation influenced the GPS covariance more than it affected the GPS-IMU EKF and GPS-ADM EKF covariances. When a satellite was lost or gained in Figure 17, *P GPS* in Figure 19 increased or decreased (compare a rise of approximately 8 m at 40 seconds for *P GPS* with a rise of approximately only 1 m for *P IMU* and *P ADM*). The change in protection levels due to satellite changes for the GPS-IMU EKF and GPS-ADM EKF were not as significant. This shows less dependence of the EKF architectures on good satellite geometry than the GPS-only architecture.

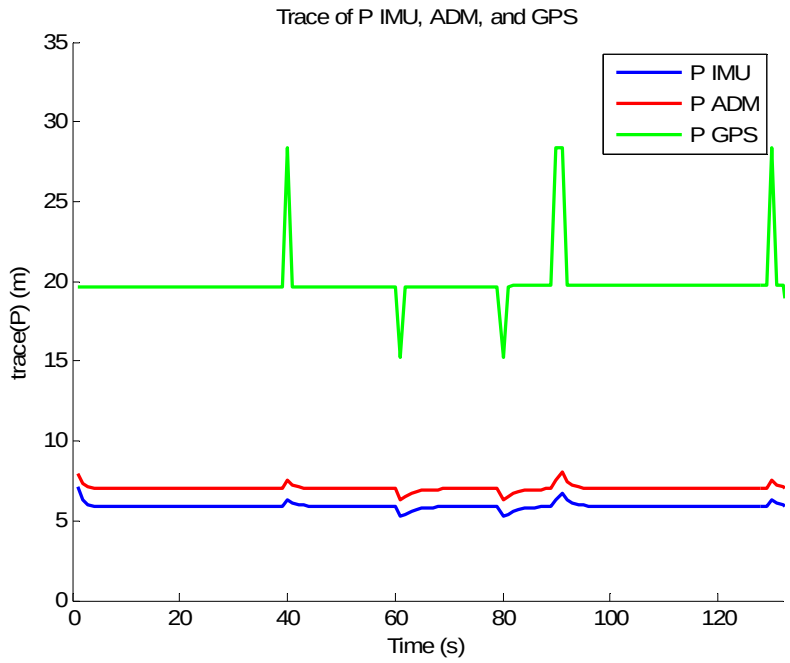

Figure 19 ***Comparison between error covariances of GPS-IMU EKF, GPS-ADM EKF and GPS, showing a reduction with GPS-IMU EKF and GPS-ADM EKF.***

Now the accuracy will be compared against the accuracy requirements of Table 2. For the horizontal case Figure 20 compares the accuracy (d_{major}) for the standalone GPS architecture, GPS-IMU EKF and GPS-ADM EKF against the requirement ($d_{major-\max}$ as indicated by the black line) as per Section 3.7.3. The accuracy of the GPS-IMU EKF and GPS-ADM EKF was approximately 1.2 m and 1 m which was lower than the GPS-only accuracy of approximately 1.8 m. It can be seen that the GPS, GPS-IMU EKF and GPS-ADM EKF all met the accuracy requirement of 7 m.

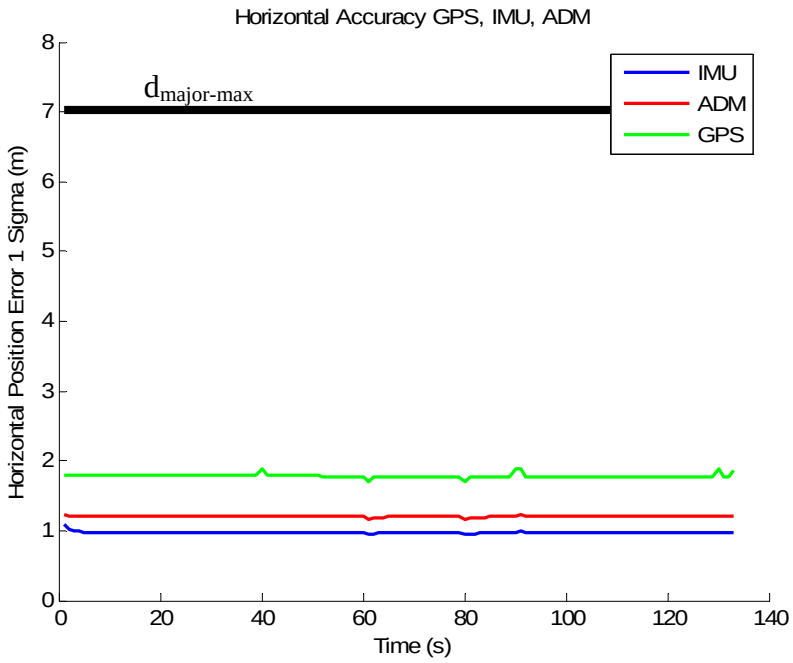

Figure 20 ***Comparison between horizontal accuracies of GPS-IMU EKF, GPS-ADM EKF and GPS, showing a reduction with GPS-IMU EKF and GPS-ADM EKF.***

For the vertical case Figure 21 compares the accuracy (σ_V) for the standalone GPS architecture, GPS-IMU EKF and GPS-ADM EKF against the requirement ($\sigma_{V-\max}$, as indicated by the black line) as per Section 3.7.3. The accuracy of the GPS-IMU EKF and GPS-ADM EKF was approximately 2 m and 2.1 m which was lower than the GPS-only accuracy of approximately 3.8 m. It can be seen that all architectures met the accuracy requirement of 8.5 m.

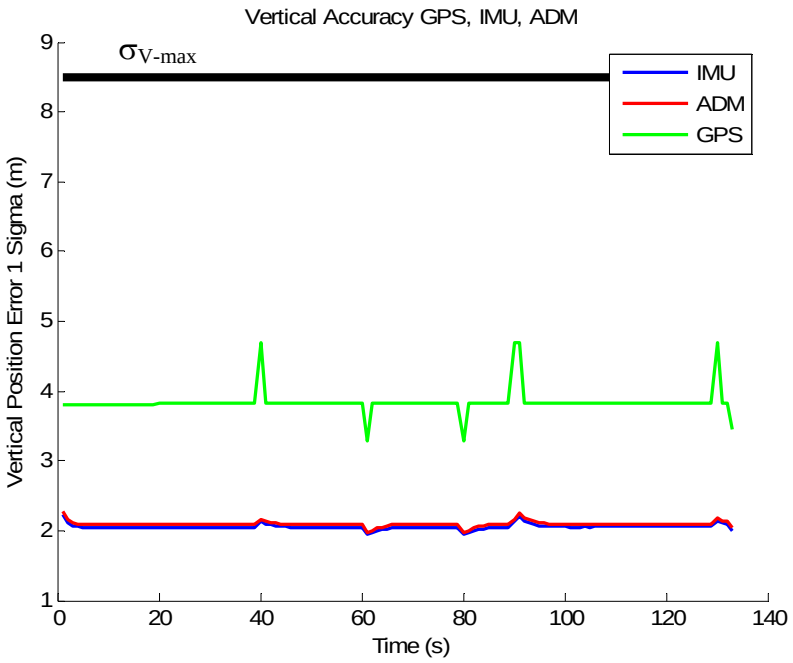

Figure 21 ***Comparison between vertical accuracies of GPS-IMU EKF, GPS-ADM EKF and GPS, showing a reduction with GPS-IMU EKF and GPS-ADM EKF.***

Now that the accuracy requirement is seen to be satisfied in this scenario, the following section will compare the protection levels.

4.3.2 Protection Level Comparison

The aim of this section is to compare the protection levels of the GPS-only fault detection architecture of Section 3.12, with the GPS-IMU EKF of Section 3.8 and GPS-ADM EKF of Section 3.9.

Figure 22 compares the HPL against the HAL requirement (40 m). As can be seen the GPS-IMU EKF had the smallest protection levels at approximately 10 m, followed by the GPS-ADM EKF at approximately 11 m and finally the GPS, which had the largest protection levels at approximately 19 m. The GPS-IMU EKF HPL was calculated to 48.5% lower and the GPS-ADM EKF HPL was 43.7% lower than the GPS HPL, averaged over the whole simulated approach. All systems met the horizontal alert requirement, since the protection levels were smaller than the alert limit.

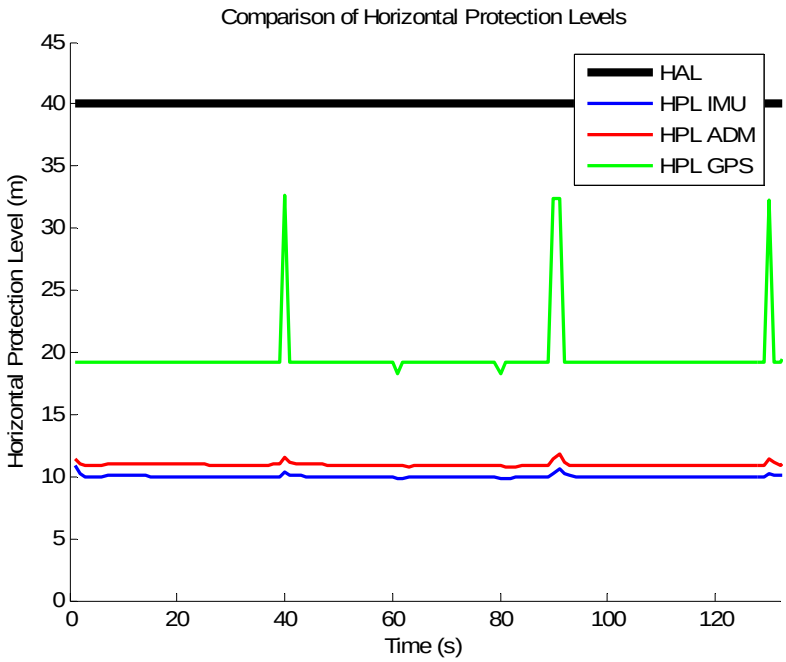

Figure 22 ***Comparison between HPL of GPS-IMU EKF, GPS-ADM EKF and GPS, showing a reduction with GPS-IMU EKF and GPS-ADM EKF.***

Figure 23 compares the VPL against the VAL requirement (50 m). The results are similar to the HPL seen previously. The GPS-IMU EKF had the smallest protection levels, approximately 13.2 m, followed by the GPS-ADM EKF at approximately 13.3 m and finally the GPS, which had the largest protection levels at approximately 26 m. The GPS-IMU EKF VPL was calculated to 49.6% lower and the GPS-ADM EKF VPL was 49.2% lower than the GPS VPL, averaged over the whole simulated approach. As seen, the GPS-IMU EKF and GPS-ADM EKF systems met the alert limit requirements all of the time but the GPS VPL exceeds the VAL three times (at about times 40 s, 90s and 130 s) due to the drop in visible satellites.

Sudden “spikes” in HPL and VPL of the GPS can be noticed in Figure 22 and Figure 23 which shows the large influence which the satellite geometry can have on the protection levels. In general, as the number of satellites decrease (resulting in poorer geometry), the uncertainty in the position estimates increases, leading to an increase in protection levels. As mentioned in Section 2.5.3 the current GPS constellation is not supportive of APV integrity. This is one justification for using a filtered fault detection method and filtering the GPS measurements with an IMU or ADM instead of a snapshot GPS-only method. The fusion of the IMU or ADM with

the GPS means there is greater information available to the system to perform fault detection and there is less dependency upon having good GPS satellite geometry. The reduction in protection levels possible by fusing GPS with IMU or ADM can result in greater availability of the fault detection function, helping to meet the demanding *Availability* requirement of 99.999% in Table 2. This will be investigated further in Section 4.6 where the average protection levels over different satellite geometries in a 24-hour period are compared.

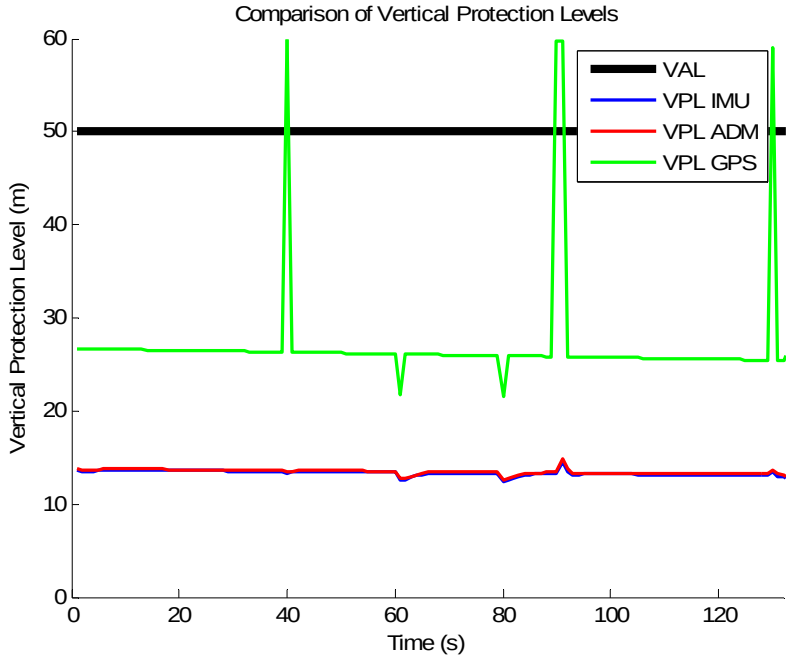

Figure 23 ***Comparison between VPL of GPS-IMU EKF, GPS-ADM EKF and GPS, showing a reduction with GPS-IMU EKF and GPS-ADM EKF.***

It has been seen that fusing GPS with the ADM can result in a smaller HPL and VPL than GPS alone. However fusing GPS with the IMU gave the lowest protection levels overall. The following results will compare the GPS-IMU EKF, GPS-ADM EKF and GPS-only architecture in detecting ramp faults.

4.3.3 Ramp Fault Detection Comparison

The previous section compared the protection levels against the alert limit requirements. The purpose of this section is to investigate the performance of detecting a 0.5 m/s ramp fault and a 2.5 m/s ramp fault. The ramp fault was applied on the pseudorange of the "most difficult to detect" satellite starting at 25 seconds into the simulation. As shown in Figure 24, according to the requirements [28] if the

phase of flight is known the fault must be detected before the position error exceeds the alert limit within the Time to Alert (TTA).

First the case for the 0.5 m/s ramp fault was tested. Then the test was repeated with the 2.5 m/s ramp fault. These magnitudes of ramp fault were chosen because they are within a test range of 0.01 m/s to 5 m/s from [28]. Slowly growing errors within this range are considered to be difficult to detect. 0.5 m/s was found by trial and error in the simulations to be the smallest ramp fault which caused a significant enough position errors to exceed the protection levels before the simulated flight was over. Ramp faults smaller than 0.5 m/s may be considered for further research, however extremely slow growing faults are likely to be detected by the GPS control segment [54].

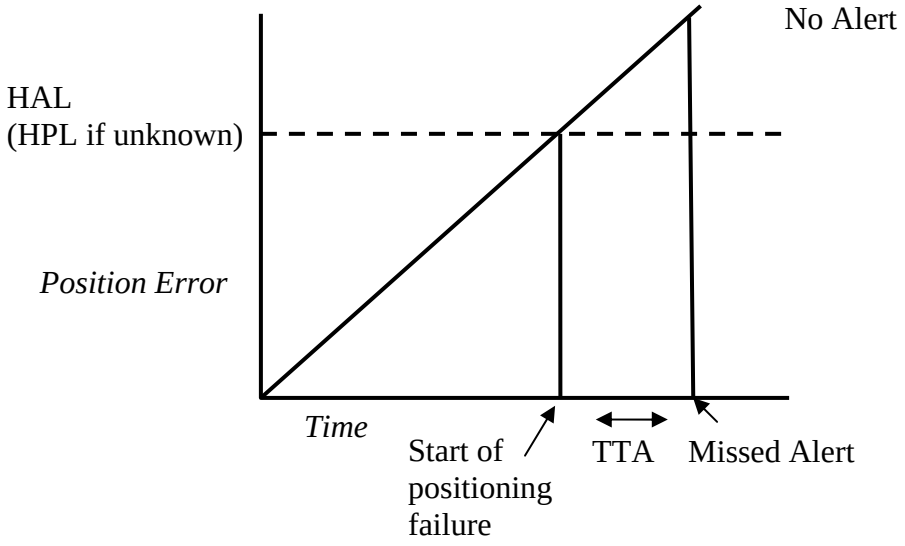

Figure 24 ***Position Error causing Missed Alert.***

Figure 25 shows the horizontal test statistics versus thresholds for the GPS-IMU EKF. The Horizontal Position Error (HPE) and HPL are also given. The fault is detected when the test statistic exceeds the threshold as indicated on the diagram and it should be detected before the HPE exceeds the HPL, in accordance with the horizontal P_{md} requirement. As indicated on Figure 25 by the arrow, the fault was detected at time 57 s before the HPE crossed the HPL at time 75 s.

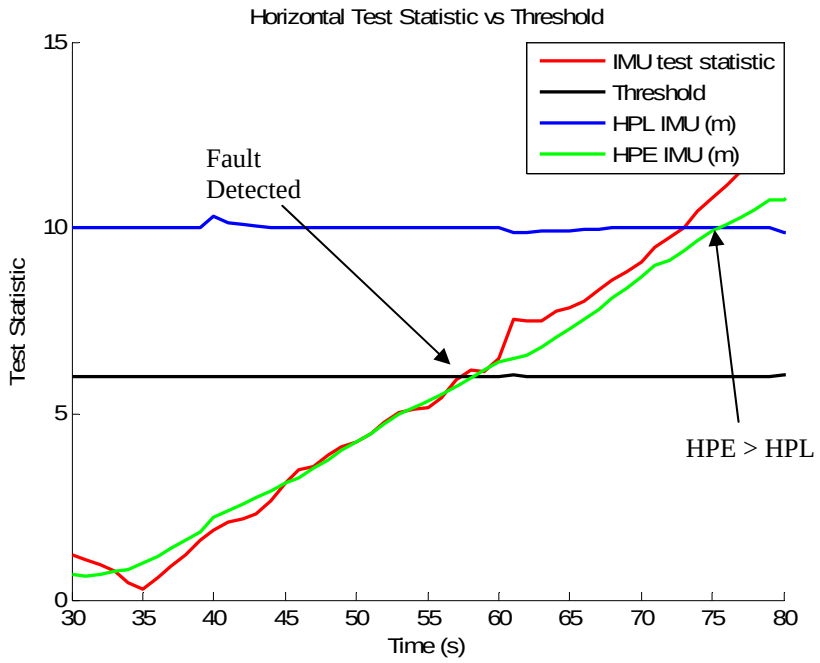

Figure 25 ***Horizontal Test Statistic vs Threshold for GPS-IMU EKF, showing the ramp fault being successfully detected.***

Figure 26 shows the vertical test statistics versus thresholds for the GPS-IMU EKF. The Vertical Position Error (HPE) and VPL are also given. The fault is detected when the test statistic exceeds the threshold as indicated on the diagram and it should be detected before the VPE exceeds the VPL, in accordance with the vertical P_{md} requirement. As indicated by the arrow, the fault was detected at time 58 s one second after the VPE crossed the VPL at time 57 s. In each of the horizontal and vertical cases the fault was detected well before the position errors exceeded the HAL and VAL requirements (40 m HAL and 50 m VAL).

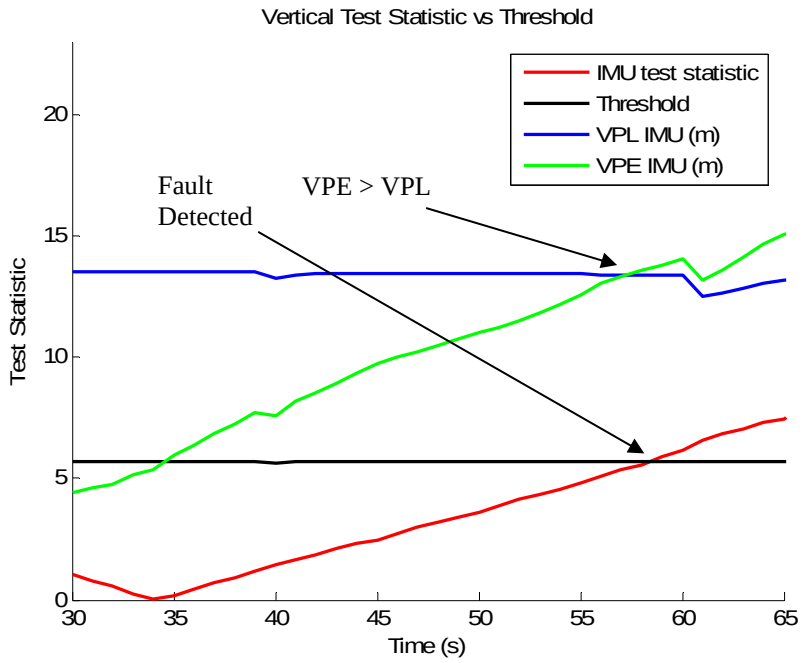

Figure 26 ***Vertical Test Statistic vs Threshold for GPS-IMU EKF, showing the ramp fault being successfully detected.***

Results were similar for the GPS-ADM EKF. Figure 27 and Figure 28 show the horizontal and vertical test statistics versus thresholds for the GPS-ADM EKF. In Figure 27 the fault was detected at time 59 s before the HPE crosses the HPL at time 79 s. In Figure 28 the fault was detected at time 58 s after the VPE crossed the VPL at time 57 s. The GPS-ADM EKF showed a similar capability in detecting the ramp fault as the GPS-IMU EKF.

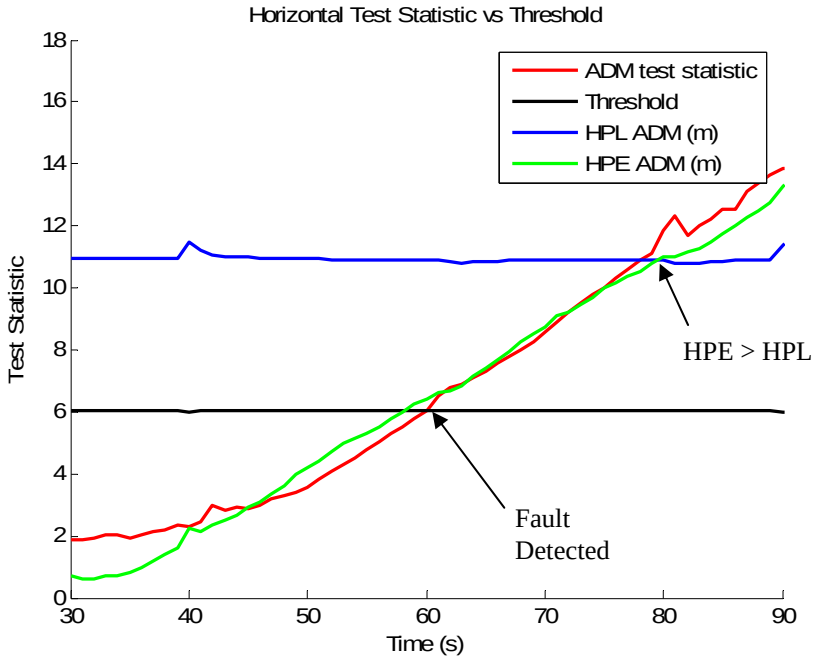

Figure 27 ***Horizontal Test Statistic vs Threshold for GPS-ADM EKF, showing the ramp fault being successfully detected.***

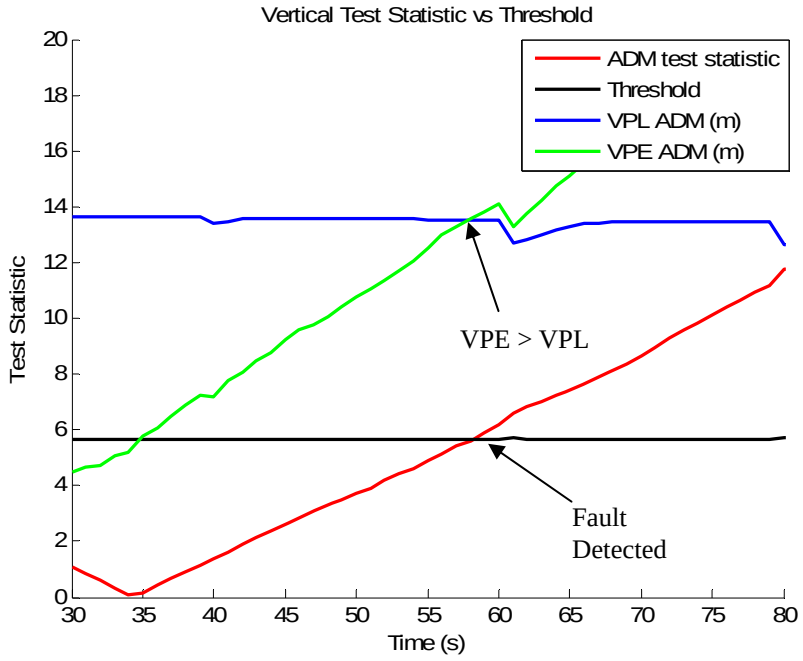

Figure 28 ***Vertical Test Statistic vs Threshold for GPS-ADM EKF, showing the ramp fault being successfully detected.***

Whilst the faults were detected before the HPE exceeded the HPL, it appears that for both the GPS-IMU EKF and GPS-ADM EKF it was more difficult to detect the fault in the vertical direction since the VPE exceeded the VPL about 1 second before the fault was detected. However this does not necessarily mean that the protection

level requirement is not met. Monte Carlo simulation would be required to verify that the P_{md} requirement is met. For a P_{md_V} of 0.045, it would be expected that out of 10,000 runs, 475 runs would show the fault not being detected before the position error exceeds the protection level. However GARDSim is not able to do such extensive Monte Carlo simulation within any practical time-frame to verify that P_{md} is met, therefore this is left for further work. If it is found that the P_{md} requirement is not met, the statistics may need to be adjusted (recall that greater allocation of P_{md} was given to the vertical case in Section 3.7.1, for example increase from 95% allocation to the vertical to 99% allocation) to give an increase in VPL. Alternatively the filters may need to be tuned more conservatively to give a corresponding increase in VPL to ensure that the P_{md} requirement is met.

Figure 29 and Figure 30 show the horizontal and vertical test statistics versus thresholds for the GPS-only architecture. In Figure 29 the fault was detected at time 79 s before the HPE crossed the HPL at time 113 s. In Figure 30 the fault was detected at time 79 s before the VPE crossed the VPL at time 98 s.

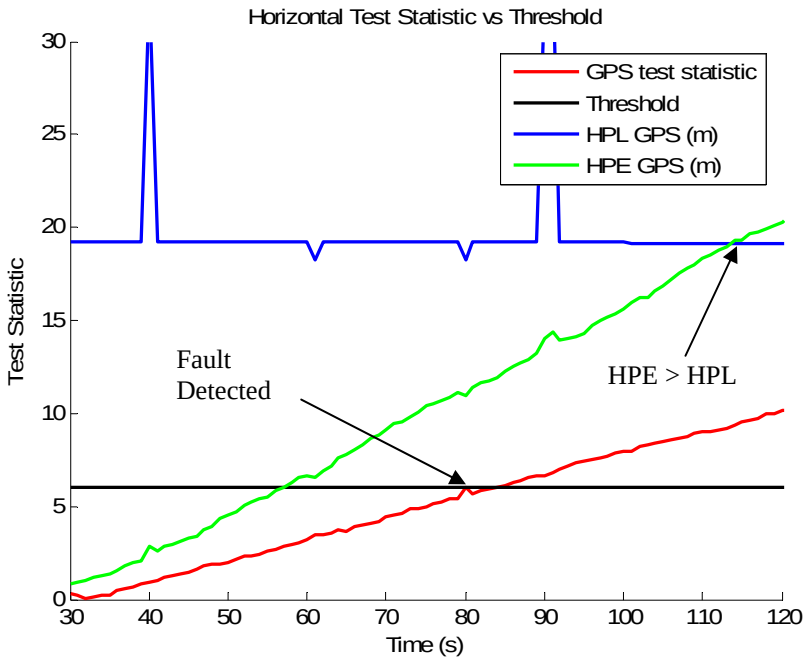

Figure 29 ***Horizontal Test Statistic vs Threshold for GPS, showing the ramp fault being successfully detected.***

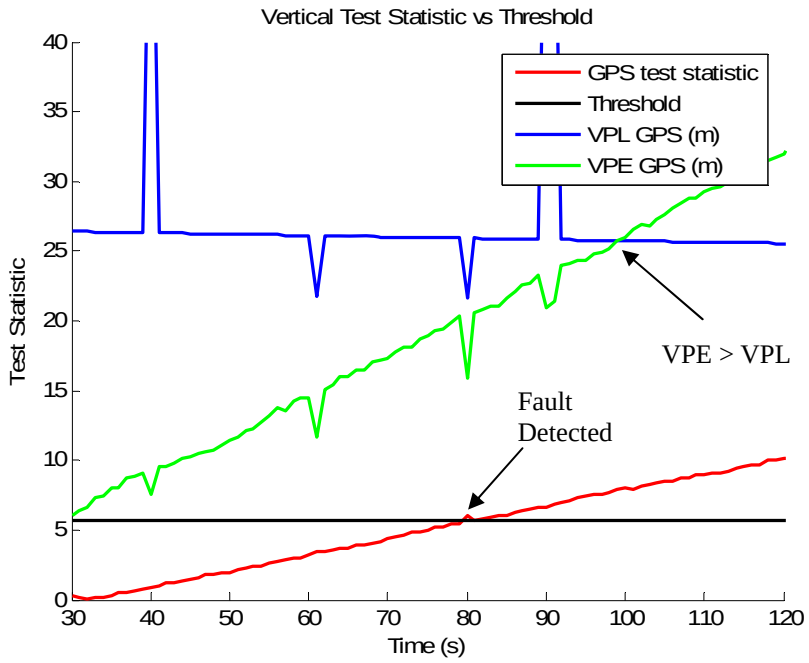

Figure 30 ***Vertical Test Statistic vs Threshold for GPS, showing the ramp fault being successfully detected.***

The same test was repeated for a 2.5 m/s ramp fault. The results are summarized in Table 4. In Table 4, *Time to Detection* is the time it took until the fault was detected, from the onset of the fault to the time when the fault is detected. *Time to NSE > PL* is the time it took for the Navigation System Error (NSE) to exceed the protection level (PL). As seen the GPS-IMU EKF was the fastest in detecting the faults for the 0.5 m/s case, approximately 1 second sooner than the GPS-ADM EKF and 20 seconds sooner than the GPS methods. For the 2.5 m/s case there is less difference between the *Time to Detection* which was approximately 3 seconds sooner for the GPS-IMU EKF and GPS-ADM EKF compared to the GPS.

These results demonstrate that fault detection of 0.5 and 2.5 m/s ramp faults is achievable using GAGIS and gives a relative comparison of the times to detection for the different architectures for this single case. The results also show that the GPS-IMU EKF and GPS-ADM EKF can detect slowly growing ramp faults sooner than GPS-only. The HPL and VPL should bound the true error within the probability of missed detection requirement. However since these results are only for a single case these results cannot be used to guarantee that P_{md} is met. Although the NSS method has analytically-derived protection levels, the EKF is a suboptimal filter and whilst the EKF is tuned to be consistent in these simulations, the covariance calculated by

the EKF may not be exactly equal to the true covariance. For this reason extensive Monte Carlo simulation consisting of many simulation runs can be used to validate that the P_{md} is met but this is time consuming [66]. GARDSim is not able to do extensive Monte Carlo simulation within a practical timeframe therefore validation that GAGIS meets the P_{md} requirement is left for further work.

Whilst the protection levels may need to be increased or decreased slightly as necessary pending the outcome of any Monte Carlo simulations, a more dangerous situation is if the position error exceeds the HAL or VAL without being detected. It can be seen that all systems detected the fault before the error ever grows large enough to not be detected. Also, other fault detection methods may have better performance at detecting slowly growing ramp faults in GAGIS such as a rate detector algorithm as presented in [50]. Investigation of this is left for further work.

	0.5 m/s ramp fault		***2.5 m/s ramp fault***	
Architecture	***Time to Detection (s)***	***Time to NSE > PL (s)***	***Time to Detection (s)***	***Time to NSE > PL (s)***
GPS-IMU EKF H	32	50	9	12
GPS-IMU EKF V	33	32	9	9
GPS-ADM EKF H	34	54	8	12
GPS-ADM EKF V	33	32	9	9
GPS H	54	88	12	18
GPS V	54	73	12	15

Table 4 ***Comparison of 0.5 m/s and 2.5 m/s Fault Detection Times, showing earlier fault detection for GPS-IMU EKF and GPS-ADM EKF.***

4.3.4 Conclusion

In Section 4.3 the aim was to compare and investigate the GPS-IMU EKF, GPS-ADM EKF and stand-alone GPS architectures in accuracy, protection levels and detection of a 0.5 m/s and 2.5 m/s ramp fault.

In Section 4.3.1 the results for accuracy were presented. Firstly the position covariances were compared. It was shown that the GPS-IMU EKF and GPS-ADM EKF covariances were smaller than the GPS. This is a benefit of fusing GPS with IMU or ADM. The accuracy was then compared against the requirements and shown that all systems met the accuracy requirements.

In Section 4.3.2 the protection levels were compared. The GPS-IMU EKF HPL was calculated to be 48.5% lower and the GPS-ADM EKF HPL was 43.7% lower than the GPS HPL, averaged over the whole simulated approach. The GPS-IMU EKF VPL was calculated to be 48.5% lower and the GPS-ADM EKF VPL was 43.7% lower than the GPS VPL, averaged over the whole simulated approach. Although fusing GPS with either IMU or ADM resulted in a reduction in protection level, GPS-IMU EKF protection levels were lower than the GPS-ADM EKF. This is to be expected that the ADM would be less accurate and have greater uncertainty than the IMU since the ADM cannot measure the uncertain wind for example, whereas the IMU can. It was also seen that the GPS-only protection levels were more dependent upon satellite geometry than the EKF architectures and the GPS VPL exceeded the VAL momentarily on three occasions. The change in protection levels due to satellite changes for the GPS-IMU EKF and GPS-ADM EKF were not as significant.

In Section 4.3.3 the performance of the GPS-only, GPS-IMU EKF and GPS-ADM EKF architectures was compared in detecting a 0.5 m/s and 2.5 m/s ramp fault applied on the pseudorange of the “most difficult to detect” satellite. It was found that the GPS-IMU EKF and GPS-ADM EKF detected the faults approximately 20 seconds sooner than the GPS. It shows that GAGIS can detect the 0.5 m/s and 2.5 m/s faults and gives relative comparisons between the different architectures. However this is only a single case and does not prove that the P_{md} is met. Although

with the NSS method the protection levels can be verified analytically without the need for Monte Carlo simulation, in GAGIS it was used with the EKF which is an approximate filter. Whilst the EKF was tuned conservatively and consistently in the simulations, the EKF may not estimate the true covariance because it is really a pseudo-covariance (Section 3.6). To verify that the P_{md} is met, Monte Carlo simulation is required which is beyond the capability of GARDSim. Therefore this is left for further work. If it is found that P_{md} is not met, it may require re-tuning of the filters giving an increase in protection levels to ensure that they bound the error. This may be a limitation of using the EKF in practice. Inaccurate covariance estimates, if significant enough, may justify the investigation into using nonlinear filters such as the UKF [64].

Whilst the GPS-ADM EKF could not achieve protection levels as low as the GPS-IMU EKF, it did improve the performance over the GPS-only architecture. The ADM may serve to replace or supplement the IMU as the provider of dynamic information in the filters in instances where an IMU fails. For example, a loss of a single accelerometer may be supplemented or replaced by the information provided from the ADM. This will be investigated in Section 4.8

The following section will investigate the protection levels of the GPS-ADM EKF with Wind Estimation architecture of Section 3.10.

4.4 GPS-ADM EKF with Wind Estimation Architecture Results

The purpose of this section is to investigate the protection levels of the GPS-ADM EKF with Wind Estimation architecture of Section 3.10 and whether or not correcting the ADM with wind estimates can result in lower protection levels.

In Section 4.3 a scenario was simulated where the wind contained a constant mean velocity and gust component (Table 3). For the results in this section another simulated flight was run whilst considering the effects of wind shear.

The Aerosim wind gust and shear models applied a shear component to the aircraft body angular rates (*p*, *q*, *r*) and a mean velocity plus turbulence (gust) component to the body velocities (*u*, *v*, *w*) of the aircraft [73]. Because the effects of wind are simulated during generation of the truth data using Aerosim, another approach had to be flown. During the approach the wind conditions were changed to simulate wind shear at altitudes chosen arbitrarily in the following sequence:

The specified mean wind velocities input to Aerosim's wind model were labeled wind conditions W1 through to W4.

(W1)10 kn (5.14 m/s) North, 10 kn (5.14 m/s) East, 2 kn (1.03 m/s) Down from 1500 ft to 1200 ft. This was the initial wind.

(W2) -10 kn (-5.14 m/s) North, -10 kn (-5.14 m/s) East, 2 kn (1.03 m/s) Down at an altitude of 1200 ft. This was an opposite change in horizontal direction, with the same magnitude as in (W1).

(W3) 15.8 kn (8.14 m/s) North, 10 kn (5.14 m/s) East, 5.9 kn (3.03 m/s) Down at an altitude of 600 ft. This was another opposite change in horizontal direction as well as an increase in magnitude.

(W4) 10 kn (5.14 m/s) North, 10 kn (5.14 m/s) East, 2 kn (1.03 m/s) Down at an altitude of 450 ft. The winds were changed to the same as (W1) just before the MAP.

Figure 31 is a plot of the wind velocity magnitudes in the north, east, down directions over time. The times when the wind conditions W1 to W4 were simulated are indicated on the figure. Encountering three wind direction changes would be a case of severe wind shear since only one wind direction change is usual on a real approach. It was considered to see if the GPS-ADM EKF could perform in these conditions.

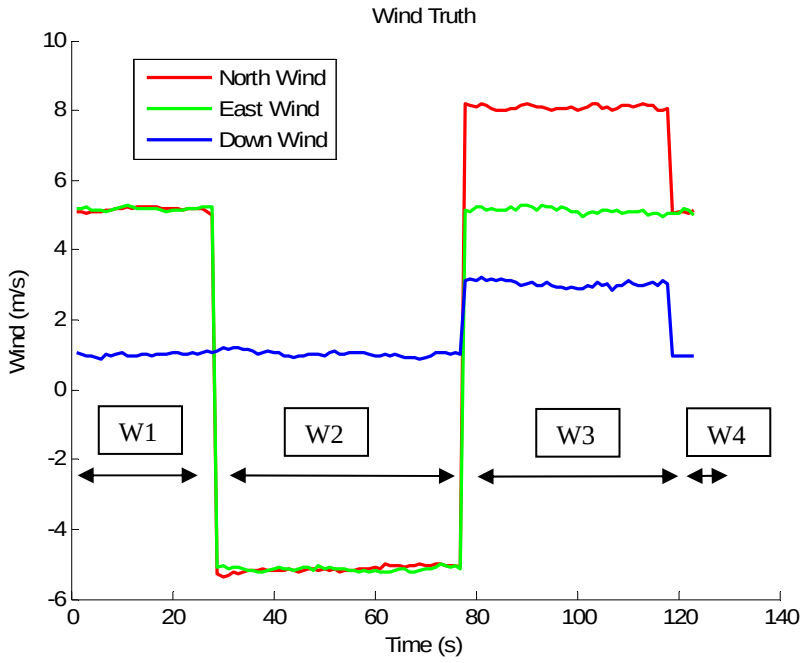

Figure 31 ***Simulated North, East, Down Wind Velocities.***

The simulated flight path is given in Figure 32. The sudden changes in wind meant the aircraft had to be steadied to keep it at a constant rate of descent. This resulted in momentary disruptions in the flight path as indicated on Figure 32, due to sudden changes in wind direction. If significant enough these disruptions may mean that the assumptions of steady state flight for the linear ADM are not valid and a nonlinear model may provide better performance (refer Section 3.5.2). However GPS updates correct for this modeling error at 1 Hz. Whether an improvement may be gained by using a nonlinear ADM is an area for possible further research.

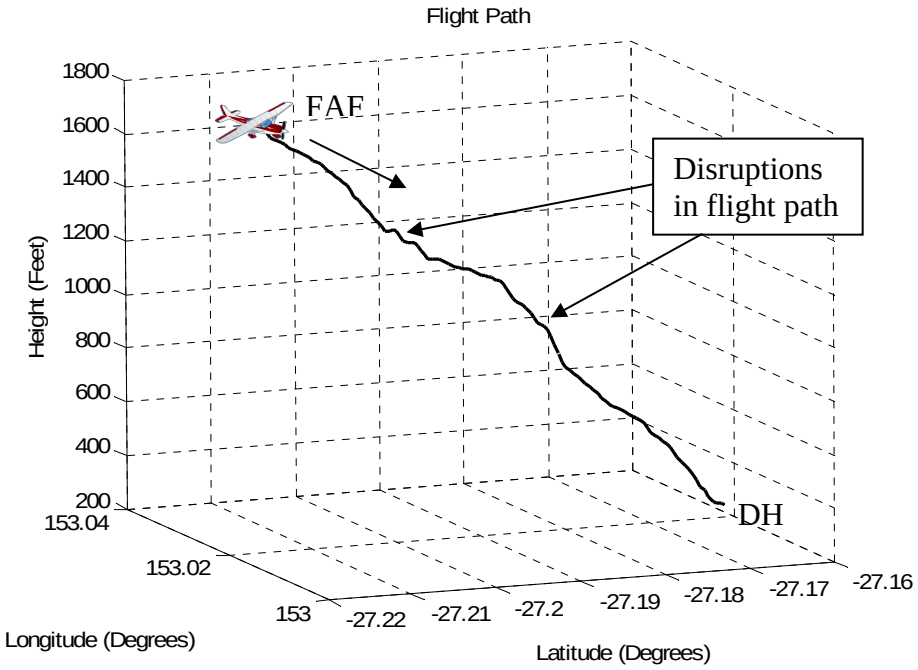

Figure 32 ***The Simulated APV Approach with Wind Shear.***

The attitude changes of the aircraft resulted in decreases and increases of between 7 and 9 satellites as can be seen in Figure 33. This was due to roll angle changes of approximately 10 degrees and pitch angle changes of approximately 5 degrees as seen in Figure 34.

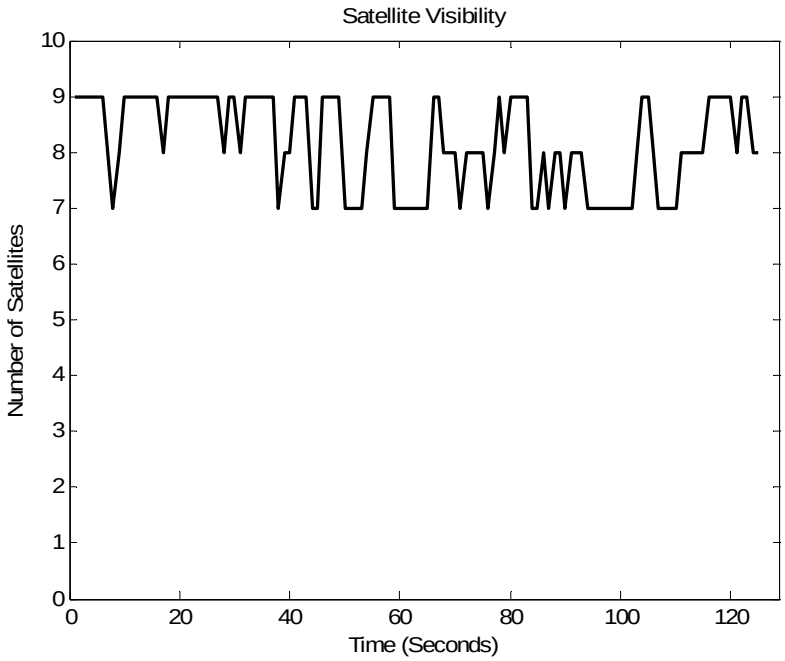

Figure 33 ***Satellite Visibility for wind shear scenario.***

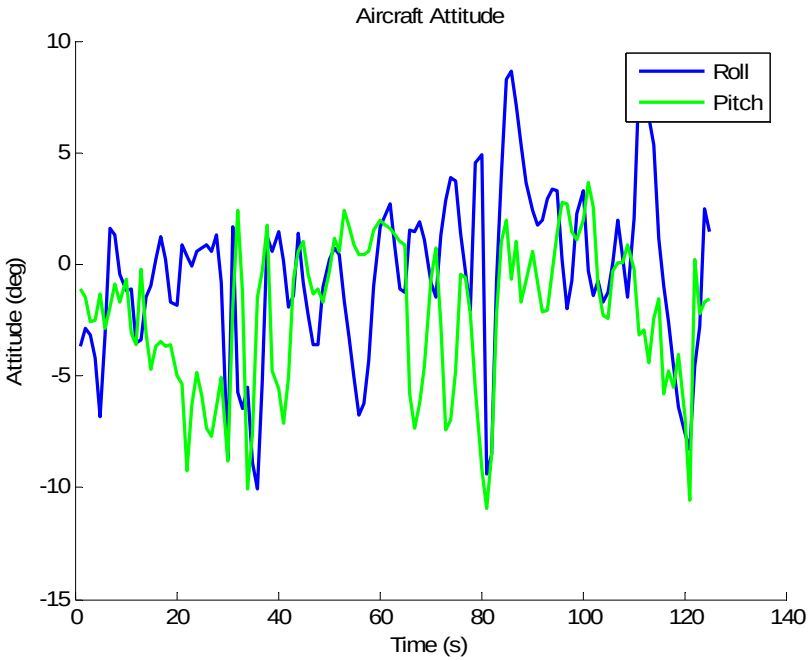

Figure 34 ***Aircraft Attitude on simulated APV approach with wind shear.***

The following section will present results for estimating the wind in the EKF using the method presented in Section 3.10.1.

4.4.1 Wind Estimation in the EKF Results

The purpose of this section is to investigate the accuracy of the wind estimates using the method in Section 3.10.1. This method estimated wind by augmenting the EKF state with North, East, Down wind estimates which were modeled as random walks. The magnitudes of the driving white noises for the wind estimates in (107) were specified as 10 m/s (1 sigma) in each direction.

Figure 35, Figure 36 and Figure 37 show the north, east and down wind velocity estimates compared to the true values of wind. As seen the wind was not estimated well, particularly for the Down wind estimate. Because wind is uncontrollable and unobservable it is a challenge to estimate it without any additional sensors. It should be noted the wind states in the Kalman filter are unobservable. Specially designed manouvres may help to achieve observability in the wind estimates as conducted in [14]. However an aircraft on the final approach would be unable to do any special maneuvers for estimating the wind so this is impractical. A better solution is to include air data and IMU measurements which will be investigated in the following

section.

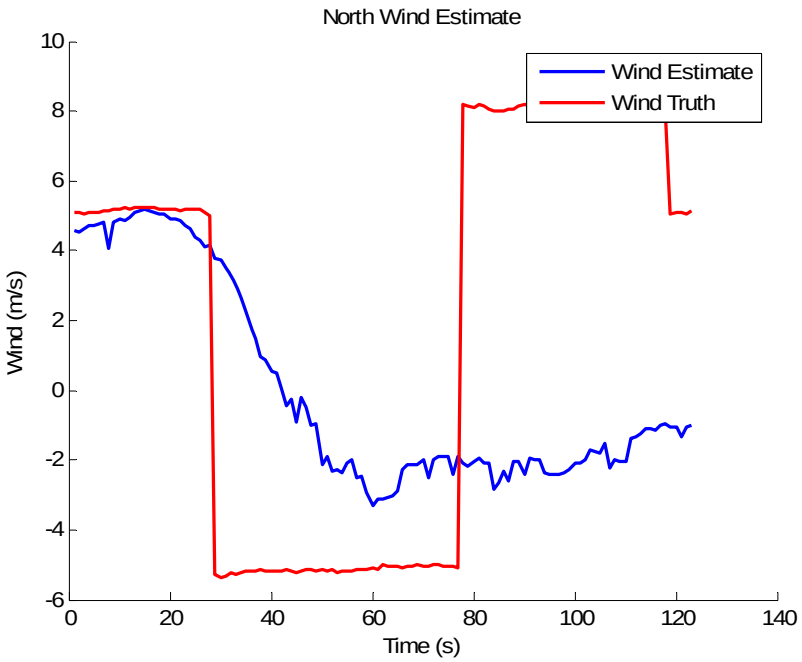

Figure 35 ***EKF North Wind Estimates.***

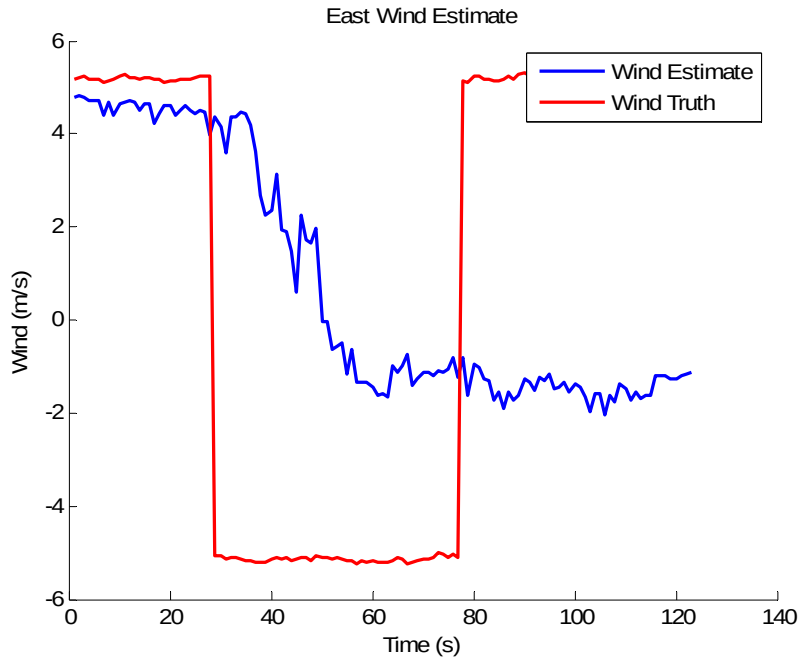

Figure 36 ***EKF East Wind Estimates.***

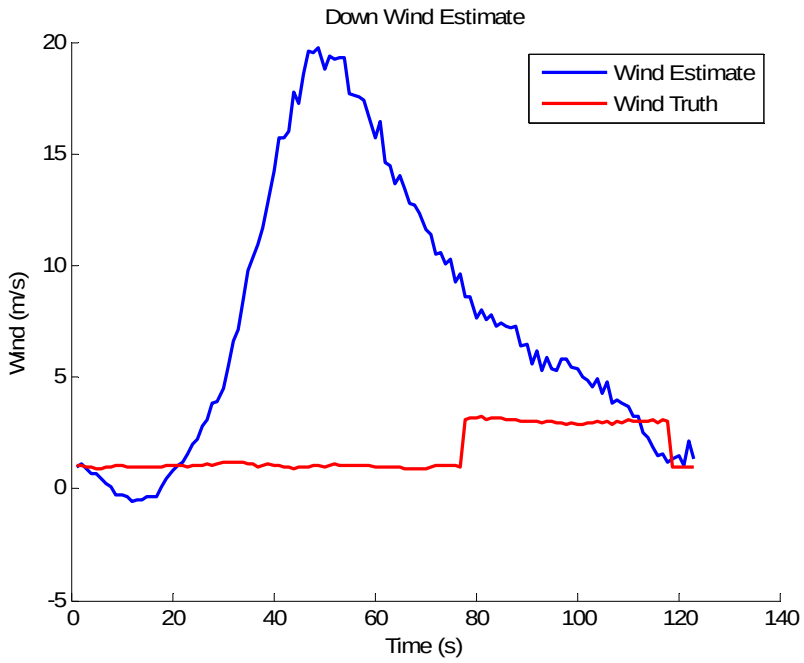

Figure 37 ***EKF Down Wind Estimates.***

In this section the accuracy of the wind estimates using the method in Section 3.10.1 was presented. The following section will present wind estimation results for the architecture in Section 3.10.2 which includes air data sensors and IMU.

4.4.2 Wind Estimation with Air Data Sensor and IMU Results

The purpose of this section is to evaluate the accuracy of the wind estimates with the aid of the IMU and air data sensors as per Section 3.10.2. Table 3 gives the values for a bias and noise assumed to be on the air data measurements. Figure 38, Figure 39 and Figure 40 show the north, east and down wind velocity estimates compared to the true values of wind. As seen, the wind estimates were more accurate with air data measurements than the previous results and the response was almost immediate when the wind conditions change at about 30 and 80 seconds. It can be seen that the estimates were biased which is due to the attitude estimate errors and the uncorrected bias on the air data measurements.

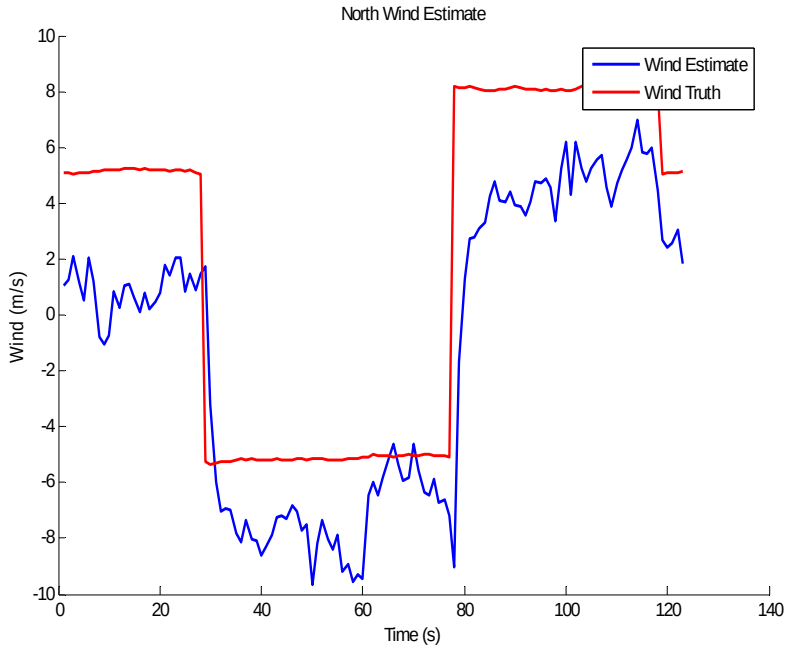

Figure 38 ***Air Data North Wind Estimates.***

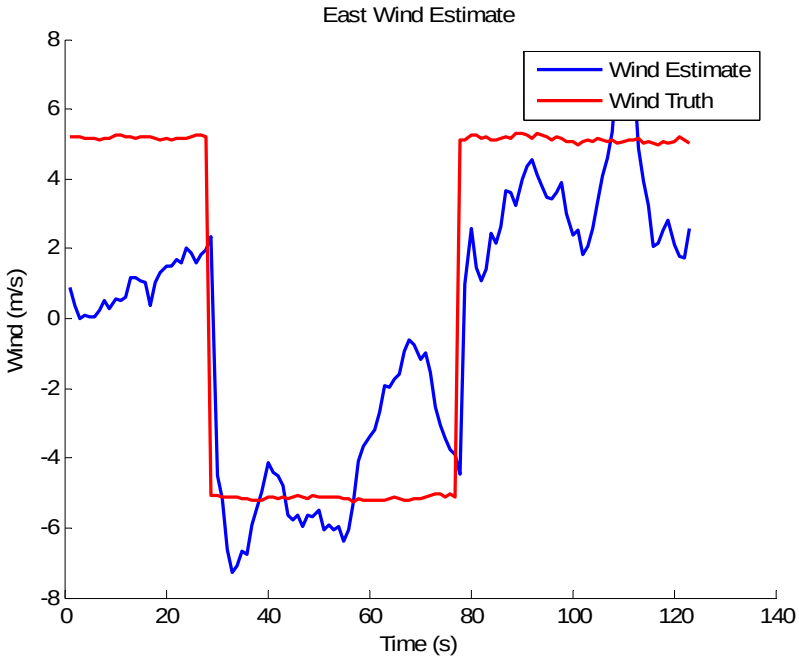

Figure 39 ***Air Data East Wind Estimates.***

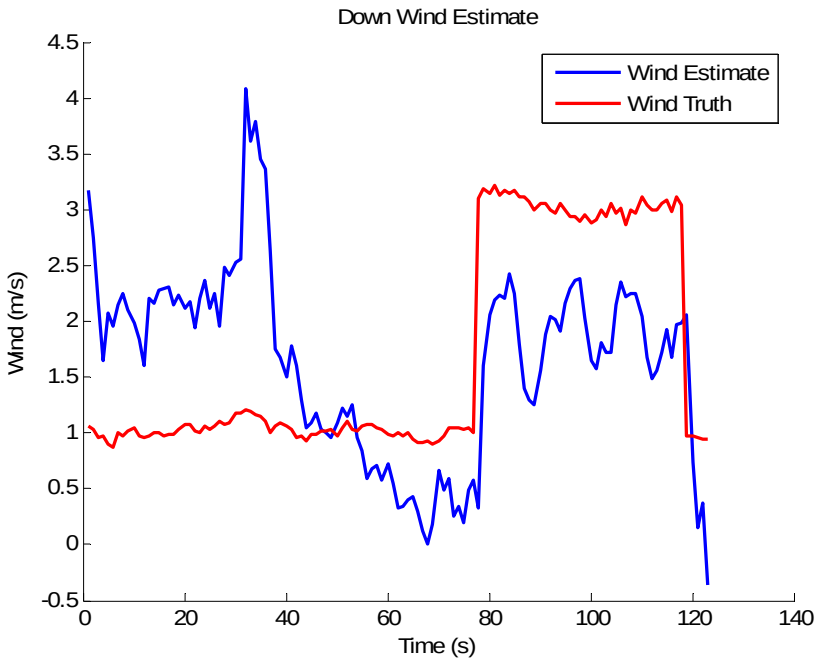

Figure 40 ***Air Data Down Wind Estimates.***

Wind estimation accuracies were presented for the architecture in Section 3.10.2. The following section will compare the protection levels of the GPS-ADM EKF with wind estimation architectures.

4.4.3 Protection Level Comparison

The purpose of this section is to compare the protection levels of the GPS-ADM EKF with wind estimation using the EKF, against with the GPS-ADM EKF which does not make any wind estimates. Referring to the legends of Figure 41 and Figure 42 *HPL ADM Wind* and *VPL ADM Wind* is the HPL and VPL using the wind estimates provided from the Kalman Filter as per Section 3.10.1 . *HPL ADM AD* and *VPL ADM AD* is the HPL and VPL using the wind estimates from air data sensors as per Section 3.10.2. *HPL ADM* and *VPL ADM* is the HPL and VPL calculated using the GPS-ADM EKF of Section 3.9, which does not estimate the wind at all. In each case the filters were tuned to be consistent.

Comparing the results, as seen in Figure 41 and Figure 42, *HPL ADM Wind* and *VPL ADM Wind* were too high to meet the APV requirements. *HPL AD* and *VPL AD* were lower however the requirements were not met for much of the approach, as they exceed the HAL and VAL on a number of occasions. The lowest protection levels

were *HPL ADM* and *VPL ADM* which did not correct the ADM with wind estimates.

This shows that not attempting to estimate the wind gave lower protection levels than if it were estimated. It was observed that the GPS-ADM EKF with wind estimates architecture had higher position covariance than the GPS-ADM EKF with no wind estimates. This resulted in higher protection levels than without wind estimates. In the GPS-ADM EKF with no wind estimates, the frequent GPS update rate (1 Hz) corrects for any errors in the ADM due to wind changes. Because the GPS measurements were weighted more than the ADM process model, the wind shear did not affect the system too significantly. Only if the GPS update rate was slower, or if the wind shear was severe enough in one second to cause the aircraft to travel off course, over tens of metres in one second for example, might this show a significant impact. For these reasons it might be better not to attempt to estimate the wind at all, but rather account for it by the injection of artificial process noise in the ADM process model within the EKF. Only if the wind could be measured much more precisely with lower uncertainty on its estimates, might the inclusion of wind estimates give improved performance. However this would require very accurate air data sensors and possibly a highly accurate IMU for the attitude estimates.

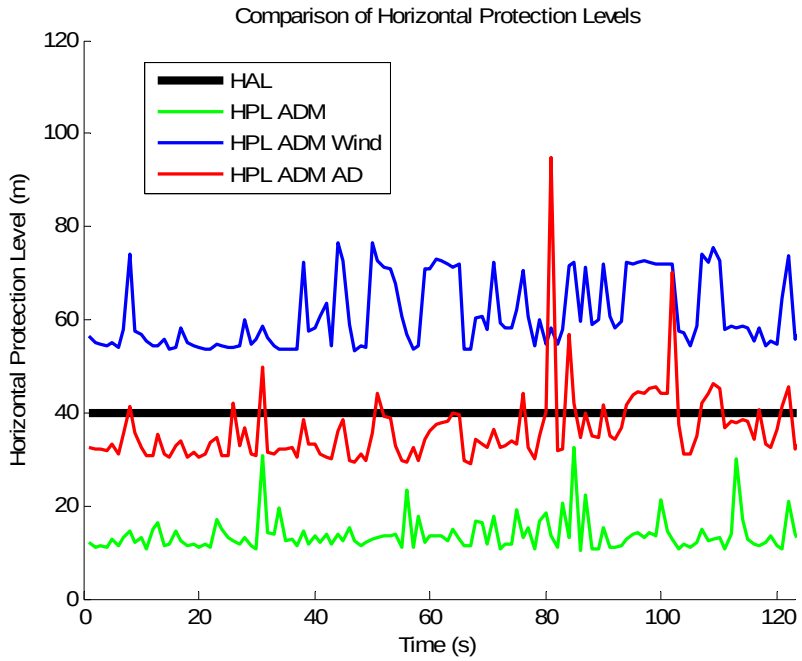

Figure 41 ***Comparison between HPL of GPS-ADM EKF with and without wind estimates.***

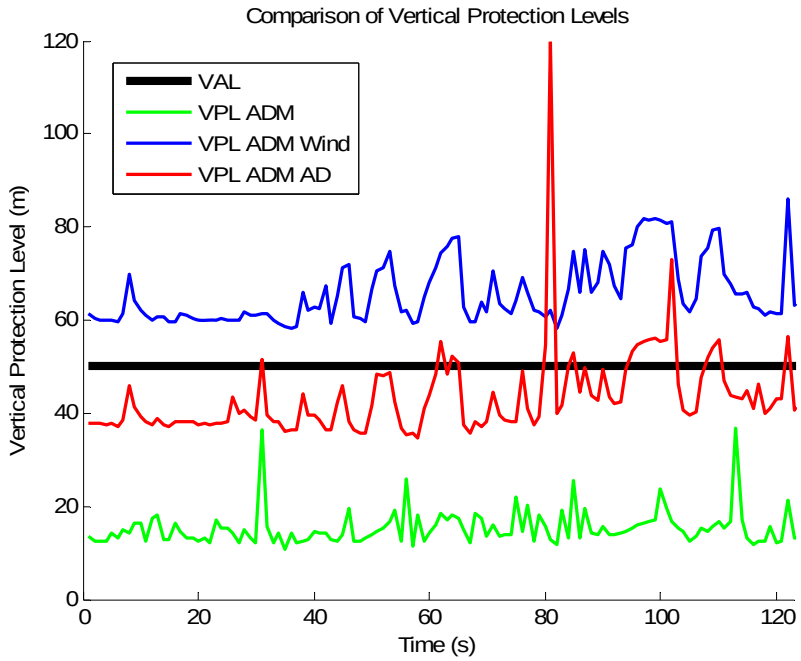

Figure 42 ***Comparison between VPL of GPS-ADM EKF with and without wind estimates.***

4.4.4 Conclusion

In this section the protection levels of the GPS-ADM EKF with wind estimation using the EKF and with air data sensors were compared with the GPS-ADM EKF which did not have any wind estimation. The aim was to investigate whether or not including wind estimates in the ADM can allow for lower protection levels over not including them. Results for a new simulated APV approach with changing wind conditions (wind shear) over the flight were presented.

In Section 4.4.1 the wind estimation accuracy of the GPS-ADM EKF with Wind Estimation architecture of Section 3.10 were investigated. Recall that this architecture modeled wind as a state within the EKF and no air data sensors were used. This resulted in poor wind estimates. Because wind is uncontrollable and unobservable it is a challenge to estimate it, especially without measurements such as from air data and IMU. The accuracy of the wind estimates using the method in Section 3.10.1 which used air data and attitude measurements was presented. The wind estimates were more accurate with air data measurements than the previous results and the response was almost immediate when the wind conditions change.

Comparing the protection levels of the GPS-ADM EKF with wind estimate architectures against the GPS-ADM EKF it was found that estimating the wind at 1 Hz within the filter structure and incorporating this into the ADM estimates resulted in higher, rather than lower protection levels. The use of air data sensors and IMU to measure the wind was found to improve the wind estimates but the ADM HPL and VPL was still too large to meet APV-I requirements. The GPS-ADM EKF without wind estimates had the lowest protection rather than when wind estimates were made. Because the GPS-ADM EKF with wind estimates had higher position covariances than the GPS-ADM EKF, this resulted in a corresponding increase in protection levels. For this reason it is better to not make wind estimates but rather let the wind uncertainty be dealt with by the GPS update. The uncertainty of the wind estimates made by air data and attitude estimates are not accurate enough to see a reduction in protection levels.

The following section will compare the protection levels between the GPS-IMU-ADM EKF and GPS-IMU EKF.

4.5 Protection Levels of GPS-IMU-ADM EKF Architecture

The purpose of this section is to compare the GPS-IMU EKF and GPS-ADM EKF with the GPS-IMU-ADM EKF in protection levels. This is to investigate whether or not a reduction in protection levels can be achieved by fusing the ADM and IMU estimates together using MMF. As explained in Section 3.11, combining the IMU and ADM process models together may reduce the state covariance estimates of each, resulting in reduction to the protection levels.

Firstly the apriori error covariances will be compared because the covariances influence the protection levels. If there is a change in covariance due to fusing the IMU and ADM this is expected to be seen on the protection levels also. Figure 43 compares the trace of the position components of the apriori error covariance of the GPS-IMU EKF (P^- *IMU* in the legend) with the IMU state covariance of the GPS-IMU-ADM EKF (P^- *IMU with MMF* in the legend). It can be seen that the P^- *IMU with MMF* was approximately 0.7 m lower than the P^- *IMU* and this reduction was calculated to be an average of 5% over the whole simulation. As stated in Section in 3.11, the reduction in covariance is due to exploiting the correlations between the IMU and ADM.

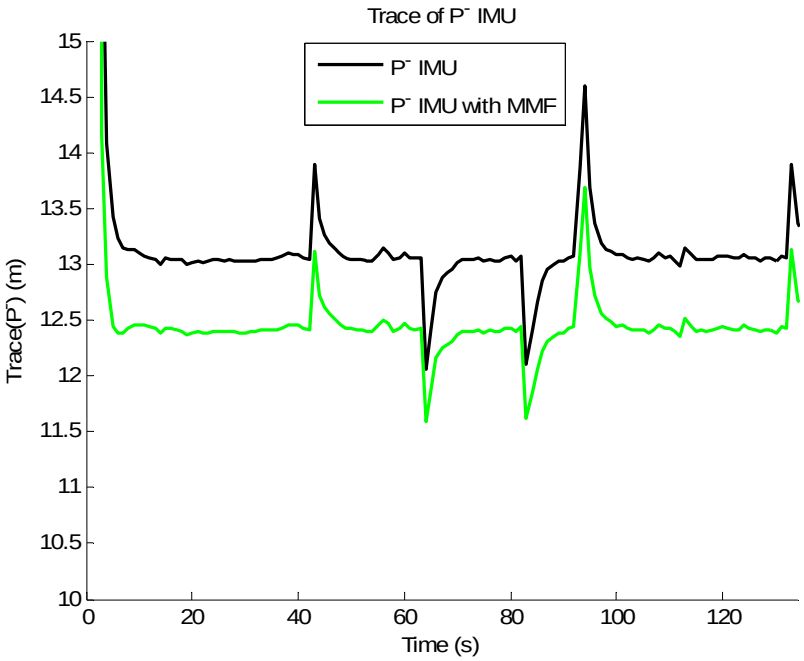

Figure 43 ***Comparison between apriori error covariance of GPS-IMU EKF and GPS-IMU-ADM EKF, showing a reduction with GPS-IMU-ADM EKF.***

Figure 44 compares the trace of the position components of the apriori error covariance of the GPS-ADM EKF (P^- *ADM* in the legend) with the state covariance of the GPS-IMU-ADM EKF (P^- *ADM with MMF* in the legend). There was calculated to be an average 6.8% reduction in P^- *ADM with MMF* than P^- *ADM*. This reduction is larger than for the IMU seen previously (5%) because the ADM had higher covariance than the IMU and so gained greater benefit by being fused with the IMU.

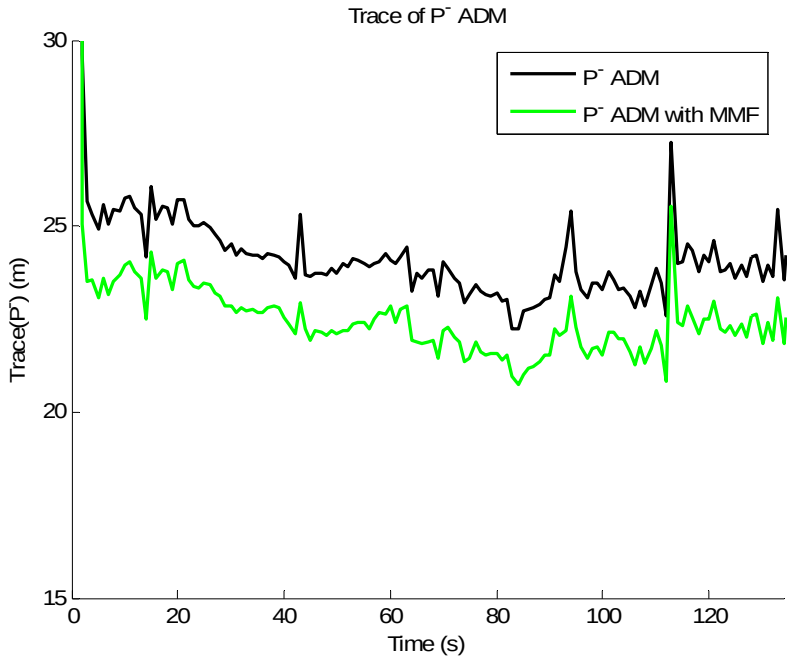

Figure 44 ***Comparison between apriori error covariances of GPS-ADM EKF and GPS-IMU-ADM EKF, showing a reduction with GPS-IMU-ADM EKF.***

The reductions in the error covariances after the GPS updates are shown in Figure 45 and Figure 46. There was calculated to be an average 5.8% reduction in *P IMU with MMF* in Figure 45 and a 20% reduction in *P ADM with MMF* and Figure 46, than *P IMU*.

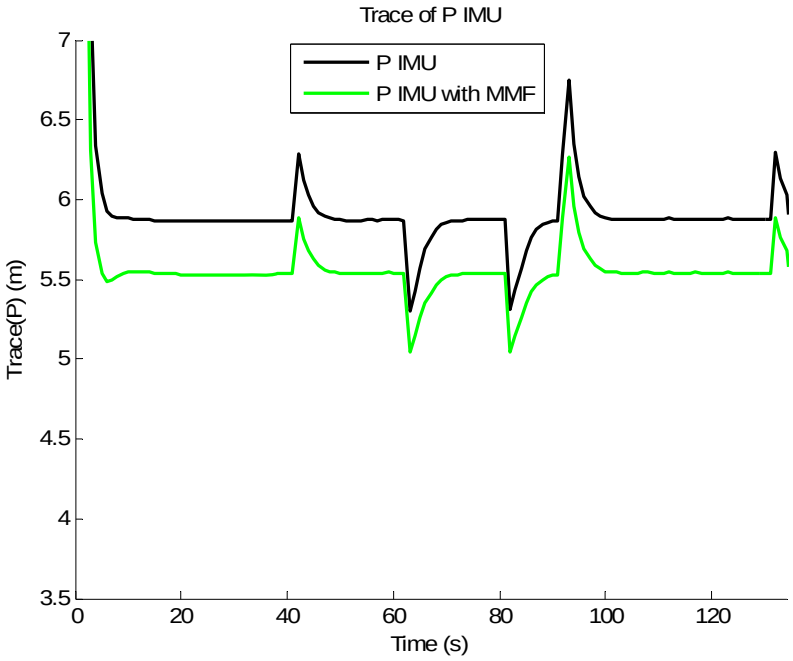

Figure 45 ***Comparison between error covariances of GPS-IMU EKF and GPS-IMU-ADM EKF, showing a reduction with GPS-IMU-ADM EKF.***

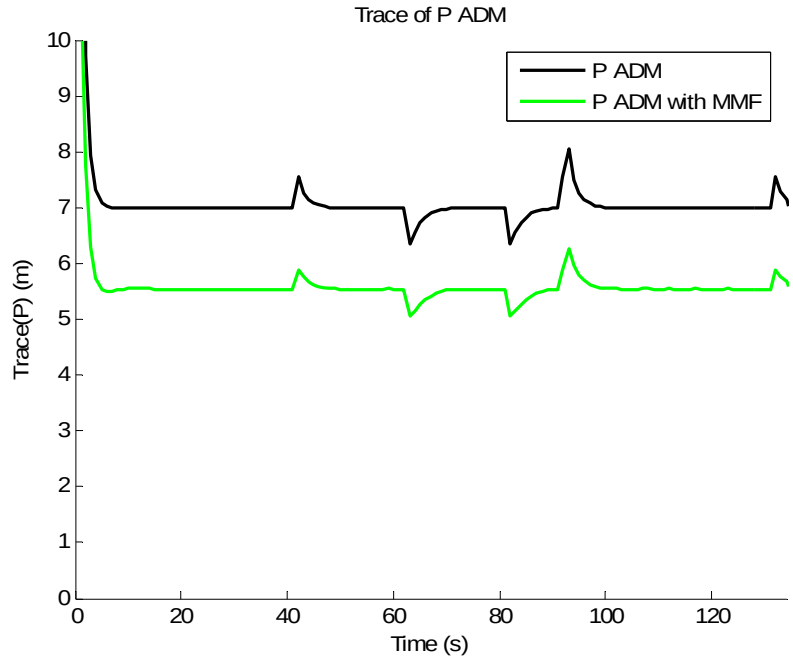

Figure 46 ***Comparison between error covariances of GPS-ADM EKF and GPS-IMU-ADM EKF, showing a reduction with GPS-IMU-ADM EKF.***

Because the HPL and VPL depend partly on the estimated covariances (Section 3.7.5), any reduction in covariance due to MMF should have an effect in reducing the HPL and VPL in the integrity monitoring algorithm whose values are based on the

filter estimates.

Figure 47 and Figure 48 below show a reduction in HPL and VPL with the GPS-IMU-ADM EKF (*HPL IMU-ADM* and *VPL IMU-ADM* in the legends) compared to the GPS-IMU EKF (*HPL IMU* and *VPL IMU* in the legends). Averaged over the whole simulated approach, the *HPL IMU-ADM* was 2.6% lower than *HPL IMU* and the V*PL IMU-ADM* was 4% lower than V*PL IMU*.

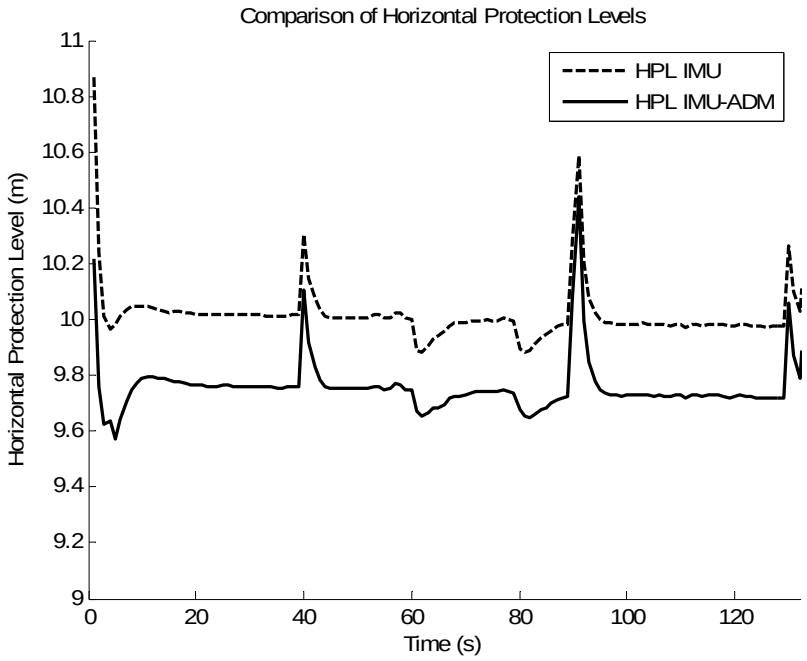

Figure 47 Comparison between HPL of GPS-IMU EKF and GPS-IMU-ADM EKF showing a reduction with GPS-IMU-ADM EKF.

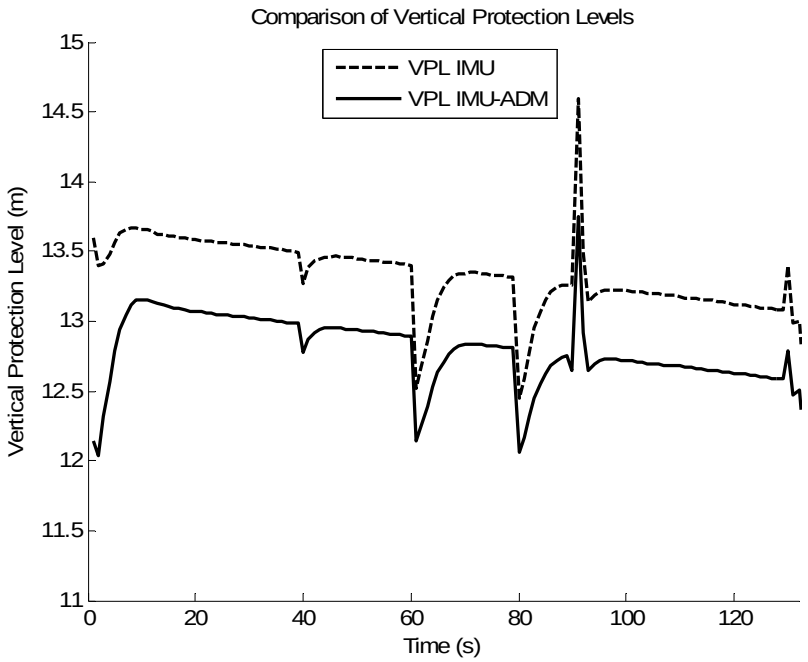

Figure 48 ***Comparison between VPL of GPS-IMU EKF and GPS-IMU-ADM EKF showing a reduction with GPS-IMU-ADM EKF.***

Similarly, there was found to be a reduction compared with the GPS-ADM EKF as seen in Figure 49 and Figure 50. Averaged over the whole simulated approach, the *HPL IMU-ADM* was 10.9% lower than the *HPL ADM* and the *VPL IMU-ADM* was 5% lower than the *VPL ADM*. Note that there was a greater reduction in protection levels for the ADM than for the IMU. Recall that the ADM covariance (Figure 44) was higher than the IMU (Figure 43). Fusing the IMU and ADM together had an effect in reducing the covariance the most of whichever process model is most uncertain and improving the confidence in those estimates.

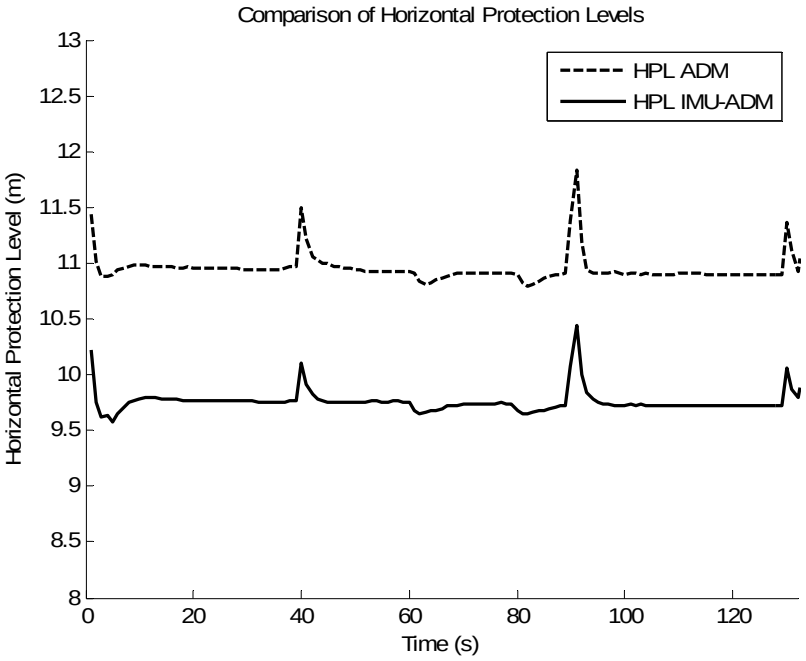

Figure 49 ***Comparison between HPL of GPS-ADM EKF and GPS-IMU-ADM EKF showing a reduction with GPS-IMU-ADM EKF.***

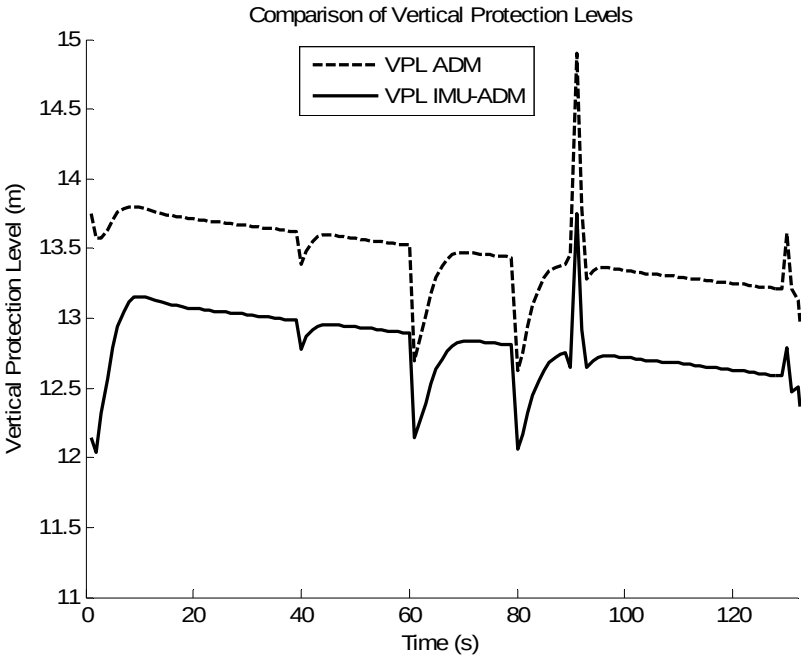

Figure 50 ***Comparison between VPL of GPS-ADM EKF and GPS-IMU-ADM EKF showing a reduction with GPS-IMU-ADM EKF.***

4.5.1 Conclusion

The purpose of this section was to compare the GPS-IMU EKF with the GPS-IMU-ADM EKF. This was to investigate whether or not any reduction in protection levels can be gained by fusing the ADM and IMU estimates together using MMF. As explained in Section 3.11, combining a low quality IMU and ADM together may lower the state covariance estimates of each, resulting in a reduction to the protection levels. This is because both make similar yet different assumptions about the aircraft's motion. The low quality MEMS IMU is a sensor corrupted with random noise and biases, whereas the ADM provides estimates based on the known aerodynamics of the aircraft and measured control inputs. Firstly it was shown that fusing the IMU and ADM together resulted in lower apriori and post-measurement update covariances. Then it was found that the HPL and VPL of the GPS-IMU-ADM EKF was 2.6% and 4% lower than the GPS-IMU EKF. The GPS-IMU-ADM EKF HPL and VPL was 10.9% and 5% lower than the GPS-ADM EKF.

The question is, is this reduction significant enough to warrant fusing the IMU with the ADM? Although the HPL and VPL were below the alert limits for all cases in these simulations, there may be times (due to poor GPS satellite geometry for example) when the HPL or VPL is "borderline", that is, slightly below the HAL or VAL. In such cases a small reduction in HPL and VPL could mean the difference between a missed approach and a successful landing. Alternatively, the small reductions may have more significance if tighter HAL and VAL requirements are needed to be met. In terms of the integrity requirements, because the integrity function is not available if the HPL or VPL exceeds the HAL and VAL, any reduction in HPL and VPL can contribute to greater availability of the integrity monitoring function. However without extensive Monte Carlo simulation it is unknown what improvement it may give to availability and whether or not this is significant. This is left for further work as this is beyond the capabilities of GARDSim. On the other hand, given that the fusing of the IMU with the ADM results in a more complex system than GPS-IMU EKF or GPS-ADM EKF, the small reduction achieved may not justify fusing them together.

The following section investigates the protection levels of the GPS-IMU EKF, GPS-ADM EKF and GPS-IMU-ADM EKF over changing satellite geometries in a

24-hour period.

4.6 GAGIS Integrity Monitoring Performance over 24 Hour Period

The aim of this test is to investigate the protection levels over a 24 hour period of changing satellite geometries and compare the integrity monitoring performance of the GPS-only fault detection architecture, GPS-IMU EKF, GPS-ADM EKF and GPS-IMU-ADM EKF. This will show how the changing satellite geometry affects the protection levels of the different architectures. Poor geometry may result in poor availability of the fault detection (Section 2.4.1). The fault detection availability is also calculated for this one approach. 70 simulation runs were made each using the same simulated APV flight as Section 4.2 but at different times over the day with an interval of one approximately every 20 minutes over a 24 hour period. This can be thought of as one aircraft conducting a 2 minute approach every 20 minutes, where each aircraft flies the exact same trajectory. Only 70 simulation runs were made due to the limitation of the slow running speed of GARDSim. The only difference at each run was the satellite geometry, as the same random number seed was used for each.

Before the results for 70 simulation runs are presented, results for one worst-case satellite geometry will be presented here. In this case there was an average of 7 satellites available, however the number of satellites varied due to aircraft motion, occasionally dropping down to 6 as shown in Figure 51. In this case the stand-alone GPS fault detection was frequently unavailable at times due to the protection level exceeding the alert limit.

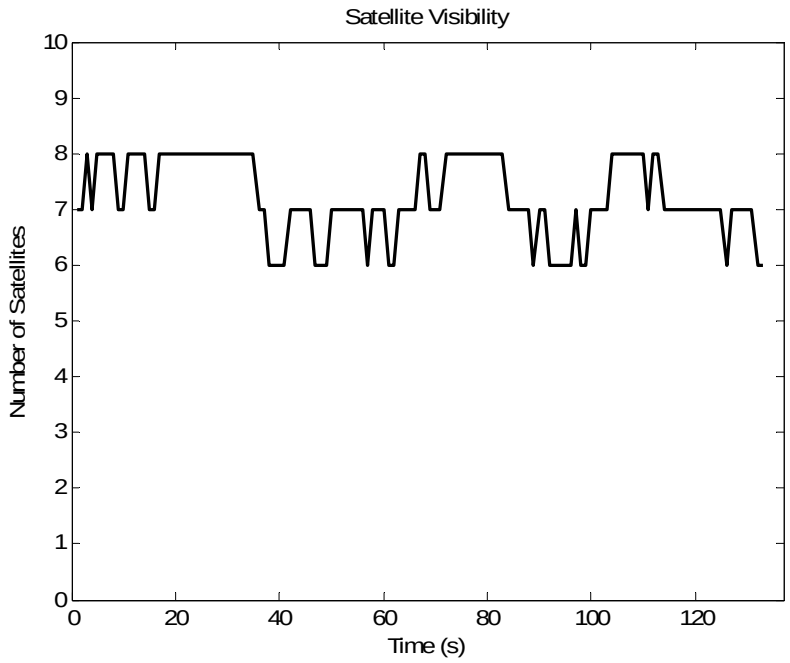

Figure 51 ***Satellite Visibility for worst case run.***

It can be seen in Figure 52 and Figure 53 that the HPL and VPL for the GPS was much higher and more dependent upon the satellite geometry than the HPL and VPL for the GPS-IMU EKF or GPS-IMU-ADM EKF. Averaged over the whole simulated approach, the GPS-IMU EKF HPL was 49.9% lower than the GPS HPL and similarly the VPL was 57.9% lower.

The HPL and VPL of the GPS-IMU-ADM EKF were lower than GPS-IMU EKF. Averaged over the whole simulated approach, the GPS-IMU-ADM EKF HPL was 1.4% lower than the GPS-IMU EKF HPL and the VPL was 5.3% lower.

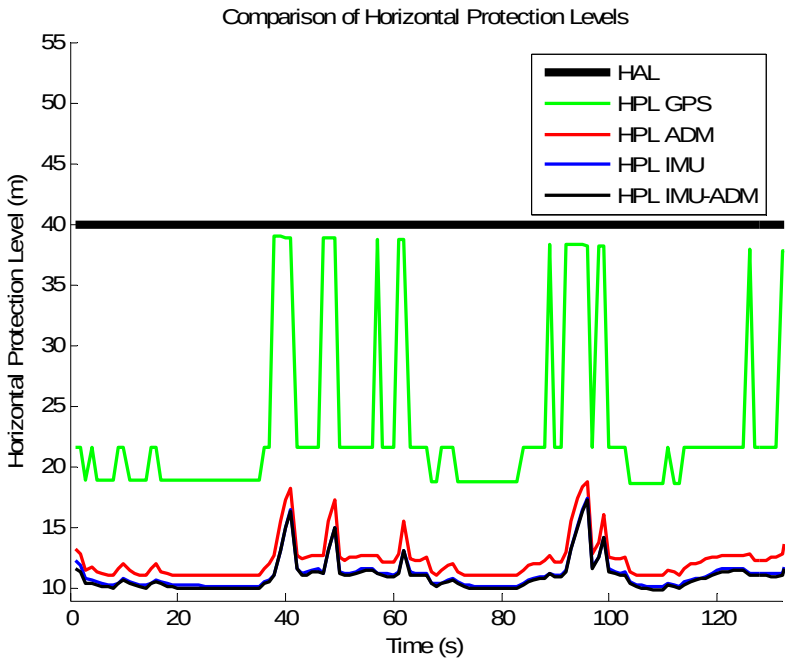

Figure 52 ***Comparison between HPL of GPS, GPS-ADM EKF, GPS-IMU EKF and GPS-IMU-ADM EKF for worst case run.***

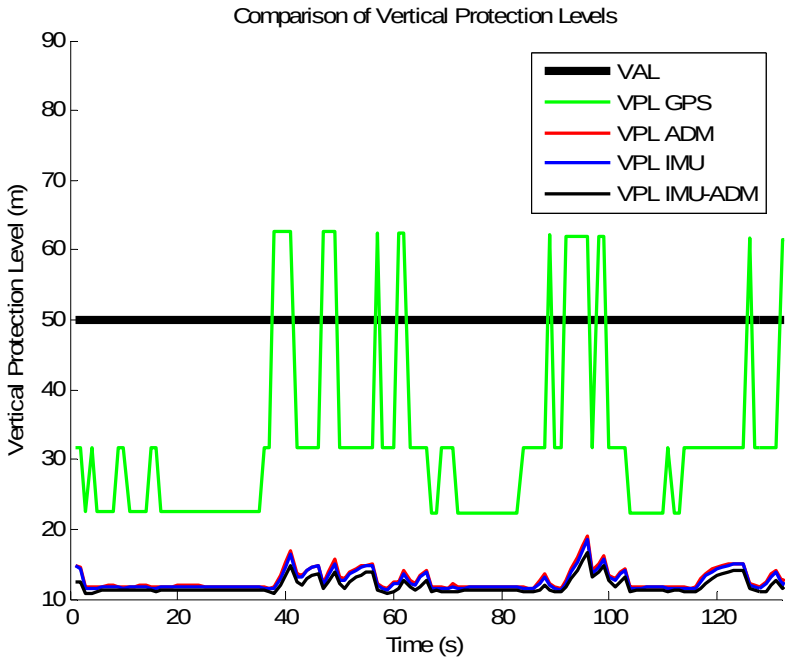

Figure 53 ***Comparison between VPL of GPS, GPS-ADM EKF, GPS-IMU EKF and GPS-IMU-ADM EKF for worst case run.***

Figure 54 and Figure 55 show the HPL and VPL which has been averaged over the 70 simulation runs. As can be seen the HPL and VPL for the GPS were much higher than for the filtered cases. Averaged over all simulation runs, the GPS-IMU EKF

HPL was 48.2% lower than the GPS and the VPL was 54.5 % lower. Averaged over all simulation runs, the GPS-ADM EKF HPL was 44.2% lower than the GPS and the VPL was 54.2 % lower. Averaged over all simulation runs, the GPS-IMU-ADM EKF HPL was 2.7% lower than the GPS-IMU EKF and the VPL was 5.6 % lower. The GPS-IMU-ADM EKF HPL was 9.8% lower than the GPS-ADM EKF and the VPL was 6.34 % lower.

To consider the availability of the fault detection the different architectures over the 70 simulations, it was calculated that fault detection was available for stand-alone GPS, 85% of the time, whereas the availability of the other architectures was 100%. Comparing with a requirement of 99% availability (Table 3), it can be seen that GAGIS has better chance of having fault detection function availability than standalone GPS. An aircraft equipped with GAGIS may be less likely to have disruptions and less risk of a missed approach or diversion. This is particularly important if in the future general aviation relies on satellite navigation alone.

For the GPS-IMU-ADM EKF, as already stated in Section 4.5 any reduction in protection level may contribute to an improvement in availability but it is unknown by how much without extensive simulation. In these results all filtered systems achieved 100% availability so it cannot be determined from this scenario how much improvement to availability the GPS-IMU-ADM EKF gives over the GPS-IMU EKF or GPS-ADM EKF. Availability varies not just with satellite geometry, but the past time history of the aircraft's flight path and so would require extensive Monte Carlo simulation to calculate any improvements. For these reasons availability analysis is left for possible further work.

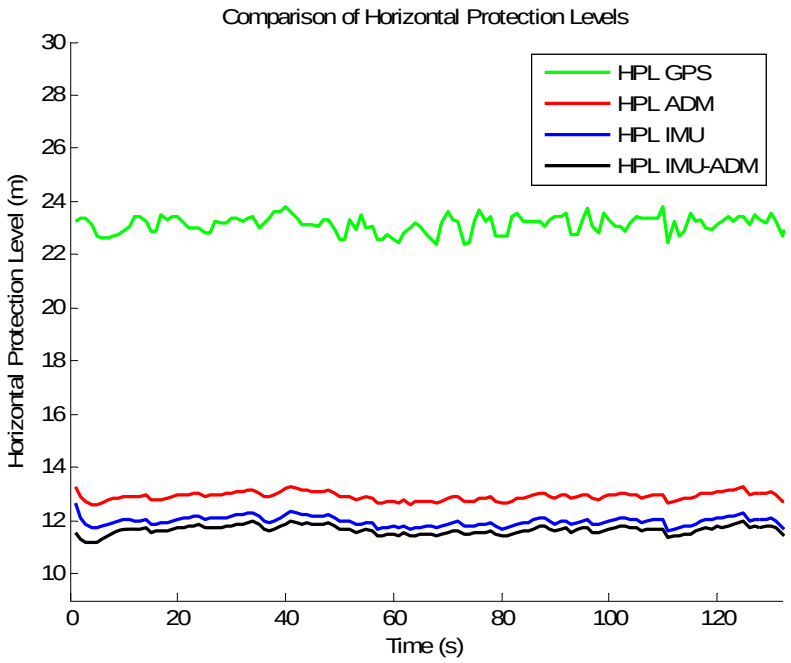

Figure 54 ***Comparison between HPL of GPS, GPS-ADM EKF, GPS-IMU EKF and GPS-IMU-ADM EKF, averaged over 70 simulation runs.***

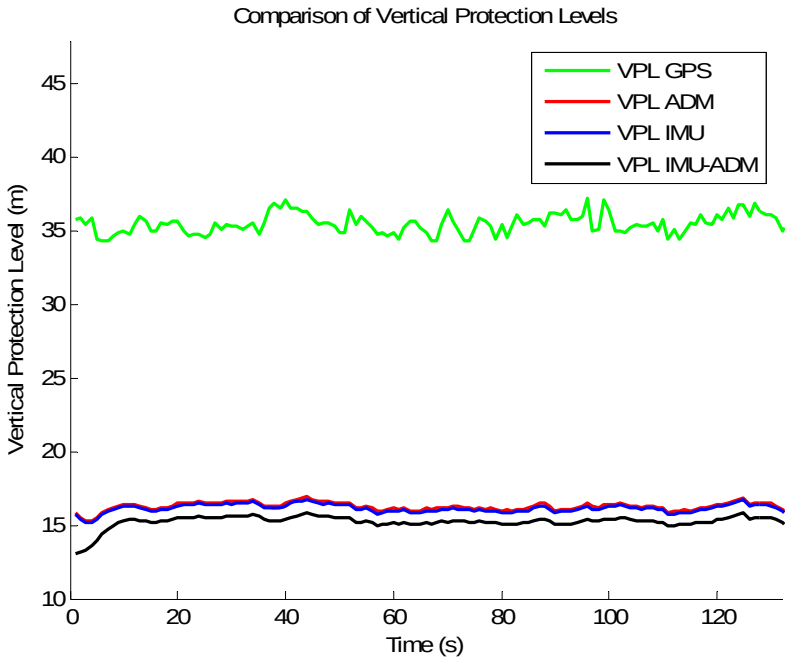

Figure 55 ***Comparison between VPL of GPS, GPS-ADM EKF, GPS-IMU EKF and GPS-IMU-ADM EKF, averaged over 70 simulation runs.***

4.6.1 Conclusion

The aim of this test was to investigate how the changing satellite geometry affected the protection levels of the different architectures. The protection levels which have been averaged over 70 simulation runs of the GPS-only fault detection architecture, GPS-IMU EKF, GPS-ADM EKF and GPS-IMU-ADM EKF were compared.

For one "worst case" situation where the GPS protection levels exceeded the alert limits at times, averaged over the whole simulated approach the GPS-IMU EKF HPL was 49.9% lower than the GPS HPL and similarly the VPL was 57.9% lower. Also, averaged over the whole simulated approach, the GPS-IMU-ADM EKF HPL was 1.4% lower than the GPS-IMU EKF HPL and the VPL was 5.3% lower. This demonstrates the benefit of fusing GPS with IMU or ADM to achieve lower protection levels, whereas without augmentation, the GPS protection levels may exceed the alert limits.

Averaged over the 70 simulation runs, the GPS-IMU EKF HPL was 48.2% lower than the GPS and the VPL was 54.5 % lower .The GPS-ADM EKF HPL was 44.2% lower than the GPS and the VPL was 54.2 % lower. The GPS-IMU-ADM EKF HPL was 2.7% lower than the GPS-IMU EKF and the VPL was 5.6 % lower. The GPS-IMU-ADM EKF HPL was 9.8% lower than the GPS-ADM EKF and the VPL was 6.34 % lower. These results averaged over different satellite geometries show a similar trend and no significant difference to the results given in previous sections. For example, for the single case in Section 4.5 it was found that the HPL and VPL of the GPS-IMU-ADM EKF was 2.6% and 4% lower than the GPS-IMU EKF which is not significantly different from the 2.7% and 5.6% averaged over the 70 simulation runs.

To consider the availability of fault detection over the 70 simulation runs, it was calculated that 85% of the time the GPS HPL or VPL exceeded the HAL or VAL requirements. In contrast, the availability of fault detection was 100% for each of the GPS-IMU EKF, GPS-ADM EKF and GPS-IMU-ADM EKF. Although this was not an extensive availability analysis, this showed that fusing GPS with low-cost IMU may achieve greater availability than GPS-only schemes and confirmed that stand-

alone GPS with the current constellation may have problems achieving a high availability of integrity monitoring for APV as given in Section 2.5.3.

Because the availability was 100% for both the GPS-IMU EKF and GPS-IMU-ADM EKF, no difference in availability could be seen in these results. Further availability analysis could be made in order to assess any improvement of the GPS-IMU-ADM EKF over GPS-IMU EKF in availability.

So far the results have focused on the Navion aircraft. The following section will present simulation results for a faster approach speed typical of faster aircraft such as personal business jets.

4.7 GAGIS with Fast Approach Speed

The simulation results for the previous sections only considered a Navion general aviation aircraft which had an approach speed of approximately 70 knots. However, the category of general aviation is broad and it includes faster flying aircraft such as business jets for example. Therefore to consider a faster flying aircraft the aim of this section is to determine whether the performance of GAGIS might change significantly with a faster approach velocity of 120 knots. The protection levels and ramp fault detection times of the GPS-only fault detection architecture, GPS-IMU EKF and GPS-ADM EKF will be compared. The GPS-IMU-ADM EKF will also be compared.

Using the Navion aircraft model an arbitrary descent was simulated starting from an altitude of 4500 ft and descending at average speed of 120 knots. This was also a steeper rate of descent and the approach time was shorter than previous simulations. A 0.5 m/s ramp fault was placed on the most difficult to detect satellite, starting as 25 seconds. The corresponding satellite visibility plot is given below.

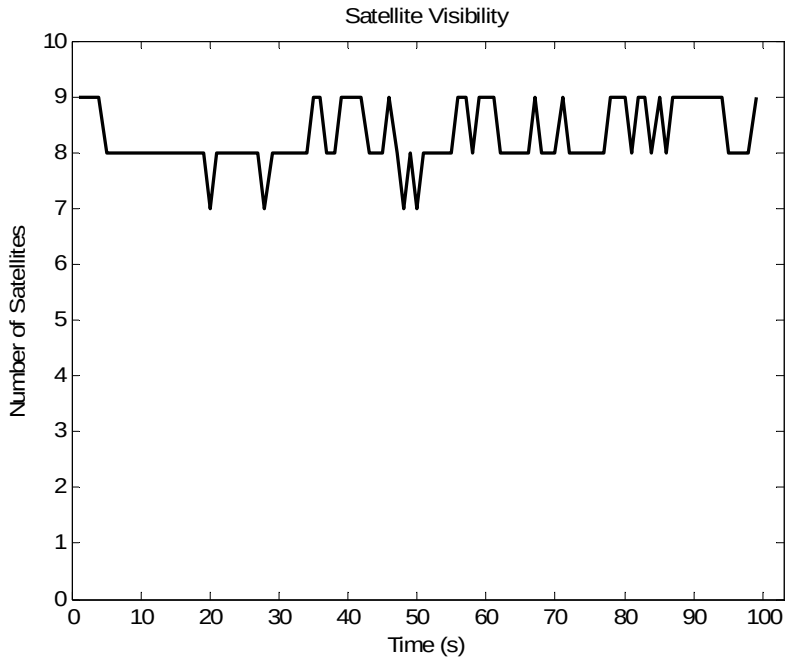

Figure 56 ***Satellite Visibility for fast approach speed.***

Figure 57 shows the HPL for the fast approach speed. *HPL IMU* was calculated to be 52.4% lower than *HPL GPS* and *HPL ADM* was 47.9% lower.

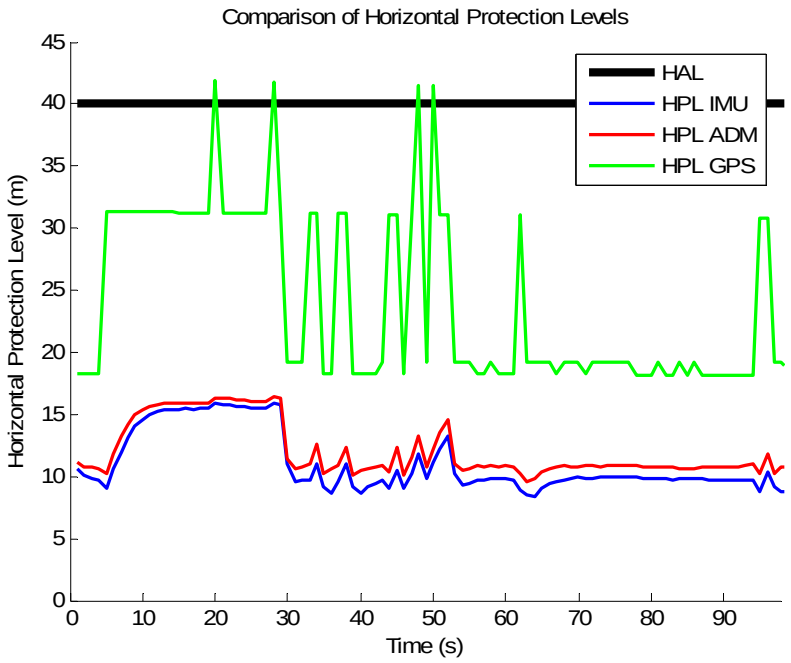

Figure 57 ***Comparison between HPL of GPS, GPS-ADM EKF and GPS-IMU EKF for fast approach speed, showing a reduction with GPS-ADM EKF and GPS-IMU EKF.***

Figure 58 shows the VPL for the fast approach speed. *VPL IMU* was calculated to be 51.2% lower than *VPL GPS* and *VPL ADM* was 50.4% lower.

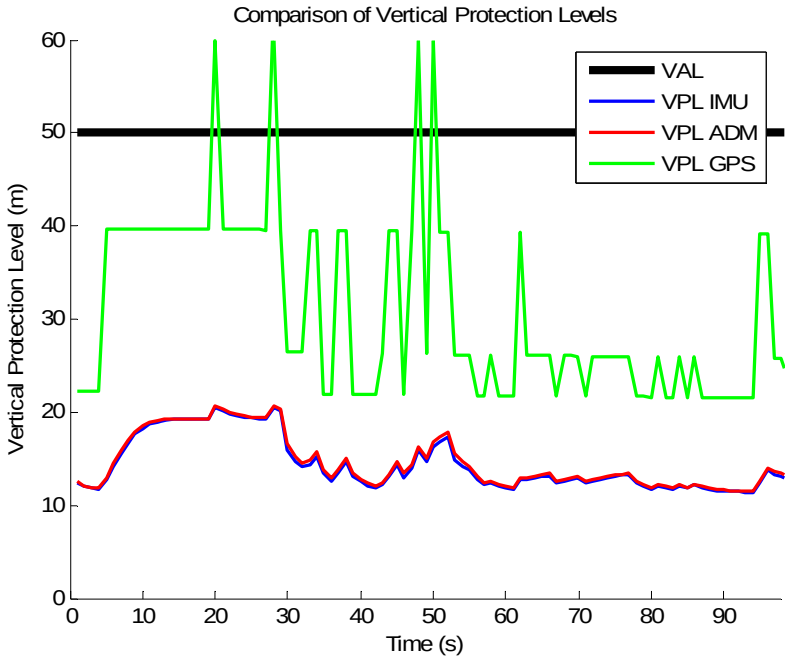

Figure 58 ***Comparison between VPL of GPS, GPS-ADM EKF and GPS-IMU EKF for fast approach speed, showing a reduction with GPS-ADM EKF and GPS-IMU EKF.***

To compare these results which will be called *Fast Approach Speed* with the results of the previous Section 4.3 which will be called the *Slow Approach Speed.*

	Compared to GPS (%)	
Architecture	***Fast Approach Speed***	***Slow Approach Speed***
GPS-IMU EKF HPL	52.4	48.5
GPS-IMU EKF VPL	51.2	49.6
GPS-ADM EKF HPL	47.9	43.7
GPS-ADM EKF VPL	50.4	49.2

Table 5 ***Protection level comparison between Fast Approach Speed and Slow Approach Speed.***

For the detection of ramp faults only the 0.5 m/s ramp fault results will be compared. Table 6 presents the fault detection times. Note that the *NSE > PL* result for the GPS H and GPS V is > 100 s because the simulation had finished before the NSE had exceeded the PL. It is shown that the fault was detected on all systems and the trend was similar to previous results where the GPS-IMU EKF gives fastest detection followed by the GPS-ADM EKF and lastly the GPS. For both the *Fast* and *Slow approach speed* results, GAGIS detected the fault approximately 20 seconds sooner than the GPS. Therefore it cannot be said that there is any significant difference between the results of the slow approach speed and the fast approach speed.

	0.5 m/s ramp fault Fast approach speed		***0.5 m/s ramp fault Slow approach speed***	
Architecture	***Time to Detection (s)***	***Time to NSE > PL (s)***	***Time to Detection (s)***	***Time to NSE > PL (s)***
GPS H	44	> 100	54	88
GPS V	41	> 100	54	73
GPS-IMU EKF H	23	52	32	50
GPS-IMU EKF V	25	50	33	32
GPS-ADM EKF H	27	56	34	54
GPS-ADM EKF V	26	51	33	32

Table 6 ***Fault Detection Times for fast approach speed, showing earlier detection times for the GPS-IMU EKF and GPS-ADM EKF and comparison with slow approach speed.***

Comparing the protection levels of the GPS-IMU-ADM EKF, Figure 59 compares

the HPL of the GPS-IMU EKF against the GPS-IMU-ADM EKF. *HPL IMU-ADM* was 3.1% lower than *HPL IMU*. For VPL in Figure 60, V*PL IMU-ADM* was 4.3% lower than *VPL IMU*. Although no plots are shown for the GPS-ADM EKF, the HPL for the GPS-IMU-ADM EKF was 11.7% lower than GPS-ADM EKF and VPL was 5.8% lower.

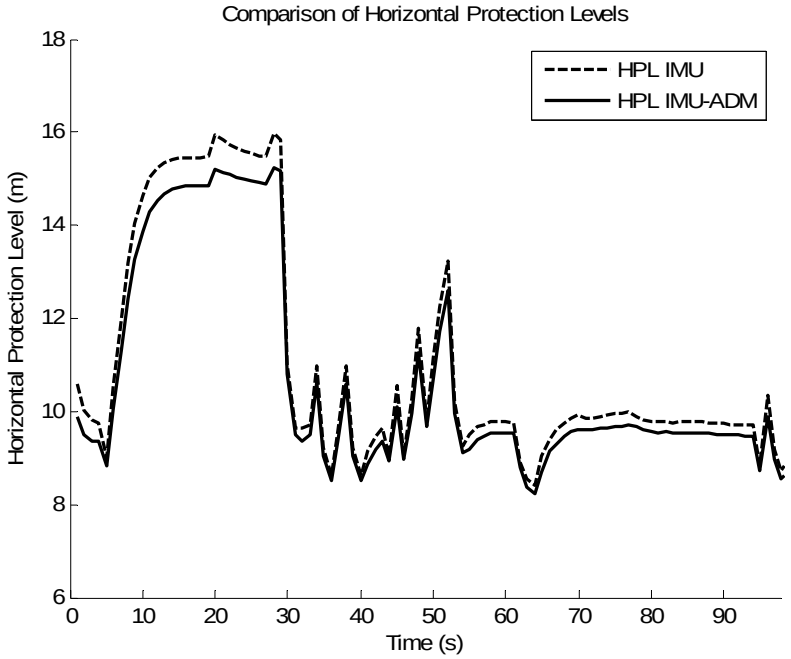

Figure 59 ***Comparison between HPL of GPS-IMU EKF and GPS-IMU-ADM EKF for fast approach speed, showing a reduction with GPS-IMU-ADM EKF.***

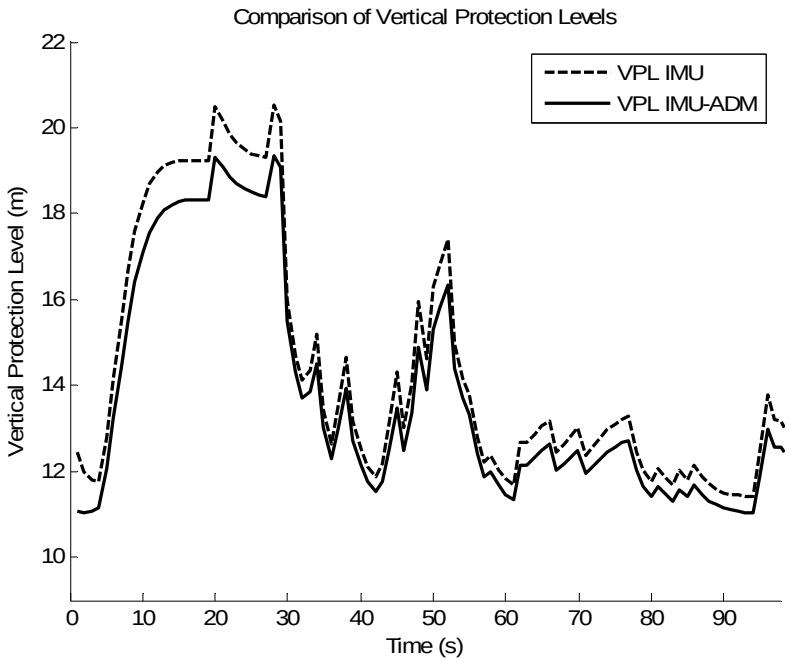

Figure 60 ***Comparison between VPL of GPS-IMU EKF and GPS-IMU-ADM EKF for fast approach speed, showing a reduction with GPS-IMU-ADM EKF.***

To compare these results with the results of previous Section 4.5, the results are summarized in Table 7. As can be seen there is no significant difference between the results with the *Fast Approach Speed* compared to the *Slow Approach Speed*.

	Compared to GPS-IMU EKF (%)		***Compared to GPS-ADM EKF (%)***	
Architecture	***Fast Approach Speed***	***Slow Approach Speed***	***Fast Approach Speed***	***Slow Approach Speed***
GPS-IMU-ADM EKF HPL	3.1	2.6	11.7	10.9
GPS-IMU-ADM EKF VPL	4.3	4	5.8	5

Table 7 ***Comparison of Protection Levels between slow and fast approach speeds, showing no significant differences.***

4.7.1 Conclusion

The aim of this section was to investigate the performance of GAGIS with a faster approach velocity that may be due to the system being used on a faster aircraft such as a business jet. An arbitrary descent was simulated starting from an altitude of 4500 ft and descending at average speed of 120 knots, as compared to 70 knots in the previous simulations.

Protection levels and 0.5 m/s ramp fault detection times were compared with the GPS-only fault detection architecture, GPS-IMU EKF and GPS-ADM EKF. Following this the protection levels of the GPS-IMU-ADM EKF were compared. It was found that there was no significant difference in the results as compared to the results for the slower approach speed of sections 4.3 and 4.5. The dynamics experienced by a faster flying aircraft on APV approach are not expected to be high enough to see any great difference in performance with GAGIS.

The following section investigates substituting IMU measurements with ADM estimates which may be useful for redundancy purposes.

4.8 Substituting IMU Measurements with ADM Estimates

Section 2.7.2 stated that the ADM may contribute to navigation system robustness. The aim of this section is to investigate this possibility by combining IMU and ADM information in the one filter. Besides the existence of a GPS-ADM EKF which may operate independently of the GPS-IMU EKF, another way in which it may be useful is to be the source of dynamic information for the filters in the case of a partial IMU failure. The possibility of this is investigated here. Note this is a different approach to the GPS-IMU-ADM EKF where the IMU and ADM were fused together. Assuming that the measurements from all three accelerometers of the IMU are unusable due to an IMU failure, Figure 61 and Figure 62 show the protection levels *HPL IMU* and *VPL IMU* in the case where the three-axis acceleration estimates were replaced by acceleration measurements from the ADM. The three-axis angular rates continue to be provided by the IMU. The noise statistics were changed accordingly in the filters and tuned until consistent.

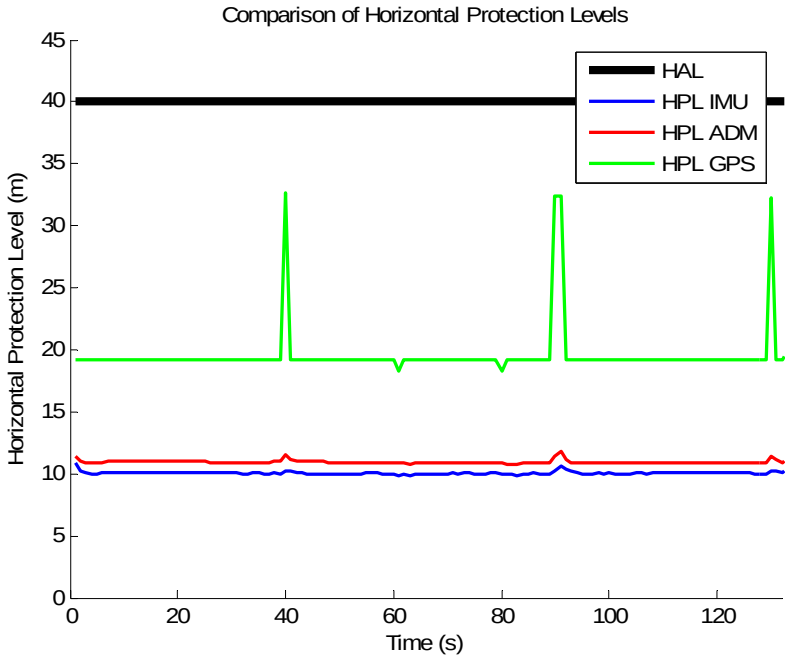

Figure 61 ***Comparison between HPL of GPS-IMU EKF using ADM-provided acceleration estimates, GPS-ADM EKF and GPS.***

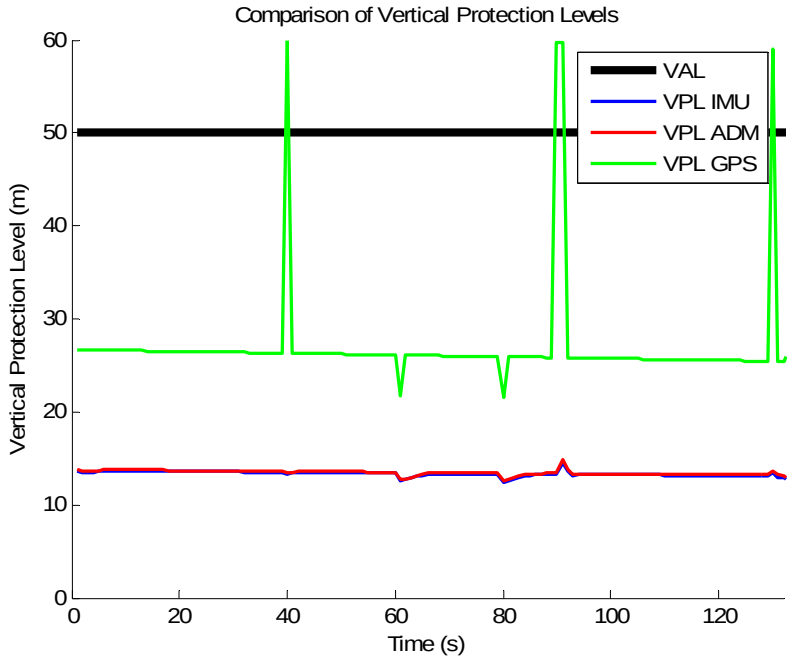

Figure 62 ***Comparison between VPL of GPS-IMU EKF using ADM-provided acceleration estimates, GPS-ADM EKF and GPS.***

If compared to results of Section 4.3.2 it can be seen that there was no significant difference in the *HPL IMU* of Figure 61 which was approximately 9.83 at 55 seconds (point chosen arbitrarily for comparison) and *HPL IMU* of Figure 22 which was approximately 9.81 m. Likewise for the *VPL IMU* which was approximately 13.06 in Figure 62 and 13.04 m in Figure 23.

There is a slightly higher protection levels when replacing IMU measurements with ADM estimates since the ADM estimates are less accurate than the IMU. However care needs to be taken in the filter tuning and an adaptive tuning approach may be necessary to properly tune the filters with the mixture of ADM and IMU information. Otherwise it may lead to filter instability. Also a process for detecting an IMU fault and transitioning to the ADM information on the approach will be required. However this demonstrates the possibility of substituting IMU acceleration and angular rate measurements with estimates from the ADM whilst meeting the alert limit requirements.

4.8.1 Conclusion

The aim of this test was to investigate substituting the IMU with the ADM, in the

situation of three IMU accelerometers failing example. This was to determine whether or not using partial information from the ADM can improve the redundancy in the navigation system. It was found that the IMU measurements may be replaced with ADM estimates without any significant increase in protection levels. This has potential for improving the robustness of the navigation system. For example, if a partial IMU failure occurs where one or more of the accelerometers or gyroscopes have failed and cannot be used, the ADM may be used instead. However care needs to be taken in the filter tuning and an adaptive tuning approach may be necessary to properly tune the filters with the mixture of ADM and IMU information. Also a process for detecting an IMU fault and transitioning to the ADM information on the approach will need to be developed and has not been considered in these results. These considerations are likely to make this approach of combining ADM and IMU measurements difficult in practice. Also, it may be more cost effective simply to have additional IMU's for backup rather than the ADM, considering that the ADM is not normally used in general aviation aircraft.

5 Conclusions

APV approaches can result in improved safety and cost savings for general aviation operations by using GPS but GPS must meet APV integrity monitoring requirements. Augmentation systems can assist GPS to meet the requirements however systems such as SBAS may be too expensive or not adopted by some countries such as Australia due to sovereignty concerns. Lower cost alternatives such as GRAS may not be able to provide complete coverage for all general aviation operations. Instead, ABAS may provide the required integrity monitoring performance by augmenting GPS with other sensors local to the aircraft.

Past ABAS designs rely upon an accurate inertially-derived reference trajectory in Kalman filters. However these high-quality inertial sensors are too expensive for general aviation aircraft. As an alternative, augmenting GPS with low quality MEMS IMU's may provide the necessary augmentation in lower-cost ABAS designs for general aviation. Augmenting GPS with aircraft dynamic information may also be useful. The purpose of this thesis was to investigate using an Aircraft Dynamic Model (ADM) and low-cost IMU in an ABAS architecture for general aviation. As given in Section 1.2 the fundamental research question was:

What GPS integrity monitoring performance can be achieved by augmenting a GPS with an ADM and low-cost IMU for a general aviation aircraft on an APV approach?

From this, the sub-questions were:

(a) Can augmenting a GPS with a low-cost IMU or ADM provide improved GPS integrity monitoring performance over GPS alone and if so by how much?

(b) How does augmenting a GPS with an ADM compare to using a low-cost IMU in ABAS for general aviation?

(c) Can an ADM be used as an IMU replacement to improve navigation system redundancy?

(d) Is there any benefit to GPS integrity monitoring in fusing an IMU with an ADM?

To answer these questions and evaluate the performance of an ABAS design with low-cost IMU and ADM, in Chapter 3 a new navigation system architecture concept named the General Aviation GPS Integrity System (GAGIS) was presented. Each of the components of GAGIS including the GPS, MEMS IMU, ADM, EKF and FD algorithm were explained. Different possible configurations of GAGIS which were a GPS-IMU EKF, GPS-ADM EKF and GPS-IMU-ADM EKF architectures were presented. In Chapter 4, a computer simulation environment in MATLAB called GARDSim was used was to investigate the performance of the GPS-IMU EKF, GPS-ADM EKF and GPS-IMU-ADM EKF architectures. A simulated aircraft approach was hand-flown using a joystick to simulate a pilot's approach. Typical GPS, IMU, ADM and environmental errors were simulated.

Based on the results of the simulations a contribution to research was made in answering the question "*Can augmenting GPS with a low-cost IMU or ADM provide improved GPS integrity monitoring performance over GPS alone and if so by how much?"*

The GPS-IMU EKF and GPS-ADM EKF were compared with a stand-alone GPS architecture. It was found that the GPS-IMU EKF and GPS-ADM EKF gave improved performance over stand-alone GPS in accuracy, detection of 0.5 m/s and 2.5 m/s ramp faults, protection levels and availability of the fault detection function.

Results presented in 4.3.1 showed that all systems met the accuracy requirements. However the GPS-IMU EKF was the most accurate, followed by the GPS-ADM EKF and lastly the GPS. For protection level results it was found that the GPS-only performance was highly dependent upon the satellite geometry, whereas the changing geometry did not affect the GPS-IMU EKF or GPS-ADM EKF as much (for example see Figure 22). It was also found that augmenting GPS with the IMU or ADM resulted in lower protection levels where a typical reduction was approximately 50% (Section 4.6).

A lowering in protection levels gives an improvement in fault detection availability. Whilst no extensive availability analysis was conducted because it was beyond the capability of GARDSim, the availability was calculated to be 85% for the GPS and 100% for the GPS-IMU EKF and GPS-ADM EKF as shown in Section 4.7, calculated over 70 different satellite geometries in a 24-hour period. An improvement in availability may improve the general aviation operations, resulting in fewer missed approaches and diversions. It may also allow operations in areas which may otherwise be subject to poor GPS satellite availability.

The ramp fault detection performance of GAGIS was evaluated where the GPS-IMU EKF and GPS-ADM EKF and GPS were shown to be able to detect slowly growing 0.5 m/s and 2.5 m/s ramp faults. Typically the GPS-IMU EKF and GPS-ADM EKF detected the fault approximately 20 seconds sooner for the 0.5 m/s case. However for the 2.5 m/s case, the GPS-IMU EKF and GPS-ADM EKF detected the fault approximately only 3 seconds sooner than the GPS. Faster detection of faults can give greater time for any subsequent fault exclusion attempts or if exclusion fails can give quicker notification to the pilot that there is a problem so that they can take the necessary precautions.

These results show that the use of low-cost IMU has potential in ABAS designs for general aviation. The ADM also has potential. However, although the ADM is essentially only a piece of software with associated sensors to measure pilot inputs, the ADM is not normally used in navigation systems. There would be costs involved in fitting aircraft with sensors, not to mention the development costs of the ADM for a particular aircraft type. To investigate how the ADM compared with the IMU, another contribution to research was made in answering the question *"How does augmenting a GPS with an ADM compare to using a low-cost IMU in an ABAS for general aviation?"*

To answer this question, the simulation results for the GPS-IMU EKF were compared with the GPS-ADM EKF. The simulations consisted of wind, environmental and aerodynamic coefficient error on the ADM with the values given in Table 3. Justification for the choice of these values was given in Appendix B. The

goal was to choose typical values and consider as many of the main errors on the ADM as possible for comparison with the IMU.

It was found that with all these errors the accuracy of the GPS-ADM EKF was poorer than the GPS-IMU EKF. This is to be expected considering the ADM does not measure the wind and would have more uncertainty on its estimates than the IMU which does measure wind. On average the protection levels for the GPS-ADM EKF were approximately 2% higher than the GPS-IMU EKF, but still met the alert limit requirements. Of course, this depends on the IMU sensor quality and the ADM accuracy. In general it can be expected that if a higher accuracy IMU was used or less accurate ADM, the difference would be much greater, all else being equal. Or if a more accurate ADM or less accurate IMU were used, the difference between the two would be less, all else being equal. Note however that the performance is also dependant upon the GPS and the filters.

It was thought that including wind estimates into the ADM might improve the ADM accuracy and result in improved integrity monitoring performance over not including wind estimates. However in Section 4.4 it was found that estimating the wind at 1 Hz within the filter structure and incorporating this into the ADM estimates resulted in higher rather than lower protection levels. This was because it resulted in an increase in the position covariance estimates leading to higher protection levels. The uncertainty in the wind estimates made by air data and attitude estimates are not small enough to see a reduction in protection levels. For this reason it is better to not make wind estimates but rather let the wind uncertainty be dealt with by the frequent GPS update.

Given that it is unlikely that the GPS-ADM EKF performance will match that of the GPS-IMU EKF (as results have shown), yet fusing GPS with the ADM can result in an improvement over GPS alone, a contribution to research was made in answering the question *"Can an ADM be used as an IMU replacement to improve navigation system redundancy?"*

The ADM could be present in the navigation system to improve fault detection performance should the IMU be unavailable. This could consist of the GPS-ADM

EKF performing fault detection in parallel and independently to a GPS-IMU EKF. But it may also be possible to substitute part IMU information with the ADM. This was investigated in Section 4.8 where IMU accelerometer measurements were substituted with ADM estimates, simulating the case where three IMU accelerometers failed. It was shown that the IMU acceleration measurements were able to be substituted with the ADM-provided accelerations and angular rates whilst still meeting APV alert limit requirements. This may be useful if the IMU experiences a partial failure and then the ADM could replace the IMU as the provider of dynamic information in the filters. However this may be difficult to achieve in practice due to the need for consistent filter tuning, the possibility of filter instability and considering that the ADM is not normally used in general aviation aircraft. For a practical navigation system for general aviation, it may be more cost-effective simply to add another IMU rather than use an ADM. Although the ADM in navigation systems has been shown to be beneficial in past literature (Section 2.7.2), if low-cost MEMS IMU technology continues to improve there may never be a justification for using an ADM in practical systems for general aviation.

Besides treating the IMU and ADM separately, the possibility of fusing the IMU and ADM information together to achieve greater performance than either was investigated. A contribution to research was made in answering the question "*Is there any benefit to GPS integrity monitoring in fusing an IMU with an ADM?*"

It was found by 70 simulation runs with changing satellite geometry that the HPL and VPL of the GPS-IMU-ADM EKF was approximately 3% and 6% lower on average than GPS-IMU EKF as shown in (Figure 54, Figure 55). This small reduction in protection levels may result in an increase in fault detection availability. However the availability for both the GPS-IMU EKF and GPS-IMU-ADM EKF was 100% in Section 4.6. More extensive simulation would be required to determine what improvement in availability the GPS-IMU-ADM EKF gave, but given that only small reductions in protection levels were achieved this too is expected to be small. A small improvement in availability may be more significant where the performance requirements are much tighter (such as APV II) or satellite geometry is poor. On the other hand, a small improvement may not be large enough to justify the effort and cost of fusing an ADM with the IMU. There is also a disadvantage of fusing the IMU

with ADM which is that the architecture is less robust against IMU or ADM faults as stated in Section 3.11, since a fault on either one will mean a fault affecting the whole system. This is likely to be a problem for practical systems if IMU and ADM reliability cannot be assured.

However, it was interesting that the fusion of the ADM with the IMU achieved a reduction in protection levels. In general it may be said that if a more accurate IMU were used, or perhaps a poorer ADM, the improvement in fusing the two together would be even less or none at all. On the other hand, if the ADM accuracy was improved or the IMU accuracy was poorer there would be greater benefit in fusing the ADM with the IMU. However this comparison is assuming all else is equal. Any improvement in fusing the IMU and ADM together is also dependent upon the GPS, the filtering and the aircraft dynamics.

Whilst only a Navion aircraft was modeled for most of the results, a question might be asked whether or not the performance of GAGIS might change significantly if used in a faster aircraft. Further simulations for a faster approach velocity were conducted to investigate this. It was found that there was no significant difference in the results as compared to the results for the slower approach speed (sections 4.3 and 4.5). The dynamics experienced by a faster aircraft on APV approach are not expected to be high enough to see any great difference in performance with GAGIS.

5.1 Publications

The following publications were made over the course of the PhD candidature.

Refereed Journal Papers

Bruggemann, Troy S. and Greer, Duncan G. and Walker, Rodney A. Investigating GPS Fault Detection with a MEMS IMU and Aircraft Dynamic Model for Approaches with Vertical Guidance (accepted 6 July 2009, for publication in IEEE Transactions on Aerospace and Electronic Systems).

Refereed Conference Papers

Bruggemann, Troy S. and Greer, Duncan G. and Walker, Rodney A. (2007) GPS Integrity Monitoring with an Aerodynamic Model and Low Quality INS. In Proceedings International Global Navigation Satellite Systems Society IGNSS Symposium 2007, Sydney, Australia.

Greer, Duncan G. and Bruggemann, Troy S. and Walker, Rodney A. (2007) Sigma Point Kalman Filters for GPS Navigation with Integrity in Aviation. In Dempster Andrew, Eds. Proceedings IGNSS 2007, Sydney, Australia.

Bruggemann, Troy S. and Greer, Duncan G. and Walker, Rodney A. (2006) Chip Scale Atomic Clocks: Benefits to Airborne GNSS Navigation Performance. In Proceedings International Global Navigation Satellite Systems Society Symposium 2006, Holiday Inn, Surfers Paradise, Australia.

Greer, Duncan G. and Bruggemann, Troy S. and Walker, Rodney A. (2006) Integrity Coasting Concept for General Aviation Users of the Ground Based Regional Augmentation System. In Proceedings IGNSS 2006, Holiday Inn Surfers Paradise, Gold Coast, Australia.

Non-Refereed Conference Papers

Bruggemann, Troy S. and Walker, Rodney A. (2007) GPS, MEMS INS and Aircraft Model Integration for GPS Integrity Monitoring. In Proceedings Smart Systems 2007 Postgraduate Research Conference, Brisbane, Australia.

Bruggemann, Troy S. and Greer, Duncan G. and Walker, Rodney A. (2005) GARDSim - A GPS Receiver Simulation Environment for Integrated Navigation System Development and Analysis. In Goh, Roland and Ward, Nick, Eds. Proceedings Smart Systems 2005 Postgraduate Research Conference, Brisbane.

5.2 Recommendations

To further the research in low-cost ABAS for general aviation, more work could be done in the following areas:

1. Investigation of fault exclusion with GAGIS could be made since fault exclusion was not investigated in this research. Whilst this research showed some benefits for fault detection it is expected that a corresponding benefit to fault exclusion can be found as well.

2. It is hoped that this research can be furthered to consider the practical implementation, issues and integrity performance of GAGIS by flight testing since only simulation results were conducted.

3. An extensive Monte Carlo simulation analysis for HPL/VPL validation and availability study of GAGIS may be required to validate some of the statistics. This is a challenge however considering that the number of runs required for small probabilities is large. To do this it is expected that an alternative simulation environment to MATLAB will be required as GARDSim is not able to do it in any practical timeframe.

4. Detection of faults slower than 0.5 m/s and different fault detection algorithms. It may be worth researching detection of faults slower than 0.5 m/s. Investigation could be made with other fault detection methods such as the rate detector algorithm in [15].

5. Consideration of MEMS IMU and ADM failures and reliability issues with GAGIS and how to minimise, detect, exclude or accommodate them. MEMS inertial technology is an active area of research in the literature but there appears to be little research in applying this technology to ABAS. There is further research potential in addressing the robustness and reliability issues of MEMS sensors with respect to low-cost ABAS.

A. Appendix *GARDSim – The GRAS Airborne Receiver Development Simulation Environment*

The purpose of this section is to describe the computer simulation environment named the GRAS Airborne Receiver Development Simulation Environment (GARDSim). GARDSim is a set of functions and scripts written in MATLAB developed by the author and fellow PhD student Duncan Greer over the course of the PhD program. The simulation environment itself encompasses approximately three years of work and was continually updated and refined throughout the course of the research by the author and Duncan Greer. The following section describes the GARDSim truth model.

A.1 GARDSim Truth Model

Figure 63 is a block diagram showing the components of GARDSim. "Truth" data is generated using the Aerosim Blockset for Simulink by Unmanned Dynamics [73]. Aerosim's model includes a full 6 degree-of-freedom nonlinear aircraft model, propulsion model and earth models. It includes typical environmental effects such as changing gravity, air density, air temperature and wind turbulence and shear effects on the aerodynamics. The aircraft model is "flown" using a joystick to control the elevator, aileron, rudder and throttle and the FlightGear Simulator [87] which has a simulated cockpit display is used for visualisation of the flight. The use of the joystick and FlightGear results in pilot-like inputs and responses to changes in the environment such as wind.

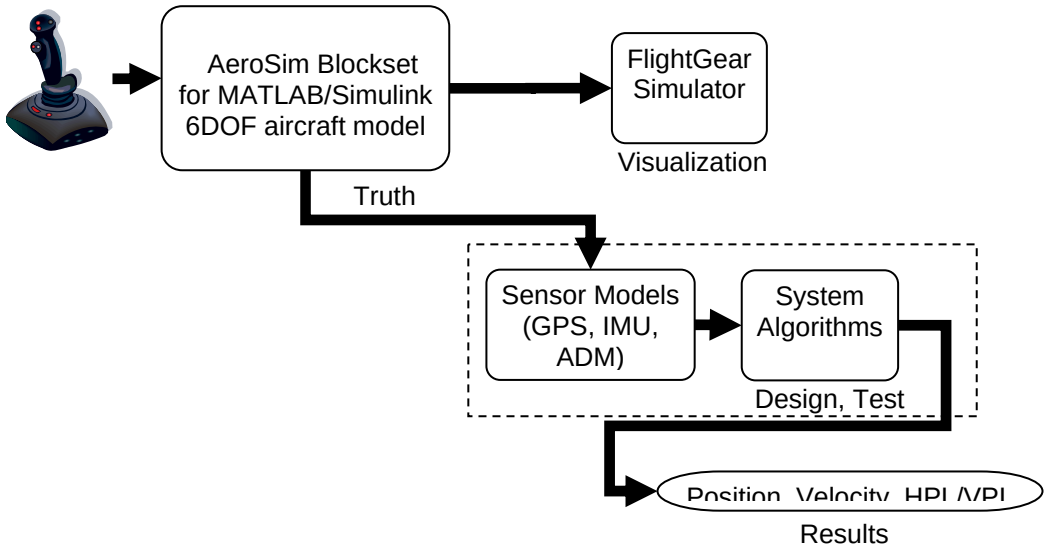

Figure 63 ***GARDSim Architecture.***

After the truth data is generated, sensor models are run to corrupt the truth data with noises to simulate the various sensors. A description of the sensor models in GARDSim is provided in the following section.

A.2 Sensor Models

A.2.1 GPS Sensor Model

GPS pseudorange and pseudorange rate noises are modeled as a sum of Gauss-Markov processes for correlated noises plus Gaussian white noise for measurement noise based upon [67]. For the GPS satellite constellation the changing 24-satellite optimized GPS constellation from [28] is used.

The model for the simulated L1 GPS pseudorange measurements (m) is:

$$\tilde{\rho} = \rho + c(dt - dT) + \varepsilon_{eph} + d_{ion} + d_{trop} + \varepsilon_{mp} + v_{rcvr} + \Delta PR_{\Omega} \quad (134)$$

Where ρ is the geometric range between satellite and user, c is the speed of light, dt is the GPS receiver clock bias, dT is the satellite clock bias, ε_{eph} is ephemeris error, d_{ion} is ionospheric delay, d_{trop} is tropospheric delay, ε_{mp} is multipath, v_{rcvr} is

C/A code measurement noise, $\Delta PR_{\dot{\Omega}}$ is error due to earth rotation.

The simulated L1 GPS pseudorange rate is calculated by differencing simulated carrier phase between successive epochs. The model used for the simulated GPS carrier phase measurements (m) is:

$$\lambda\tilde{\Phi} = \rho + c(dt - dT) + \varepsilon_{eph} - d_{ion} + d_{trop} + \varepsilon_{mp\_carr} + v_{rcvr\_carr} \tag{135}$$

Where λ is the carrier wavelength, ε_{mp_carr} is carrier phase multipath, v_{rcvr_carr} is carrier phase measurement noise. Integer ambiguity was not simulated as it cancels through differencing.

Referring to the table of simulation parameters, Table 3 in Chapter 4, the values for ephemeris, residual L1-L5 ionospheric and residual tropospheric delay noise were chosen based upon [88] and [89]. These values for ionosphere and troposphere represent the residual errors on the GPS measurements after the dual frequency corrections and tropospheric models have been applied. Values for the code and carrier multipath and receiver noises were obtained from the values for narrow correlator technology in [67]. The unknown GPS receiver clock bias and drift is modeled using a typical crystal oscillator model from [48]. Residual satellite clock error is not modeled as it is assumed to be negligible. An antenna mask angle model was included which accounts for GPS signal masking due to aircraft attitude. A 5 degree antenna elevation mask angle was chosen because it is a test condition in [28]. To verify the choice of noises used in this model it was compared with GPS data obtained from a Novatel OEM-V GPS receiver operating from a Spirent GPS Signal Simulator. The sample rate for the simulated GPS measurements was 1 Hz.

A.2.2 IMU Sensor Model

The IMU accelerometer and gyroscope errors were modeled as a first-order Gauss Markov process for the bias plus an additive white noise component. Note that this is not a complete error simulation of the raw outputs of the sensors, but a model of the errors which the filters “see” after sensor calibration (for temperature for example).

The random bias represents the dominant bias on the sensors which is the sum of many different errors and random noise is modeled as Gaussian white noise. This model is also justified by the fact that the simulation times considered are short (approximately 2 minutes). The values shown in Table 3 for the noises and biases were chosen based on values from our lab test of a Crossbow MicroNAV. The sample rate for the simulated IMU measurements was 100 Hz.

A.2.3 ADM

The ADM was a 6-Degree-of-Freedom nonlinear rigid body model as presented in Section 3.5. Control input, aerodynamic coefficient, mass and inertia, centre of gravity, thrust and environmental (wind, air density, speed of sound) errors were considered, as given in Table 3. The values for mass, inertia, centre of gravity error were chosen based upon judgment and the gravity error chosen based on values in [90] assuming an EGM-96 gravity model is used. The values for the control input measurements were based upon error values given in [74] assuming potentiometers are used for measuring control surface deflections. The sample rate for the control input measurements was 100 Hz.

[12] states that the aerodynamic coefficients can typically be known up to 10% of their true values. In this study the aerodynamic coefficient uncertainties were modeled as independent first-order GM processes with values as given in Table 3. The time constants were chosen to give some slowly varying random variation of the parameters over the flight rather than modelling them as constants. This noise was added to the true values of the aerodynamic parameters which were obtained from Aerosim's Navion model. The following aerodynamic parameters were corrupted with this noise:

Coefficient of lift C_L

$C_{L_0}, C_{L_\alpha}, C_{L_q}, C_{L_M}, C_{L_{\delta e}}$

Coefficient of drag C_D

$C_{D_0}, C_{LD_0}, k, C_{D_M}, C_{D_{\delta e}}, C_{D_{\delta a}}, C_{D_{\delta r}}$

Coefficient of side force C_Y

$C_{Y_\beta}, C_{Y_p}, C_{Y_r}, C_{Y_{\delta a}}, C_{Y_{\delta r}}$

Coefficient of pitch moment C_m

$C_{m_0}, C_{m_\alpha}, C_{m_q}, C_{m_{\dot{\alpha}}}, C_{m_M}, C_{m_{\delta e}}$

Coefficient of roll moment C_l

$C_{l_\beta}, C_{l_p}, C_{l_r}, C_{l_{\delta a}}, C_{l_{\delta r}}$

Coefficient of yaw Moment C_n

$C_{n_\beta}, C_{n_p}, C_{n_r}, C_{n_{\delta a}}, C_{n_{\delta r}}$

A.2.4 Air Data Sensor Models

The airspeed, angle of attack and angle of sideslip measurement errors were modeled as the sum of a constant bias plus a white Gaussian noise. Values in Table 3 were chosen based upon [22].

A.3 Validation of Simulation Environment

Although simulated data was used for this research, over a three year period various efforts were made to validate the simulation environment as it was developed. Its performance was validated against real data, manufacturer's data sheets and published results in the literature, where possible, and given the resources available. It should be noted that GARDSim is essentially a list of functions and scripts which can work with either real or simulated data. It was therefore possible to validate most scripts and functions by comparing the results of using both simulated and real data, where possible. For example, the position and velocity solutions obtained from GARDSim's least squares function using pseudoranges from a Novatel OEM-V receiver, could be validated against the OEM-V's own position and velocity solution.

Because development of the simulation environment was conducted in conjunction with fellow PhD candidate Mr Duncan Greer, and was managed using software version control systems such as CVS (and then SVN later in the project), our related but independent work also helped provide independent validation of the various functions and scripts developed. Efforts made to validate specific parts of GARDSim are described in the sections following.

A.3.1 Simulated GPS Validation Efforts

Validation of the simulated GPS component was performed by comparing simulated pseudoranges and resultant simulated position solutions (and their variances) with real data. The accurately surveyed position of QUT's S-block GPS repeater antenna served as a useful reference position and GPS data was collected using different GPS receivers. Initially Mitel Orion and Ashtech MicroZ surveyor GPS receivers were used, but then the simulated GPS models were compared with a more modern Novatel OEM-V GPS receiver, kindly loaned by GPSat Systems Pty Ltd. Using the known location of the antenna and satellite positions calculated from precise SP3 satellite orbit data or ephemeris, the noise values of the pseudorange from real data could be compared with the simulated. Specifically, the magnitudes of the pseudorange noises and their autocorrelation sequences were compared. Actually, comparison of the simulated ranges and positions with real data revealed that the simulated values should be lowered, since values given in [67] are from 1994 and GPS accuracy has improved much since then. For this reason, rather than use all values given in [67] some components such as receiver noise were based upon and validated against information provided in the Novatel OEM-V data sheets obtainable from the manufacturer's website. Current URA values obtained from collected real data were also used as a guide to what the simulated pseudorange accuracy should be.

Not only were simulated pseudoranges and positions validated against real data using the repeater antenna, but they were also compared with GPS data obtained from the Novatel OEM-V GPS receiver running on a Spirent GPS Signal Simulator with a dynamic flight path circuit.

Efforts were made to validate the GPS receiver clock model by comparison with the calculated receiver clock bias and drift estimates from a Novatel OEM-V. In the early stages of the project in 2005 we also investigated ionospheric and tropospheric noises from real data and the ionosphere and troposphere models and values were checked accordingly. GARDSim's satellite orbit calculations were validated by comparing with precise SP3 satellite orbits.

A.3.2 Simulated IMU Validation Efforts

The simulated MEMS IMU model was validated by comparing with real data from testing of a Crossbow MicroNAV in a static environment. Specifically, the comparisons were made by comparing autocorrelation sequences. Admittedly these tests were made in a stationary environment and not an airborne dynamic environment, however the simulated noises were also compared against the typical values given in manufacturers data sheets, and simulated IMU noises modelled accordingly. Admittedly, this generic error model is only an approximation of the sum total of a wide variety of error sources within the IMU. Actually, more detailed models may be used instead of first order GM models such as described in [72], but since this research only considers short operation times and does not consider long periods of IMU stand-alone operation, it was not thought necessary to implement more detailed IMU models.

In 2006 attempts were made to validate the IMU models in a dynamic flight environment by examining IMU data collected from Boomerang UAV which flew in fourth year avionics engineering project flights. While useful to examine the performance of the MEMS sensors, this did not provide a precise comparison as there was no accurate truth reference. Some data collected from an unmanned helicopter was also examined but likewise could not provide any precise validation of the IMU model. Therefore the majority of the validation efforts of the IMU rest upon the static tests and manufacturers data sheets.

A.3.3 ADM Validation Efforts

The ADM implementation was validated by comparing with the Aerosim simulink blockset which is a commercially available software package as mentioned in Section A.1. The ADM models were developed independently of Aerosim using textbooks such as [75, 77, 91] and comparisons with Aerosim confirmed the implementation of the ADM was correct, and also verified that the Aerosim blockset was without fault.

To better understand the wind environment, wind data for Sydney and other areas at altitudes was obtained from the Australian Bureau of Meteorology and was analysed in conjunction with fellow PhD students who had common interest in the wind environment. Some time was also spent developing a control surface deflection position logger for QUT's Boomerang UAV, and the measured control surface deflections from flights were examined.

A.3.4 Simulated Architecture Validation Efforts

The implementations of the standalone least squares and EKF solutions in the simulation environment were validated in a number of ways. The implementation of the standalone GPS least squares solution was validated by comparing the calculated position and velocity with position and velocity outputs of a Novatel OEM-V receiver, using the surveyed position of the S-block repeater antenna as common reference. The simulated dilution of precision calculations and protection levels were also checked in similar manner. Implementations of the KF and EKF code were validated by comparing against stand-alone GPS KF and EKF implementations as given in [48], and compared with GPS KF, EKF and UKF solutions using real-data from a Novatel OEM-V on dynamic flight simulations with a Spirent GPS signal simulator.

For the GPS-INS EKF, the covariances and protection levels generated in simulation were compared in magnitude against covariances and protection levels of a GPS-INS EKF system developed by D. Greer and flown on a Cessna 172 in 2008. Both loosely and tightly coupled approaches were implemented and the simulated

data was compared with the results from the flight tests. Although this was not a complete test as there was no accurate truth reference, the results between real and simulated data were comparable. It should be noted that the implementations of thresholds, test statistics and protection levels had also been verified by comparing the results with papers available in the literature such as [92].

B. Notation and Definitions

Table 8 lists the symbols used in this thesis for the aerodynamic model.

Symbol	Definition
α	Angle of attack
$\dot{\alpha}$	Angle of attack rate
β	Angle of side slip
V_a	Airspeed
M	Mach number
p	Roll angular rate
q	Pitch angular rate
r	Yaw angular rate
δ_a	Aileron deflection angle
δ_e	Elevation deflection angle
δ_r	Rudder deflection angle
δ_f	Flap deflection angle
b	Wing span
$\bar{c}$	Mean aerodynamic chord
S	Wing area
k	Induced drag coefficient
C_L	Coefficient of lift
C_D	Coefficient of drag
C_Y	Coefficient of side force
C_l	Coefficient of roll moment
C_m	Coefficient of pitch moment

C_n	Coefficient of yaw moment

Table 8 ***Table of Notation for Aerodynamic Model***

Gauss-Markov Process

A discrete first-order Gauss-Markov process $GM(\sigma,\tau)$ with standard deviation of the Markov process σ and time constant, $\tau = 1/\beta$ seconds is [48]

$$x_{k+1} = e^{-\beta\Delta t} x_k + W_k \tag{136}$$

where x_k is a random variable and W_k is a white sequence,

$W_k \sim N[0,\sigma^2(1-e^{-2\beta\Delta t})]$.

Bibliography

[1] "CFIT: Australia in context 1996 to 2005," in *Flight Safety Australia*. vol. Jan-Feb, 2008.

[2] A. Polkinghorne, "APV Approach Implementation," in *9th ASTRA GNSS Implementation Team Meeting*, Melbourne, 2005.

[3] Y. C. Lee, "Receiver Autonomous Integrity Monitoring (RAIM) Capability for Sole-means GPS Navigation in the Oceanic Phase of Flight," *Aerospace and Electronic Systems Magazine, IEEE*, vol. 7, pp. 29-36, 1992.

[4] Y. C. Lee, R. Braff, J. P. Fernow, D. Hashemi, M. P. McLaughlin, and D. O'Laughlin, "GPS and Galileo with RAIM or WAAS for vertically guided approaches," in *ION GNSS*, Long Beach, CA, 2005.

[5] J. S. Leung and B. Siegel, "GPS Standard Positioning Service (SPS) Aircraft en route RAIM Availability for Continental United States," in *Digital Avionics Systems Conference, 1995., 14th DASC*, 1995, pp. 245-251.

[6] K. L. Van Dyke, "The World After SA: Benefits to GPS Integrity," in *Position Location and Navigation Symposium, IEEE 2000*, 2000, pp. 387-394.

[7] K. L. Van Dyke, "Use of stand alone GPS for approach with vertical guidance," in *ION National Technical Meeting 2001*, Long Beach, CA, 2001.

[8] W. Ely, "GRAS development, approval and implementation in Australia," Sydney: University of New South Wales, 2006.

[9] M. Brenner, "Integrated GPS/Inertial fault detection availability," in *ION GPS 95*, 1995.

[10] J. Diesel, "A New Approach to GPS Integrity/Availability: Immediate Global Sole Means Without WAAS," in *ION GPS*, 1994.

[11] R. S. Y. Young and G. A. McGraw, "Fault detection and exclusion using normalized solution separation and residual monitoring methods," *Navigation: The Journal of the Institute of Navigation*, 2003.

[12] M. Koifman and I. Y. Bar-Itzhack, "Inertial navigation system aided by aircraft dynamics," *IEEE Transactions on Control Systems Technology*, vol. 7, 1999.

[13] C. Eck, H. P. Geering, and S. C. Bose, "Model based INS/GPS navigation," in *7th Saint Petersburg International Conference on Integrated Navigation Systems*, St. Petersburg, Russia, 2000.

[14] K. P. A. Lievens, J. A. Mulder, and P. Chu, "Single GPS antenna attitude determination of a fixed wing aircraft aided with aircraft aerodynamics," in *AIAA Guidance, Navigation and Control Conference*, San Francisco, California, 2005.

[15] U. I. Bhatti, "Improved integrity algorithms for integrated GPS/INS systems in the presence of slowly growing errors," London: Imperial College London, 2007.

[16] P. Dixon and S. Harris, *Mastering GPS Flying*. New York: McGraw-Hill, 2004.

[17] C. Rizos, "Trends in GPS Technology and Applications," in *2nd International LBS Workshop*, Seoul, Korea, 2003.

[18] "www.glonass-ianc.rsa.ru," 27 October 2008.

[19] "http://www.esa.int/esaNA/SEMJQSXEM4E_galileo_0.html," 27 October 2008.
[20] G. X. Gao, A. Chen, D. D. Lorenzo, and P. Enge, "Decoding Compass Codes," in *47th CGSIC Meeting*, Fort Worth, Texas, 2007.
[21] B. Hofmann-Wellenhof, H. Lichtenegger, and J. Collins, *Global Positioning System: Theory and Practice*, 5th ed. New York: Springer-Verlag, 1997.
[22] M. Kayton and W. R. Fried, *Avionics Navigation Systems*, 2nd ed. New York: John Wiley & Sons, Inc., 1997.
[23] "L5 Satellite Launch "Indefinite"," in *GPS World*, 2008.
[24] M. S. Grewal, L. R. Weill, and A. P. Andrews, *Global Positioning Systems, Inertial Navigation, and Integration*, Second ed. New Jersey: John Wiley & Sons, 2007.
[25] "http://www.navcen.uscg.gov/gps/incidents.htm," 14 February 2006.
[26] B. W. Parkinson, J. J. Spilker Jr., P. Axelrad, and P. Enge, "Global Positioning System: Theory and Applications." vol. 1 Washington, DC: American Institute of Aeronautics and Astronautics, 1996.
[27] B. W. Parkinson, J. J. Spilker Jr., P. Axelrad, and P. Enge, "Global Positioning System: Theory and Applications." vol. 2 Washington, DC: American Institute of Aeronautics and Astronautics, 1996.
[28] "Minimum Operational Performance Standards for Global Positioning System/Wide Area Augmentation System Airborne Equipment," Radio Technical Commission for Aeronautics Inc., Washington DO-229D, 2006.
[29] "ICAO Standards and Recommended Practices Annex 10 - Aeronautical Telecommunications - Volume 1.," International Civil Aviation Organisation.
[30] "Minimum Operational Performance Standards for Airborne Supplemental Navigation Equipment Using the Global Positioning System," Radio Technical Commission for Aeronautics Inc., Washington DO-208, 1991.
[31] "Minimum Aviation System Performance Standards DGNSS Instrument Approach System: Special Category I (SCAT-I)," Radio Technical Commission for Aeronautics Inc., Washington DO-217, 1993.
[32] B. W. Parkinson and P. Axelrad, "Autonomous GPS Integrity Monitoring Using the Pseudorange Residual," *Journal of the Institute of Navigation*, vol. 35, 1988.
[33] R. G. Brown, "A Baseline GPS RAIM Scheme and a Note on the Equivalence of Three RAIM Methods," *Journal of the Institute of Navigation*, 1992.
[34] M. A. Sturza, "Navigation System Integrity Monitoring Using Redundant Measurements," *Journal of The Institute of Navigation*, vol. 35, 1988.
[35] R. G. Brown, "GPS RAIM: Calculation of Thresholds and Protection Radius using Chi-Square Methods - A Geometric Approach," RTCA Paper No. 491-94/SC159-584 1994.
[36] "Technical Standard Order," Federal Aviation Administration, Washington TSO-C146.
[37] Y.-H. Tsai, W.-C. Yang, F.-R. Chang, and C.-L. Ma, "Using multi-frequency for GPS positioning and receiver autonomous integrity monitoring," in *IEEE International Conference on Control Applications*, 2004.
[38] T. Murphy and R. Hartman, "The Use of GBAS Ground Facilities in a Regional Network," in *IEEE PLANS 2000*, 2000.

[39] R. Di Esposti, H. Bazak, and M. Whelan, "WAAS Geostationary Communication Segment (GCS) Requirements Analysis," in *Position Location and Navigation Symposium, 2002 IEEE*, 2002, pp. 283-290.
[40] K. McPherson, "Ground-based Regional Augmentation System (GRAS)," in *Satellite Navigation Summit*, Munich, 2005.
[41] "Minimum Operational Performance Standards for GPS Ground-based Regional Augmentation System Airborne Equipment," Radio Technical Commission for Aeronautics Inc., Washington DO-310, 2008.
[42] G. Frisk, "A Ground Based Augmentation Service for Gate-to-Gate Operations," in *Position Location and Navigation Symposium, IEEE 2000*, 2000, pp. 527-534.
[43] K. W. McPherson, W. S. Ely, and J. M. Stewart, "Results in Support of the ICAO GRAS Validation Test," *IEEE A&E Systems Magazine*, 2005.
[44] G. K. Crosby, W. S. Ely, K. W. McPherson, J. M. Stewart, D. K. Kraus, T. P. Cashin, K. W. Bean, and B. D. Elrod, "A Ground-based Regional Augmentation System (GRAS) - The Australian Proposal," in *ION GPS2000*, Salt Lake City, UT, 2000.
[45] R. Thompson and J. M. Kunches, "Solar Cycle Number 23 - a progress report," *GPS Solutions*, vol. 6, pp. 121-123, 2002.
[46] A. Komjathy, L. Sparks, A. J. Mannucci, and A. Coster, "The Ionospheric Impact of the October 2003 Storm Event on Wide Area Augmentation System," *GPS Solutions*, vol. 9, pp. 41-50, 2005.
[47] A. Pinker and C. Smith, "Vulnerability of the GPS Signal to Jamming," *GPS Solutions*, vol. 3, pp. 19-27, 1999.
[48] R. G. Brown and P. Y. C. Hwang, *Introduction to Random Signals and Applied Kalman Filtering*, 2nd ed. New York: John Wiley & Sons, 1992.
[49] U. I. Bhatti, W. Y. Ochieng, and S. Feng, "Integrity of an integrated GPS/INS system in the presence of slowly growing errors. Part I: A critical review," *GPS Solutions*, 2007.
[50] U. I. Bhatti, W. Y. Ochieng, and S. Feng, "Integrity of an integrated GPS/INS system in the presence of slowly growing errors. Part II: analysis," *GPS Solutions*, 2007.
[51] D. H. Titterton, J. L. Weston, and Institution of Electrical Engineers., *Strapdown Inertial Navigation Technology*, 2nd ed. Stevenage, U.K.: Institution of Electrical Engineers American Institute of Aeronautics and Astronautics, 2004.
[52] J. Farrell, R. Anoll, and E. McConkey, "IMU Coast: Not a Silver Bullet," in *ION 55th Annual Meeting* Cambridge, MA, 1999.
[53] Y. Lee and S. Ericson, "Analysis of Coast Times Upon Loss of GPS Signals for Integrated GPS/Inertial Systems," in *2003 National Technical Meeting of the Institute of Navigation* Anaheim, California 2003.
[54] Y. C. Lee and D. G. O'Laughlin, "A Performance Analysis of a Tightly Coupled GPS/Inertial System for Two Integrity Monitoring Methods," in *ION GPS*, 1999.
[55] F. van Graas and A. Soloviev, "Combining Low-Cost Inertial Systems with GPS," in *GPS World*, 2004.
[56] C. Eck and H. P. Geering, "Error dynamics of model based INS/GPS navigation for an autonomously flying helicopter," in *AIAA Guidance, Navigation and Control Conference*, Denver, CO, 2000.

[57] L. Cork and R. Walker, "Sensor Fault Detection for UAVs using a Nonlinear Dynamic Model and the IMM-UKF Algorithm," in *2007 Information, Decision and Control Conference*, Adelaide, Australia, 2007.
[58] I. Nikiforov, "Integrity Monitoring for Multi-Sensor Integrated Navigation Systems," in *ION GPS 2002*, Portland, OR, 2002.
[59] G. Welch and G. Bishop, "An Introduction to the Kalman Filter," University of North Carolina 2004.
[60] S. J. Julier and J. K. Uhlmann, "A New Extension of the Kalman Filter to Nonlinear Systems," in *International Symposium on Aerospace/Defense Sensing, Simulation and Controls*, Orlando, Florida, 1997.
[61] B. Azimi-Sadjadi, "Approximate Nonlinear Filtering with Applications to Navigation," in *Electrical and Computer Engineering*: University of Maryland, 2001.
[62] W.-J. Jun and G.-I. Jun, "A Tightly Coupled GPS/INS Integration Based on the Unscented Particle Filter," in *The 2004 International Symposium on GNSS/GPS*, Sydney, Australia, 2004.
[63] J. Wendel, J. Metzger, R. Moenikes, A. Maier, and G. F. Trommer, "A Performance Comparison of Tightly Coupled GPS/INS Navigation Systems based on Extended and Sigma Point Kalman Filters," *Journal of the Institute of Navigation* vol. 53, 2006.
[64] D. Greer, T. Bruggemann, and R. Walker, "Sigma Point Kalman Filters for GPS Navigation with Integrity in Aviation," in *International Global Navigation Satellite Systems Society IGNSS Symposium 2007* Sydney, Australia, 2007.
[65] J. Diesel and G. Dunn, "GPS/IRS AIME: Certification for Sole Means and Solution to RF Interference," in *ION GPS*, 1996.
[66] Y. C. Lee and D. G. O'Laughlin, "A Further Analysis of Integrity Methods for Tightly Coupled GPS/IRS Systems," in *Institute of Navigation National Technical Meeting* Anaheim, CA, 2000.
[67] J. Rankin, "GPS and differential GPS: an error model for sensor simulation " in *Proceedings of the IEEE Position Location and Navigation Symposium*, 1994.
[68] R. van der Merwe and E. A. Wan, "Sigma-Point Kalman Filters for Integrated Navigation," in *Proceedings of the 60th Annual ION Meeting* Ohio, 2004.
[69] W. Abdel-Hamid, "Accuracy Enhancement of Integrated MEMS-IMU/GPS Systems for Land Vehicular Navigation Applications," in *Department of Geomatics Engineering*: University of Calgary, 2005.
[70] Y. Bar-Shalom, X. R. Li, and T. Kirubarajan, *Estimation with Applications to Tracking and Navigation*: John Wiley & Sons, Inc., 2001.
[71] W. Abdel-Hamid, "Accuracy Enhancement of Integrated MEMS-IMU/GPS Systems for Land Vehicular Navigation Applications," UNIVERSITY OF CALGARY, 2005.
[72] A. Noureldin, T. B. Karamat, M. D. Eberts, and A. El-Shafie, "Performance Enhancement of MEMS-Based INS/GPS Integration for Low-Cost Navigation Applications," *IEEE Transactions on Vehicular Technology*, vol. 58, 2009.
[73] "The Aerosim Blockset User's Guide," Unmanned Dynamics, LLC.
[74] V. Klein and E. Morelli, *Aircraft System Identification: Theory and Practice*. Virginia: American Institute of Aeronautics and Astronautics, Inc. , 2006.

[75] B. L. Stevens and F. L. Lewis, *Aircraft Control and Simulation*. Toronto: John Wiley & Sons, 1992.
[76] R. C. Nelson, *Flight Stability and Automatic Control*, 2nd ed. Singapore: WCB/McGraw-Hill, 1998.
[77] J. Roskam, *Airplane Flight Dynamics and Automatic Flight Controls* vol. Part 1. Lawrence, KS, USA: Design, Analysis and Research Corporation, 2001.
[78] B. Etkin, *Dynamics of Atmospheric Flight*. New York: John Wiley and Sons, Inc. , 1972.
[79] S. J. Julier, "Process models for the navigation of high-speed land vehicles," in *Department of Engineering Science*: University of Oxford, 1997.
[80] M. L. Psiaki, S. P. Powell, and P. M. Kinter, Jr., "The Accuracy of The GPS-Derived Acceleration Vector, A Novel Attitude Reference," in *American Institute of Aeronautics and Astronautics*, 1999.
[81] "GPS SPS Signal Specification, Annex B," 1995.
[82] "CRC Handbook of Tables for Probability and Statistics ", W. H. Beyer, Ed.: Chemical Rubber Company, 1968.
[83] J. H. Kim, S. Sukkarieh, E. M. Nebot, and J. Guivant, "On the Effects of Using Heading Information During Inflight Alignment of Low-Cost IMU/GPS Integrated System," in *International Conference of Field and Service Robotics*, Finland, 2001.
[84] S. Hewitson and J. Wang, "GNSS Receiver Autonomous Integrity Monitoring (RAIM) with a dynamic model," *Journal of Navigation* vol. 60, pp. 247-263, 2007.
[85] S. J. Julier and H. F. Durrant-Whyte, "A horizontal model fusion paradigm," in *The Proceedings of the SPIE AeroSense Conference: Navigation and Control Technologies for Unmanned Systems* Orlando, FL, USA, 1996.
[86] R. G. Brown and P. Y. C. Hwang, "Introduction to Random Signals and Applied Kalman Filtering," 2nd ed New York: John Wiley & Sons, 1992, p. 430.
[87] "http://www.flightgear.org/," 20 September 2008.
[88] P. Misra, B. P. Burke, and M. M. Pratt, "GPS Performance in Navigation," *Proceedings of the IEEE*, vol. 87, 1999.
[89] P. Misra and P. Enge, "Global Positioning System : Signals, Measurements, and Performance," Lincoln, Massachusetts: Ganga-Jumana Press, 2006, p. 187.
[90] K. R. Britting, *Inertial Navigation Systems Analysis*. New York: John Wiley & Sons, 1971.
[91] R. F. Stengel, *Flight Dynamics*. Princeton: Princeton University Press, 2004.
[92] R. Kelly, "Derivation of the RAIM Algoritihm from First Principles with Performance Comparisons Between Published Algorithms," in *ION NTM Santa Monica, CA* 1996.